# From Model to Reality: Experimental and Computational Insights to Bone-Implant Mechanics

Dissertation

zur Erlangung des Grades

des Doktors der Ingenieurwissenschaften

der Naturwissenschaftlich-Technischen Fakultät

der Universität des Saarlandes

von

Kerstin Wickert

Saarbrücken

2025

Tag des Kolloquiums: 12.02.2026

| | |
|---|---|
| Dekan: | Prof. Dr.-Ing. Dirk Bähre |
| Berichterstatter: | Prof. Dr.-Ing. Stefan Diebels |
| | Prof. Dr. med. Marcel Orth |
| Vorsitz: | Prof. Dr.-Ing. Matthias Nienhaus |
| Akad. Mitarbeiter: | Dr.-Ing. Oliver Maurer |

# Kurzdarstellung

In dieser kumulativen Dissertation wurden in vier Veröffentlichungen experimentelle und rechnerische Ansätze eingesetzt, um Knochen-Implantat-Systeme unter physiologischen Bedingungen zu untersuchen. Das übergeordnete Ziel dieser Arbeit war es, das Verständnis der mechanischen Einflüsse von Frakturfixationen zu vertiefen und dadurch die Knochenheilung zu verbessern.

In diesen vier Studien wurde ein experimenteller Workflow zum Testen von Knochen-Implantat-Systemen etabliert, mit dem es zusätzlich möglich war, eine Korrelation zwischen interfragmentärer Bewegung und Implantatstabilität herzustellen. Darüber hinaus wurde ein neues Plattenkonzept (in vivo, in vitro und in silico) untersucht sowie der Einfluss der Implantatgeometrie auf das Simulationsergebnis analysiert.

Zusammen tragen diese vier Veröffentlichungen zu einem umfassenderen Verständnis des biomechanischen Verhaltens von Knochen-Implantat-Systemen bei. Sie zeigen, wie integrierte experimentelle und rechnerische Methoden eingesetzt werden können, um die Leistungsfähigkeit von Implantaten zu untersuchen, Simulationen zu validieren und klinische Entscheidungen zu unterstützen. Die entwickelten Arbeitsabläufe bieten eine solide Grundlage für zukünftige Forschungsarbeiten und besitzen das Potenzial, zu einem verbesserten Implantatdesign, einer patientenspezifischen Behandlungsplanung und letztlich zu besseren Ergebnissen in der Frakturheilung beizutragen.

# Abstract

In this cumulative dissertation, experimental and computational approaches were applied in four publications to investigate bone–implant systems under physiological conditions. The overarching aim of this work was to deepen the understanding of the mechanical influences of fracture fixation and thereby contribute to improved bone healing.

Across four studies, an experimental workflow for testing bone-implant systems was established, which additionally enabled the correlation between interfragmentary movement and implant stability. Furthermore, a novel plate design was investigated in vivo, in vitro, and in silico, and the influence of implant geometry on the simulation outcomes was examined.

Together, these four publications contribute to a more comprehensive understanding of the biomechanical behavior of bone–implant systems. They demonstrate how integrated experimental and computational methods can be used to assess implant performance, validate simulations, and support clinical decision-making. The developed workflows provide a solid foundation for future research and hold the potential to contribute to improved implant design, patient-specific treatment planning, and better outcomes in fracture healing.

# Acknowledgement

My scientific work was carried out at the Chair of Applied Mechanics at Saarland University. I would like to express my sincere gratitude to Prof. Dr.-Ing. Stefan Diebels, who made this work possible by offering me the opportunity to hold this position. I am also deeply thankful for his expertise and his continuous openness to both technical and organizational questions. The freedom to incorporate my own ideas and the trust he placed in my work have greatly contributed to my personal and professional development during this time.

Special thanks also go to Prof. Dr. med. Marcel Orth. Through him, I gained valuable insights into the medical field that I, as an engineer, would otherwise not have had. His support during the experimental research was of great help, enabling realistic experiments with clinical relevance.

I would also like to thank Dr. rer. nat. Michael Roland. His open and friendly manner made me feel part of the team from the very beginning. His extensive knowledge of the academic and scientific environment greatly facilitated my entry into research. I especially value his calm and composed nature – with his guidance, every obstacle could be overcome and every problem solved. I am truly grateful for his continuous support and the many valuable discussions we had.

A special thank you goes to my office colleague Annchristin Andres. Together, we were perhaps a bit like Bones and Booth – one half analytical and detail-oriented, the other pragmatic and solution-focused. Together, we solved even the most stubborn experimental challenges. The experiences of recent years, from business trips to excursions in anatomy, will remain some of my fondest memories.

I would like to thank my parents, my sister and her family, as well as my friends for their constant support and thoughtful advice.

Finally, I would also like to thank all those who are not mentioned by name but contributed to this work.

This work was financially supported by the Werner Siemens Foundation as part of the project *“Smart Implants 2.0”* and by the German Federal Ministry of Research, Technology and Space (BMFTR) under the grant *“VirtuS”* (FKZ: 13GW0572).

# Table of contents

# List of Abbreviations

| | |
|---|---|
| 3D | Three-dimensional |
| AO | Arbeitsgemeinschaft für Osteosynthesefragen |
| BMD | Bone mineral density |
| CT | Computed tomography |
| DIC | Digital image correlation |
| FE | Finite element |
| HA | Hydroxyapatite |
| HU | Hounsfield units |
| IFM | Interfragmentary movement |

# Outline

This work is based on the following publications

| | *Title and Journal* | *Aim* | *Methods* | *Results* |
|---|---|---|---|---|
| ***Paper* 1**  | **Simulating Physiological Conditions: A Novel Testing Device for Bone–Implant Interfragmentary Movement,** *under consideration/ review at a peer-reviewed journal owned by a major scientific publisher (2025)* | Investigate interfragmentary movement under realistic conditions | Realistic simulations of a gait cycle to human cadaveric bone using experiments and computational approaches | Workflow has been established to test bone-implant systems<br><br>With this knowledge bone healing should |
| ***Paper* 2**  | **Experimental and virtual testing of bone-implant systems equipped with the AO Fracture Monitor with regard to interfragmentary movement,** *Frontiers in Bioengineering and Biotechnology (2024)* | Define relationship between AO Fracture Monitor and computational analyses | AO Fracture Monitor as strain gauge measurement and digital image correlation to investigate implant strain and interfragmentary movement | Strong correlation defining a relationship between the different areas of interest<br><br>Computational analysis validated through experimental work |
| ***Paper* 3**  | **Integrated Study of the Distal Femur Biphasic Plate: Exploring In Vivo, In Vitro, and In Silico Methodologies,** *submitted to Frontiers in Bioengineering and Biotechnology (2025)* | Exploring biphasic plate design in context with human specimens under real world conditions | In vivo, in vitro and in silico methods were used to evaluate biphasic behavior | Biphasic plate's behavior was tested in vivo, in vitro and in silico. Biphasic states were captured in vitro. Different stress distributions of the plate depending on load cases (axial vs real world conditions). |
| ***Paper* 4**  | **CT-, 3D-Scan and Manufacturer-Based Implant Models: A Comparative Finite Element Study on Implant Geometry and Interfragmentary Movement in Distal Radius Fracture Fixation,** in progress (2025) | Investigate geometry source of the implant to computational outcome in finite element analyses | Comparing of three different implant geometries with the help of computational analyses concerning realistic loading conditions | In addition to the geometric differences, minimal implant positioning play a significant role in the calculated results. |

# Research Purposes

Following research purposes are summarized in these papers:

**Paper 1:** This paper presents the concept of a self-designed and constructed testing device for evaluating bone-implant systems under physiologically relevant loading scenarios. A workflow is described using a human cadaveric tibial bone with a distal spiral fracture treated with a plate osteosynthesis. Knee joint forces that occur during a gait cycle are applied to the treated tibia. The aim of the investigations is to determine key biomechanical parameters, during a specific loading scenario. In summary, an established, reproducible workflow has been developed that makes it possible to test bone-implant systems under physiological loading scenarios and determine key biomechanical parameters.

**Paper 2:** The second paper combines experiment and simulation. Therefore, measurements with the AO Fracture Monitor (strain gauges) and measurements using digital image correlation were used experimentally. Biomechanical simulations were done evaluating implant surface and interfragmentary movement. To link between experiment and simulation hypotheses were formulated. There is a correlation between (1) digital image correlation and interfragmentary movement executed in the experiment (2) measurements of the digital image correlation and the AO Fracture Monitor signal. With the help of digital image correlation, the quality of the simulation results can be assessed. A linear model can be developed to combine AO Fracture Monitor signal with simulated interfragmentary movement. In conclusion, digital image correlation is an effective tool to evaluate bone-implant systems. It was shown, that there is a linear relationship between strain on the implant surface and the interfragmentary movement. In addition, a correlation between biomechanical simulations and experimentally measurements could be established. However, this correlation depends on the type of fracture and the treatment.

**Paper 3:** Biphasic plate design is a new concept of plate fixation. This study examined the plate's behavior under realistic loading conditions compared to traditional plating. The biphasic plate can assume two different modes (rigid or flex), which either provide greater strength or sufficient flexibility to support the healing process. The investigations were conducted in vitro using a human cadaveric specimen, prepared with the AO Fracture Monitor to detect the different modes in a test setup under axial loading. In vivo observations were based on four patients treated with the biphasic plate, whose clinical imaging and motion capturing data additionally served as the basis for the in silico models. The study successfully explored patient-specific biomechanical simulations, using biphasic plates as a treatment option to address multidirectional forces. These individual factors are evident in the simulation results, where the maximum load is distributed along the edges of the biphasic plate rather than centrally when the plate is subjected to pure axial load.

**Paper 4:** This paper investigates the effect of implant geometry source to biomechanical simulation results. The basis builds an initial patient dataset. Three different implant geometry sets from (1) computed tomography scan (2) three-dimensional scan and (3) manufacturer data were imported to the initial dataset. In all three computational evaluations, same material assignment were used. Differences were shown in interfragmentary movement near cortex, caused by potential minimal differences during implant positioning. Another aspect using computational simulations to surgical planning or in preoperative situations is to concern the rising time during model generation and computational time with rising element sizes especially in contact areas (screw to implant, screw to bone).

# 1. Introduction

With increasing age, the risk of sustaining a bone fracture rises significantly and so does the complexity of the healing process. By the age of 55, an estimated 44 % of adults will have experienced at least one fracture [1]. Furthermore, approximately 10 % of all fractures fail to heal without complications [2].

The most frequently fractured bones include the femur (thigh bone), radius (forearm) [3], and tibia (shine bone) [4]. In Germany, the number of reported cases in 2023 included 132,445 forearm fractures, 217,593 femoral fractures, and 120,867 lower leg fractures, including those involving the ankle joint (see Figure 1) [5].

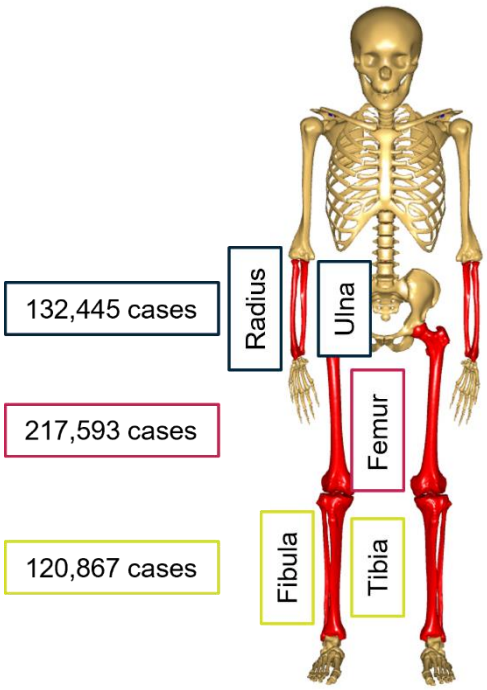


*Figure 1: Red colored bones are the most frequently fractured bones, combined with the number of reported cases in Germany in 2023 [5]. Skeletal bones were modeled with Anybody™ (AnyBody™ Technology A/S Aalborg, Denmark).*

Delays during the healing process are relatively common by these kind of fractures, resulting in lengthy treatment and recovery. In some cases, full recovery may never be achieved. The results of a protracted or incomplete recovery are long periods of absence from work and long-lasting hospital stays, which incur considerable costs. These challenges underscore the importance of personalized, well-targeted treatment strategies that can support recovery and help restore full functional mobility.

When these efforts fails, revision surgery often becomes the only remaining option, effectively resetting the healing process. It is estimated that 5-10 % of all fractures result in a so-called nonunion, requiring additional surgical intervention to initiate or support healing [6], [7].

According to the U.S. Food and Drug Administration, a fracture is classified as a nonunion if there is no radiographic evidence of healing within three months and no union has occurred by nine months post-injury [8]. Another definition states that a fracture is considered a nonunion if, in the opinion of the treating surgeon, healing is unlikely to occur without further surgical intervention [9].

Fracture healing complications, particularly nonunion, are associated with significant socioeconomic burdens [10]. Owing to global variations in healthcare systems, the cost of treating nonunion cases differs substantially between countries. In Germany, the average cost of managing lower leg fractures is approximately 6,377 € per patient, ranking second only to the cost of revision procedures for pelvic and hip fractures [7]. In the United Kingdom, the average treatment cost for nonunion is £17,200 for femoral fractures and £16,330 for tibial fractures [9].

On one hand one has to define what causes nonunion or delayed healing and on the other hand one has to clarify which factors are decisive in these cases. Delayed or absent healing can result from a variety of factors. These may be biological, (diabetes or smoking) [11] or mechanical, such as implant failure. In many cases, the cause is a combination of both. The diamond concept of fracture healing integrates these two domains and considers them equally important [8]. A strict separation between biological and mechanical influences is often not feasible, as they frequently interact. In such cases, these interdependent influences are referred to as biomechanical factors (see Figure 2).

Two fundamental biomechanical factors influencing fracture healing are implant stability and interfragmentary movement (IFM). The stability of the osteosynthesis is determined by its stiffness, which plays a direct role in the healing outcome. Together with the applied load, stiffness dictates the extent of IFM [12]. The primary function of osteosynthesis is to stabilize individual bone fragments and maintain their alignment. The fixation must strike a balance, providing enough rigidity to prevent excessive motion, while still allowing controlled micromotion to stimulate biological healing. If the construct is too unstable, excessive IFM can disrupt the healing process and lead to nonunion [13].

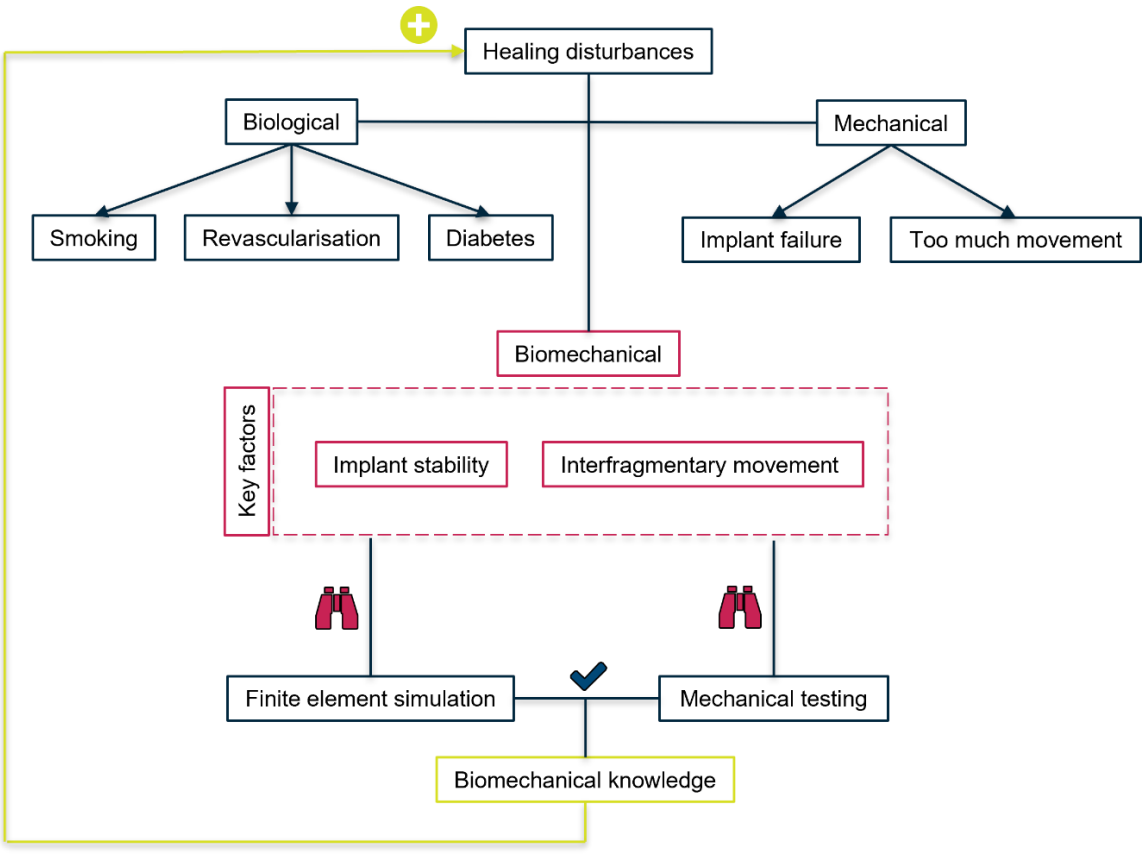


*Figure 2: Healing disturbances showing that implant stability and interfragmentary movement are biomechanical key factors influencing this process. Finite element simulation and mechanical testing investigating those key factors and widen the biomechanical knowledge to improve healing disturbances.*

This overall aim is to expand the understanding of biomechanics by focusing on the key mechanical factors that influence fracture healing. Finite element (FE) analysis is used to simulate complex physical behavior through numerical modeling, providing a framework for analyzing and interpreting mechanical conditions relevant to bone regeneration. A major advantage of this method is its ability to test alternative treatment strategies virtually, enabling clinically important questions to be addressed prior to implementation. This can lead to improved patient outcomes while also helping to reduce the risk and cost of revision surgeries. However, to ensure that simulation results are both reliable and meaningful, experimental validation is essential to confirm their accuracy and strengthen their clinical relevance. To address this, experiments are executed using custom-designed testing devices specifically developed to replicate individualized loading scenarios for bone-implant systems. With the help of FE analyses and experimental work the biomechanical knowledge will be investigated and will help to improve the healing disturbances (see Figure 2).

Figure 3 shows the established workflow to develop bone-implant systems. For realistic conditions, human cadaveric bones are prepared with standardized fractures and subsequently stabilized with implants. These specimens are then subjected to physiologically relevant loading within the experimental setup, and the resulting mechanical responses are analyzed. In parallel, FE simulations are used to model the corresponding biomechanical conditions. Clinical imaging data are used to generate subject-specific computational models, which are then exposed to the same loading scenarios as in the experiments. The simulation outcomes are subsequently compared with the experimental data to assess consistency and validate the models.

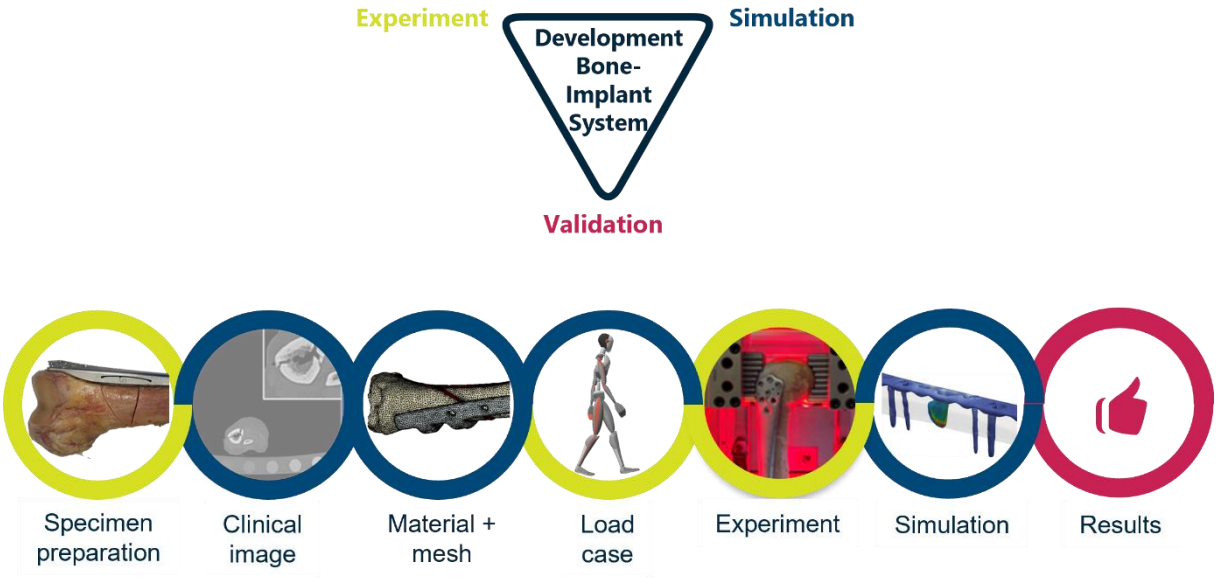


*Figure 3: Workflow shown the development of bone-implant systems using experimental and computational processes. Experimental parts highlighted in yellow, computational parts highlighted in blue and the results (validation) shown in pink.*

The individual papers led to several key outcomes:

1. Examining the fracture site using a self-designed testing device to reproduce physiological relevant loading scenarios (Paper 1).
2. Experimental and computational definition of the relationship between implant stability and IFM (Paper 2).
3. Evaluation of innovative implant designs concerning in vivo, in vitro, and in silico methodologies (Paper 3).
4. Investigation of input data influences the outcomes of FE simulations (Paper 4).

# 2. Biomechanical Basics

This chapter introduces fundamental biomechanical principles that are crucial for understanding the mechanics of fractures and their treatment. It outlines the main anatomical directions and axes, the mechanical characteristics of human bone, and the common fracture classification system. Furthermore, it provides an overview of the biological healing process, with a particular focus on mechanically relevant factors that influence bone regeneration and the stability of bone-implant systems.

## 2.1 Anatomical Axes and Directions

To understand anatomical directional terms, the following concepts are illustrated using the example of the human skeleton to show anatomical axes (see Figure 4 A) and anatomical directions (see Figure 4 B) [14]:

- Longitudinal axis (vertical axis, divides the body into front and back),
- Transverse axis (horizontal axis, divides the body into upper and lower parts),
- Sagittal axis (vertical axis, divides the body into left and right),
- Proximal (closer to the trunk or center of the body),
- Distal (further from the trunk or center of the body),
- Medial (toward the midline) and Lateral (further from the midline).

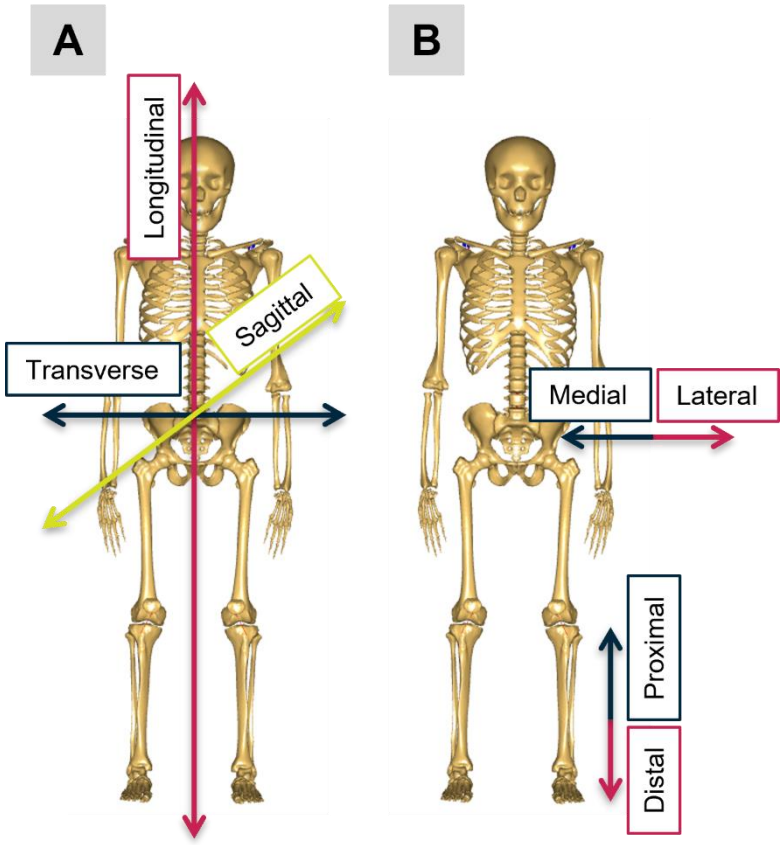


*Figure 4: A: Anatomical axes, B: Anatomical directions on human body. Skeletal bones were modeled with Anybody™ (AnyBody™ Technology A/S Aalborg, Denmark).*

## 2.2 Geometry and Mechanical Properties of Bone

The human skeleton consists of numerous bones and serves as the structural framework of the body. Among these, the radius, femur, and tibia are the three long bones with the highest incidence of fractures [3], [4]. Despite their varying locations and functions, all bones generally share a similar morphology. Approximately 80 % of bone mass is composed of a hard outer shell known as cortical bone (see Figure 5 A). This dense layer is found along the diaphysis as well as at the epi- and metaphysis (see Figure 5 B), where it encases the inner cancellous bone, or trabecular bone (see Figure 5 A) [15].

Bone quality is a key determinant of the body's load-bearing capacity, influencing the mechanical stability, strength, and adaptability of the skeleton. One of the most critical factors in assessing bone quality is bone mineral density (BMD). It is estimated that 60-70 % of a bone's mechanical competence can be attributed to its density [16]. Due to this dependence of mechanical strength on BMD, a bone with lower BMD cannot be subjected to the same higher load as a bone with higher BMD (Paper 2). Furthermore, a correlation can be established between bone density and the elastic modulus [17]. Accurate representation of material properties - such as local variations in bone density - is essential for obtaining reliable results in FE analyses.

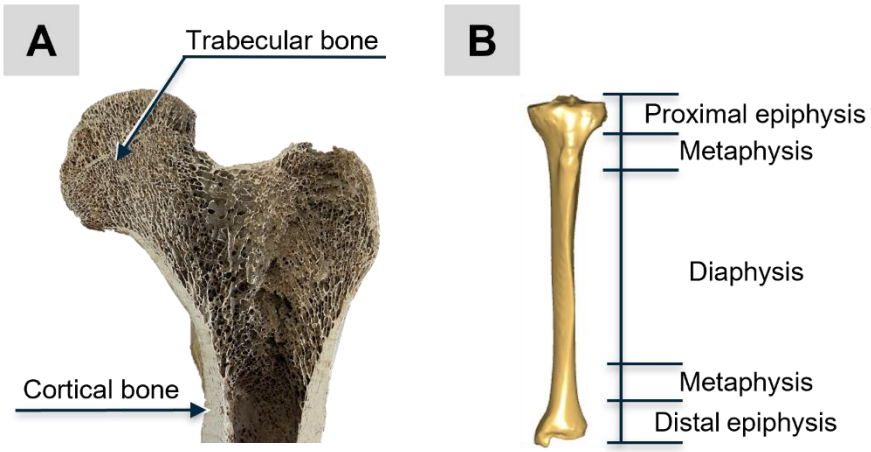


*Figure 5: A: Bone structures (cortical and trabecular) shown on femoral bone, B: Classification of single parts of human long bone shown on tibial bone. Skeletal bone was modeled with Anybody™ (AnyBody™ Technology A/S Aalborg, Denmark).*

FE models of bone structures are typically derived from computed tomography (CT) data. The CT scans are processed through image segmentation to generate a three-dimensional (3D) geometric representation of the bone. This process involves various image processing techniques, including thresholding, morphological closing, and smoothing filters. To assign material properties to the model, a relationship between bone density and the elastic modulus is required. A mathematical correlation between CT gray values and the corresponding density-modulus relationship is established.

To achieve accurate quantification of BMD from CT data, a calibration phantom is typically employed. A widely used standard is the hydroxyapatite (HA) phantom, which consists of several rods with defined HA concentrations [18], [19]. This phantom enables the calibration of CT gray values and serves as a reference for converting Hounsfield units (HU) into quantitative bone density values. It is important to distinguish between different definitions of density when deriving mechanical properties from imaging data. The most commonly referenced types are

equivalent mineral density, ash density, and apparent density. Among these, apparent density is typically used for establishing the relationship with the elastic modulus (see Figure 6).

For densitometric relationship, histograms are created for each HA phantom rod, capturing the distribution of CT gray values relative to the number of corresponding voxels. The peak of each histogram is used to define a linear relationship between HU and equivalent mineral density. By using a calibration phantom, this density metric can be directly obtained from the CT data. Equivalent mineral density exhibits a strong correlation with ash density [17], which is experimentally determined through the incineration of bone specimens in a furnace, followed by measurement of the residual mineral content. Ash density is then calculated as the ratio of the ash mass to the original mass of the specimen [17], [20].

Apparent density, which is closely linked to the elastic modulus, is derived from ash density and serves as a key parameter in establishing the density-modulus relationship [21]. It is defined as the ratio of a specimen's wet mass to its total volume. To determine apparent density experimentally, bone specimens are first cleaned and de-marrowed, then submerged in water to ensure full saturation. To eliminate entrapped air, the samples are placed under vacuum, after which they are centrifuged and weighed to obtain the wet mass [22]. The resulting apparent density is subsequently used as the basis for mechanical property assignment in the FE model.

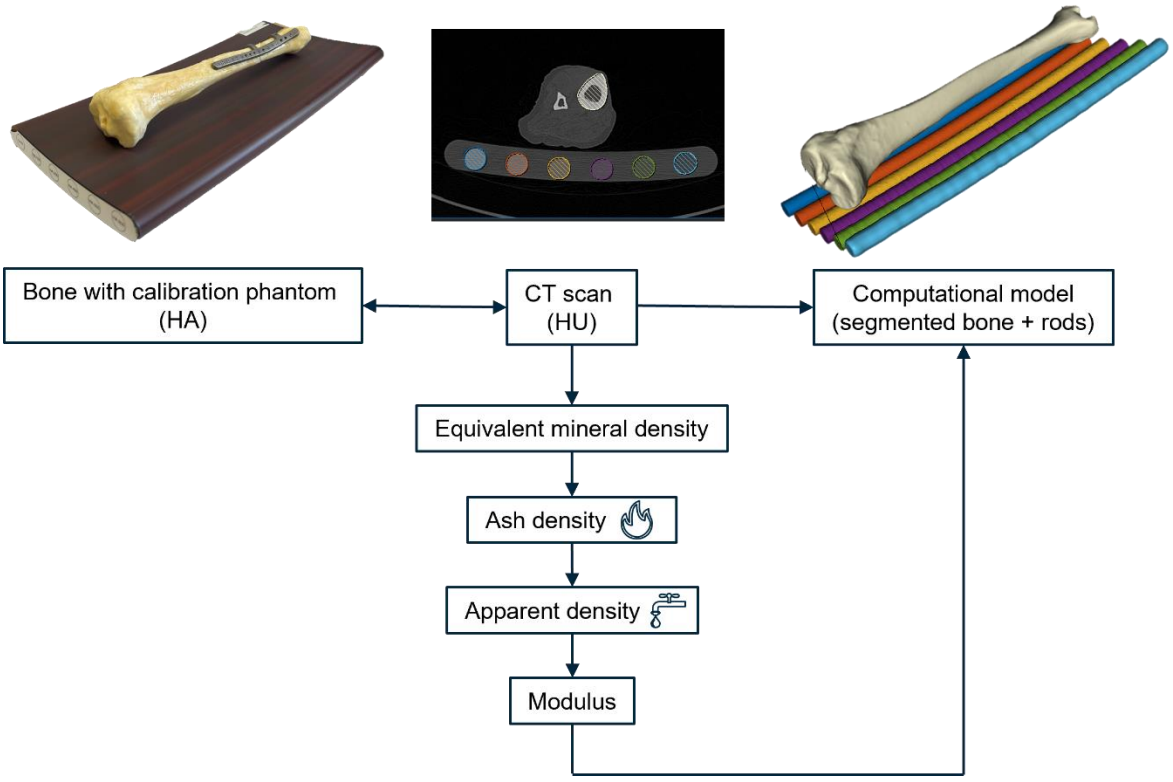


*Figure 6: Modulus calculation from computed tomography (CT) scan in (Hounsfield Units (HU)) using a hydroxyapatite (HA) calibration phantom.*

BMD is among the most frequently assessed parameters for evaluating implant performance and monitoring the healing process. Numerous studies have demonstrated a strong correlation between BMD and implant stability and function [23].

## 2.3 Fracture Type and Treatment

The AO Foundation (Arbeitsgemeinschaft für Osteosynthesefragen) focuses on the fundamental principles of fracture management and the development of standardized treatment protocols. To support this, a globally recognized fracture classification system was established [24]. This standardized system is widely used in clinical practice and research, and is accompanied by treatment guidelines tailored to each fracture type, aiming to support consistent and evidence-based decision-making. Fractures are categorized based on anatomical location, fracture morphology, and severity.

The classification code consists of multiple components: the first number identifies the anatomical region, the second indicates the segment of the bone involved (1 = proximal, 2 = diaphyseal, 3 = distal), and the final letter denotes the type and complexity of the fracture.

For example, the code “AO 2R3A2” refers to a specific fracture with defined location and characteristics (see Figure 7 A). In this context, the number “2” refers to the forearm, and the additional letter “R” designates the radius. The “3” indicates a fracture located at the distal epiphysis, while the letter “A” denotes a simple fracture. As an added feature, the AO classification provides treatment recommendations for each specific fracture type to support optimal clinical management.

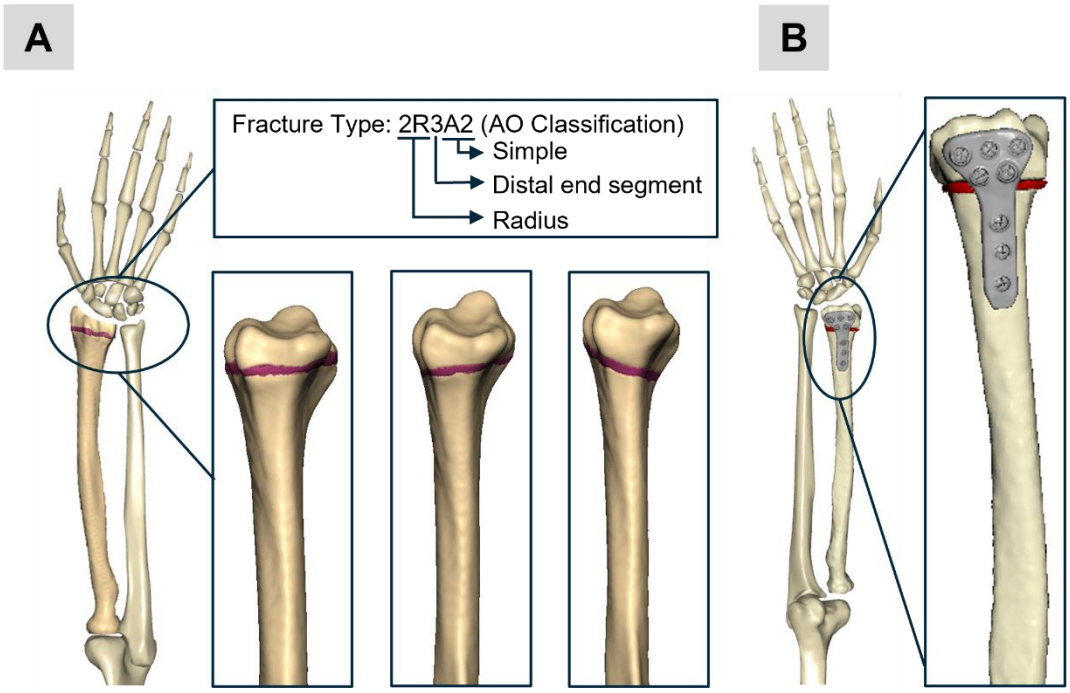


*Figure 7: A: Radius with fracture according to AO classification: Samples with different angles of a simple fracture, B: Treated fracture with individualized plate osteosynthesis. Skeletal bones except radius were modeled with Anybody™ (AnyBody™ Technology A/S Aalborg, Denmark).*

Fractures of long bones can be managed using several fixation methods, including intramedullary nails, plate osteosynthesis, and external fixators. The choice of treatment depends largely on the fracture location and the extent of the injury.

Intramedullary nails are inserted into the medullary canal of the bone, providing load-sharing that is closely aligned with the anatomical axis [25]. Because the implant is centrally positioned, this technique offers high mechanical stability and is often associated with strong primary fixation.

Plate osteosynthesis (see Figure 7 B) is commonly used for fractures near joints. Plates are affixed to the outer surface of the bone, which introduces bending loads due to the eccentric positioning. One advantage of this method is that the external placement of the implant makes it particularly suitable for experimental analysis. It allows for easy application of optical measurement techniques and the integration of instrumentation to assess implant stiffness. Additionally, since the plate is located near the fracture site, it enables a meaningful correlation between implant stiffness and IFM (Paper 2).

In cases involving significant soft tissue trauma, external fixators are often preferred . These devices are mounted outside the body and connected to the bone via pins, providing stabilization while minimizing disruption to the injured soft tissue.
In summary, primary and secondary stability serve as key indicators for assessing osseointegration, i.e., the quality of the bone-implant interface. Primary stability refers to the initial mechanical stability of the implant, whereas secondary stability is governed by biological factors [26].

## 2.4 Healing Process and Mechanical Key Factors

A detailed understanding of the fracture healing process is critical for developing targeted strategies to support and enhance bone regeneration. This requires identifying the key mechanical and biological factors that influence healing outcomes. Among the most common causes of impaired fracture healing are poor vascularization and inadequate mechanical stabilization of the fracture site [12]. Fracture healing occurs through two primary mechanisms: direct (primary) and indirect (secondary) healing (see Figure 8).

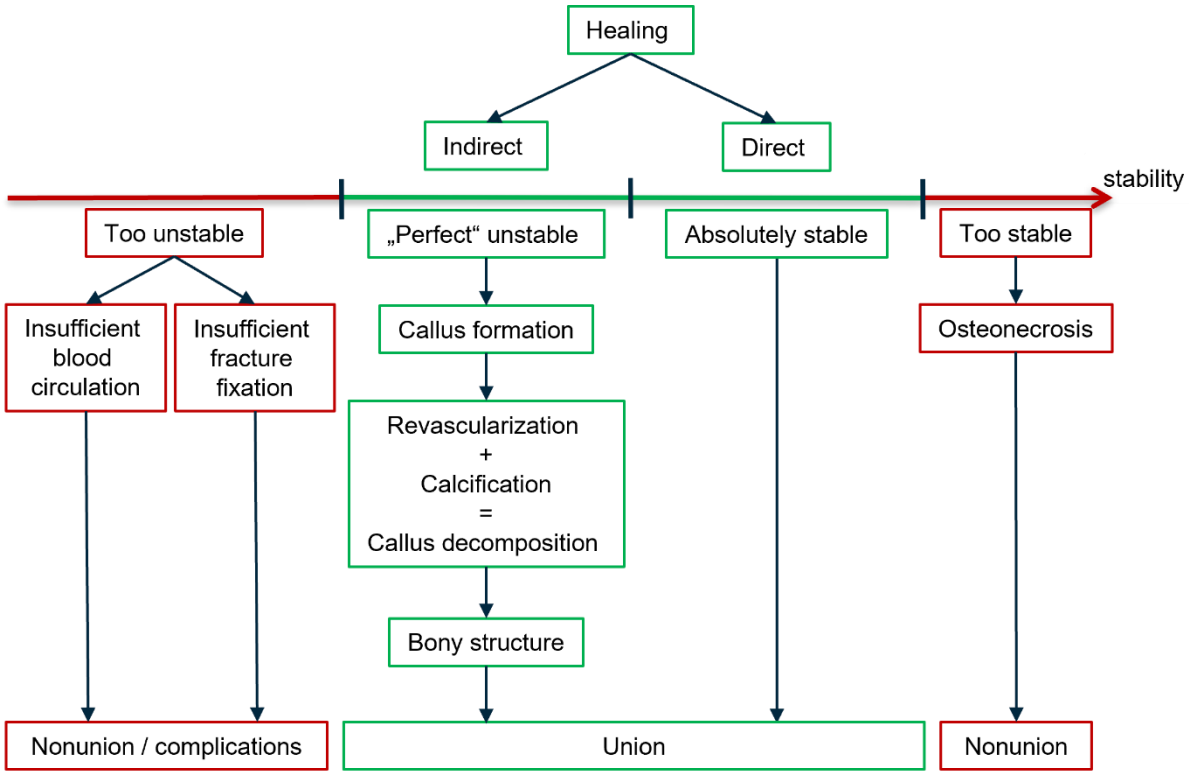


*Figure 8: Healing process in dependence of stability showing that different stability modes resulting in different healing outcomes (e.g. too unstable end up in nonunion or complications, absolutely stable and up in union).*

Direct healing requires absolute stability at the fracture interface and is typically achieved through rigid fixation [27]. However, based on Perren's strain theory, successful healing depends on maintaining a controlled range of interfragmentary strain - too much or too little can disrupt the process [28]. Excessive stability, or over-rigid fixation, may inhibit healing and

has been associated with complications such as osteonecrosis due to a lack of mechanical stimulation [29].

Indirect healing, by contrast, is characterized by new bone soft tissue that bridges the fracture gap (formation of a callus). This process is facilitated by some degree of micromotion at the fracture site, allowed by more flexible fixation methods. The optimization of the mechanobiological terms promote a fast stable callus formation (Paper 3). After revascularization and calcification, the callus gradually decomposes into mature bone, restoring structural integrity [30]. These findings underscore the close relationship between mechanical stability and the biological processes governing fracture repair.

In biomechanical research, the stability of an osteosynthesis is typically assessed through two key parameters: stiffness and IFM. Those are not feasible as direct measurements within living organisms. IFM refers to the relative movement and deformation between bone fragments at the fracture site. These kinematic parameters are strongly influenced by the fracture gap width, with which they share a direct relationship. It is known that excessive motion at the fracture interface has been shown to disrupt the healing process [13]. In stabilized fractures, interfragmentary strain is generally maintained below 10 % to promote successful healing [31].

The extent of IFM depends on the external loading conditions and the geometry of the fracture, particularly the size of the gap. When IFM remains within an optimal range, physiological bone healing can proceed. However, successful biological regeneration also depends on sufficient revascularization, which is itself influenced by IFM and fracture gap size. During the early phase of healing, IFM tends to be relatively high, as the mechanical environment is dictated primarily by the fixation stiffness and the loading scenario. As healing progresses, the developing callus begins to stiffen and assumes a greater share of the load, which gradually reduces IFM. In the final phase, as the callus mineralizes and remodels into lamellar bone, IFM is effectively eliminated and any redundant tissue is resorbed [32].

Therefore, IFM and fixation stiffness are critical mechanical factors in the regulation of the bone healing process [32].

# 3. Biomechanical Study Design

This chapter summarizes all relevant considerations for the design and implementation of biomechanical studies. Starting by presenting general methodological requirements that contribute to biomechanical investigations. Following this, the main experimental approaches are discussed in terms of their respective advantages and limitations. Finally, the chapter addresses loading scenarios relevant to bone-implant systems, highlighting their significance in both experimental and computational contexts. Together, these sections provide a structured foundation for understanding the methodological choices made in the studies presented throughout this work.

## 3.1 General

Every biomechanical study should begin with a defined hypothesis or research question that the study aims to address. The more specific the research question, the more effectively an appropriate and targeted study design can be developed. Equally important is establishing the intended context of application for the investigation. This ensures that the findings are not only scientifically robust but also practically relevant and translatable to clinical practice.

The fundamental principles of high-quality biomechanical research have been discussed extensively in the literature, e.g. Augat et al. [33]. In addition to well-established scientific quality criteria for biomechanical studies - such as those outlined by Augat et al. [33] - there are also regulatory guidelines that are particularly relevant for computational modeling of medical devices. Augat et al. [33] highlight four key criteria that can be used to evaluate the validity and impact of biomechanical studies:

1. Appropriate:

Appropriate, quantifiable outcome measures should be selected to directly address the research question. Parameters such as implant stability and IFM are commonly used, as they serve as functional indicators of bone-implant system performance.

2. Reliability and 3.Validity:

Ensuring reproducibility and transparency of the data requires a thorough description of the experimental setup and measurement procedures. Clear documentation is essential to minimize variability between test runs and to enhance the reliability and precision of the results.

4. Relevance:

The ultimate aim of any biomechanical study should be to advance patient outcomes. Achieving this requires a study design that is not only scientifically sound but also clinically relevant and reflective of real-world conditions. Experimental models should strike a balance between simplification and realism, drawing on established studies to ensure that results are both comparable and meaningfully interpretable within the broader clinical context.

To this end, the U.S. Food and Drug Administration [34] has issued a comprehensive guidance document that defines key requirements for such modeling studies. It addresses critical elements including model generation (see Paper 4), the selection and definition of appropriate material models, the specification of boundary conditions, and approaches for model verification and validation. The goal of this guidance is to enhance the transparency, reproducibility, and ultimately the clinical relevance of computational simulations, while establishing standardized criteria for their evaluation.

## 3.2 Study Design Implementation

Biomechanical research questions can be investigated at various levels: **in vivo** within a living organism, **in vitro** under controlled laboratory conditions, and **in silico** through computer-based simulations.

In vivo studies, conducted within living subjects, require clinical trials that must adhere to strict regulatory frameworks and are often associated with substantial costs. These studies must follow strict ethical and legal guidelines, including formal approval processes such as obtaining clearance from an institutional review board. One of the primary challenges in clinical research is patient selection. Answering a specific clinical question typically requires a sufficiently large and defined study population. However, assembling a homogeneous cohort is particularly difficult in clinical settings, as patients often present with a wide range of fracture types, bone densities, and comorbidities. This variability complicates standardization of testing conditions and reduces the reproducibility of results. Depending on the research objective, such heterogeneity can significantly limit the strength and comparability of study outcomes. Moreover, the practical execution of biomechanical measurements in vivo, such as assessing implant stiffness or IFM, is often technically challenging and not always feasible. As a result, studies of this nature are limited, and the availability of high-quality clinical data remains scarce.

In vitro studies, performed under controlled laboratory conditions, offer several advantages over in vivo research - particularly in terms of reproducibility and cost-effectiveness. In biomechanical research, a broad spectrum of test materials is available, ranging from synthetic bone to human cadaveric specimens and animal bones, selected based on the specific aims of the study. Importantly, the choice of material and the geometry of the specimen can influence outcomes and should be carefully considered. Standardized testing protocols can be easily replicated, which simplifies data collection, analysis, and comparison across studies. Laboratory settings enable focused investigation of specific parameters (such as implant stiffness or IFM) under controlled conditions. Such studies enable tight control over key variables and facilitate the establishment of consistent testing conditions. However, this high level of control also creates idealized experimental settings that may not fully reflect clinical reality. As a result, important biological influences (soft tissue dynamics, muscle activity, and the progressive stages of healing) are frequently absent or oversimplified, limiting the direct clinical applicability of the findings.

In silico (computational) studies represent a valuable complement to experimental and clinical approaches. However, to ensure that the results are robust and meaningful, careful validation is essential; either through comparison with experimental data or reference to established literature. It is important to recognize that the outcomes of such simulations are highly dependent on the selected input parameters, including the material properties of the modeled specimens or implants, as well as the defined loading conditions. Therefore, one of the studies investigates the influence of input data, particularly the generation of implant geometry, on the results of FE simulations. The analysis focuses on how different methods of implant geometry generation affect the simulation outcomes.

Paper 3 combines these three design implementations. The two biphasic states were captured in an in vitro study using a human cadaveric specimen. Equivalent investigations were confirmed in in silico studies. The study was completed with four patient cases (in vivo). By combining the three studies, it was possible to experimentally investigate the plate concept and its effect on the healing process.

Figure 9 summarizes the various approaches with their advantages and disadvantages.

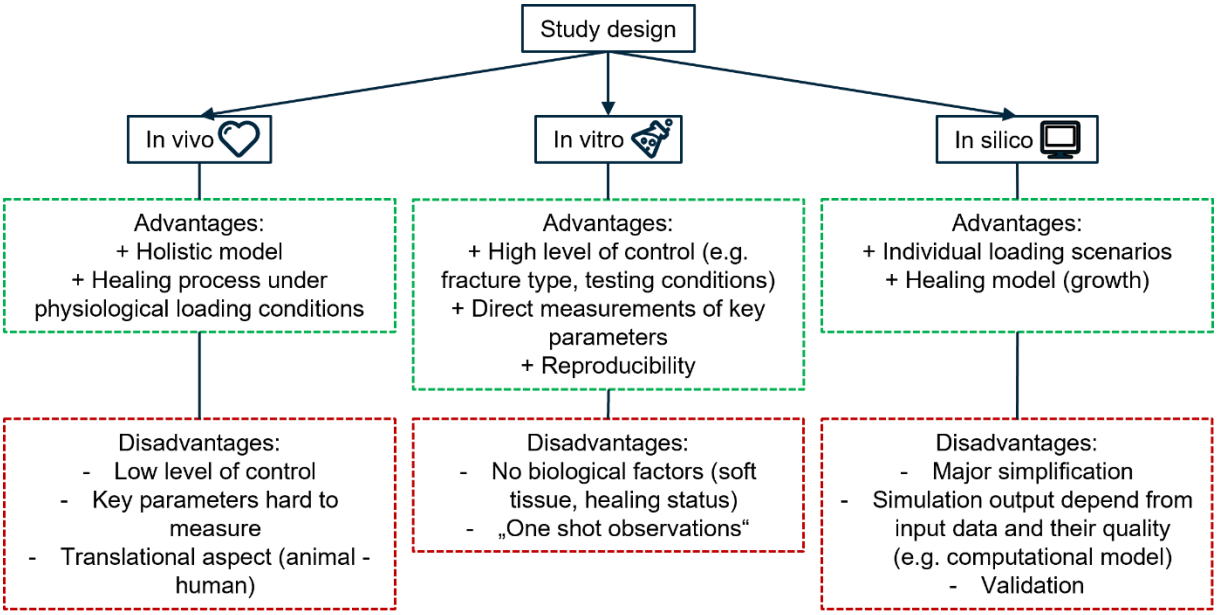


*Figure 9: Options to implement a study design showing advantages and disadvantages of in vivo, in vitro and in silico studies.*

## 3.3 Loading Conditions

Understanding how biological tissue respond to mechanical loading is central to many concepts in bone biology and biomechanics. Two foundational theories in this area are Wolff's law and the concept of the mechanical environment introduced by Perren [28]. Wolff's law [35], formulated in the late 19th century, posits that bone continuously adapts its structure - both internally and externally - based on the mechanical forces it experiences. In essence, "form follows function": bone is deposited where mechanical stress is present and resorbed where it is absent [35].

Building on this principle, Perren proposed a model linking mechanical stability, micromotion at the fracture site, and the biological process of bone healing [29]. His concept of the mechanical environment emphasizes that controlled movement at the fracture interface can promote regeneration under the right conditions. More recently, the diamond concept has broadened this view by integrating mechanical, cellular, and molecular factors into a comprehensive framework for understanding bone healing [36]. This model highlights the interplay between biomechanics and biology in driving successful tissue regeneration.

Expanding on earlier work, Claes introduced a tissue differentiation model that describes the bone healing process as a function of the mechanical stiffness of the fixation construct [12]. This model established that there is an optimal strain range within which bone regeneration can proceed effectively, without disruption.

Claes and Heigele [37] developed the concept of a "perfect healing window," which describes bone formation as a function of strain and hydrostatic pressure. When specific thresholds for strain and pressure are maintained, bone regeneration is promoted. In simple terms, within the fracture gap, distinct thresholds for strain and hydrostatic pressure delineate different tissue outcomes (resorption, bone, cartilage, fibrous tissue, or tissue damage).

This framework underscores a fundamental principle: mechanical loading is not merely a risk factor for implant failure, but also a vital stimulus for successful bone healing. Yet, in practice, biomechanical evaluations often focus on individual components of the system in isolation. For example, load transmission through the fixation device, material testing of isolated bone samples, and gait dynamics in lower limb fractures are frequently investigated as separate entities.

The following sections provide a more comprehensive perspective by examining the interrelationship between these three key components of the biomechanical system.

### 3.3.1 Implant Load Analysis

The research question is a key factor in determining the appropriate loading condition. When investigating how the underlying geometric data of the implant influences the simulation results just concerning implant load analysis, a simplified loading scenario is sufficient for initial analyses.

By limiting the mechanical input to axial loading, potential deviations in the simulation results can be more directly attributed to differences in the underlying geometric representations. This controlled setup minimizes the influence of complex boundary conditions or load interactions and thus provides a clearer assessment of the sensitivity of the FE model to geometric input data.

However, if the influence of implant geometry on overall biomechanical behavior during clinically relevant loading scenarios is the subject of the investigations, the load case changes, and within the regions of interest (Paper 4). This means that, in addition to implant analysis, IFM is also crucial.

Orthopedic implants are traditionally evaluated through material testing and regulatory approval processes that rely on standardized testing protocols. These methods typically focus on static and cyclic loading scenarios, as defined by international standards. In most cases, testing is performed using simplified setups that apply purely axial loads [38]. The use of real conditions instead of a purely axial load led to significant differences in the load distribution on the implant, with the maximum load shifting from a central distribution to the outer edges (Paper 3).

Regulatory approval processes or standardized testing protocols not always matching the real world conditions implants are exposed to. A common illustration of this simplified methodology is the approval process for radius screws [39]. To determine their mechanical performance, screws are placed vertically in a bone substitute and then pulled out axially. However, in clinical applications, these screws are rarely inserted vertically. Instead, they are placed at oblique angles, aligned with anatomical structures (Paper 4). This orientation results in more complex loading conditions involving combinations of shear, bending, and torsional forces - none of which are accounted for in standard test protocols. This mismatch between standardized testing and real-world conditions can lead to an underestimation of true failure behavior and may overlook critical biomechanical vulnerabilities.

While standardized testing protocols offer a certain level of comparability, they fall short in capturing the complex biomechanical conditions present within the human body. In clinical practice, implants are simultaneously subjected to multiple loading modes - combinations of multi-axial forces that act during different phases of specific movement patterns. Transverse loads, in particular, play a critical role in certain loading scenarios and should be accounted for in biomechanical modeling [40]. These multi-axial and dynamic loading conditions can contribute to material fatigue, micromotion at the implant interface, or even premature implant failure; factors that are often not detected through standard testing protocols .

A growing trend in implant testing is the use of anatomically accurate loading conditions based on real-life movement and force patterns [41]. Recent studies increasingly account for both translational and rotational alignment of the bone by applying loads relative to a defined anatomical coordinate system. This approach enables more physiologically relevant loading of the implant, resulting in data that better reflect its performance under clinical conditions .

Incorporating such realistic boundary conditions into implant testing represents an important step toward improving implant design, minimizing the risk of mechanical failure, and enhancing long-term in vivo stability.

### 3.3.2 Gait cycle as physiological load case

The gait cycle represents one of the most fundamental forms of human movement and serves as the primary loading condition during the healing period of lower extremity fractures. Gait analysis is widely used across disciplines - not only in clinical diagnostics but also in fields such as sports science - to evaluate walking mechanics and extract meaningful gait parameters. These analyses provide insight into the forces and moments acting on the body throughout the gait cycle.

The gait cycle is captured using a motion analysis system that records the positions and angles of individual body segments. To estimate joint reaction forces, the kinematic data are processed using musculoskeletal modeling and simulation software [42]. The Julius Wolff Institute at Charité – Universitätsmedizin Berlin provides a comprehensive database of joint reaction forces and moments [43].These data were collected from patients performing controlled movement tasks during laboratory studies under standardized conditions.

Figure 10 A illustrates the characteristic double-peak pattern of the knee joint reaction force calculated using motion capturing and musculoskeletal modeling and simulation software [44]. As reported in the literature, the knee joint force typically reaches approximately three times the body weight [45]. Figure 10 A shows an axial knee joint force of three times bodyweight. In contrast, the remaining force components are significantly smaller in magnitude. The acting forces concerning anatomical axes are shown in Figure 10 B.

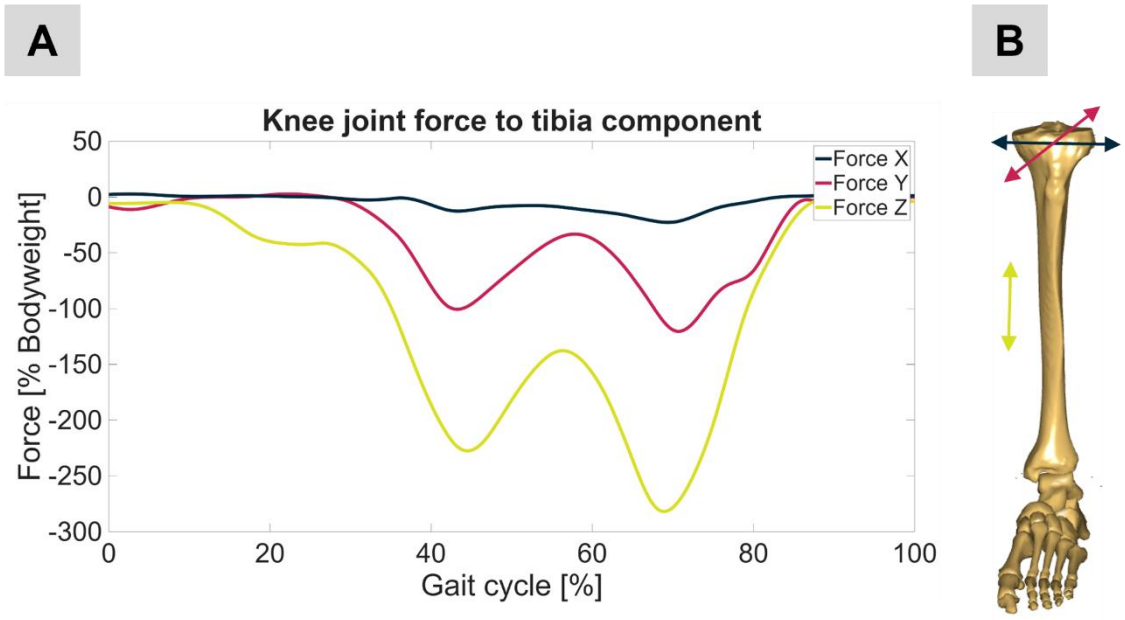


*Figure 10: A: Calculated knee joint force from motion capturing using musculoskeletal modeling and simulation software divided into anatomical axes to tibia component, B: Anatomical axes for tibial bone. Skeletal bone was modeled with Anybody™ (AnyBody™ Technology A/S Aalborg, Denmark).*

During activities such as walking, forces generated through flexion and extension of the lower limb are transmitted to the major load-bearing bones, particularly the tibia and femur. Since bone adapts to mechanical loading, walking plays a critical role in the healing process [46]. It also offers a representative loading scenario that closely mirrors the mechanical demands experienced during everyday postoperative recovery.

The gait cycle describes the time between two contacts of the same foot with the ground [47]. It is divided into two primary phases: the stance phase, which accounts for approximately 60 % of the cycle, and the swing phase, which makes up the remaining 40 % [48]. Figure 11 illustrates the gait cycle with its two main phases. The cycle begins at the moment of initial ground contact (0 %), a reference point used to assess normal gait patterns. In typical gait, the heel strikes the ground first. The cycle concludes when the same foot contacts the ground again, marking 100 % of the gait cycle. During this time, the opposite leg follows the same sequence, offset by half a cycle. It is particularly evident during the motion of the reference leg that the direction of the body vector changes throughout the gait cycle [47]. In summary, the body's center of mass shifts continuously, resulting in complex, multidirectional forces acting on the musculoskeletal system [49]. As a result, purely axial loading does not adequately capture the physiological loading conditions experienced during walking.

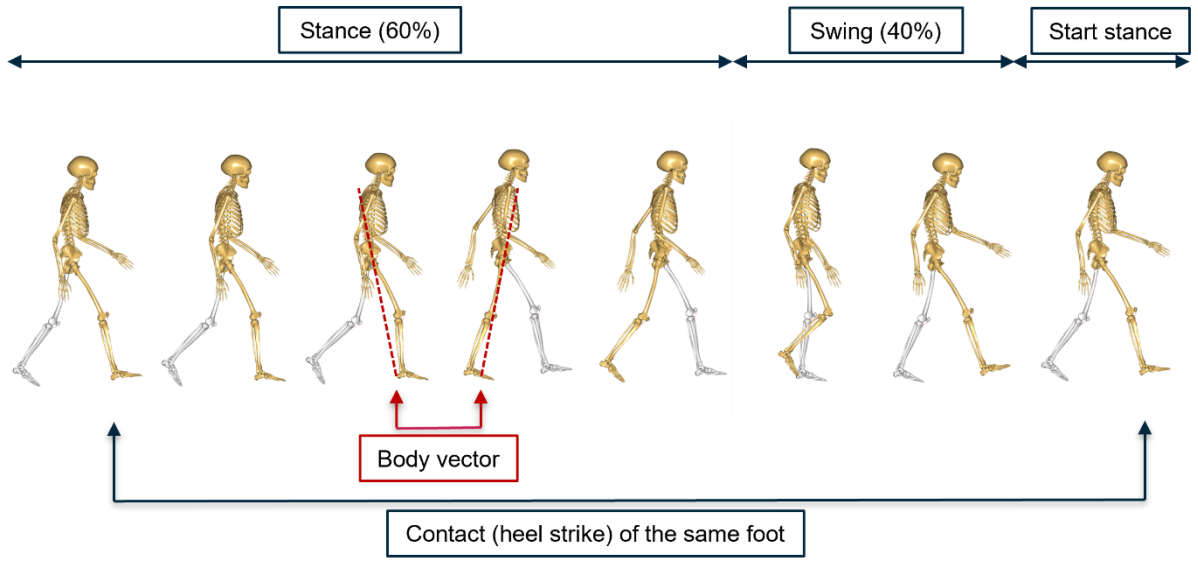


*Figure 11: Gait cycle as time between two contacts of the same foot with the ground (reference = yellow-colored leg). The other leg (transparent) follows in the same sequence, but is shifted by half a cycle. The change in direction of the body vector on the reference leg is also shown, thus illustrating the continuous mass shift during the forward movement. Skeletal bones were modeled with Anybody™ (AnyBody™ Technology A/S Aalborg, Denmark).*

### 3.3.3 Component Bone

The mechanical characterization of bone tissue is a fundamental aspect of biomechanical research. Numerous studies in the literature have investigated the material properties of bone in detail, typically distinguishing between cortical and trabecular bone due to their distinct structural and mechanical characteristics [50], [51], [52]. Key metrics such as bone density and elastic modulus are commonly used to assess bone strength and structural integrity.

The anisotropic nature of bone plays a crucial role in its mechanical behavior. In this context, anisotropy refers to the macroscopic behavior of bone, where mechanical properties depend on the direction of loading. For instance, the elastic modulus of the diaphysis in long bones ranges from approximately 17 GPa in the longitudinal direction to about 12 GPa in the transverse direction [53]. Moreover, structural differences between cortical and cancellous

bone lead to further variations in stiffness. In trabecular bone, the elastic modulus can range from 0.1 to 4.5 GPa, depending on bone density and the orientation of the trabeculae [54].

Preparing bone specimens for mechanical testing often involves the use of cadaveric material, either human or animal, and requires significant technical and logistical coordination. To perform standardized tests, samples must be machined into precise geometries, commonly cubes, cylinders, or tensile specimens, to ensure consistency across experiments [17], [52], [55]. This process demands meticulous handling and specialized equipment designed for working with biological tissue, which must be kept separate from other testing systems to maintain hygiene and avoid cross-contamination.

The preservation technique used for cadaveric specimens plays a crucial role in maintaining the integrity of biomechanical test results. In practice, samples are typically either frozen or chemically fixed using solutions such as formalin, saline solutions, or nitrite-based curing solutions [22], [56], [57]. Studies have shown that preservation technique can significantly influence the mechanical properties of bone, with effects varying by species [50], [51]. For instance, formalin fixation has been reported to cause substantial changes in the mechanical behavior of human bone, whereas bovine bone appears relatively unaffected [51]. During testing, maintaining tissue hydration is also essential. Specimens are carefully moistened throughout the experiment to prevent drying, which can alter material properties and compromise the integrity of the results.

Handling cadaveric specimens requires not only technical care but also an ethically grounded and respectful approach. Beyond logistical challenges such as storage and transport, strict adherence to safety regulations is essential to protect personnel and maintain proper lab protocols.

As research on bone-implant systems evolves, there is growing recognition of the importance of a holistic perspective. While studies on isolated bone samples offer valuable mechanical insights, they fall short of capturing the complex, dynamic interaction between bone, implant, and physiological loading. Animal models have helped bridge this gap, but differences in anatomy and function limit their direct applicability to human clinical scenarios.

Given these limitations, it is essential to critically evaluate each study's design and consider its relevance and translational value within a clinical context.

# 4. Application Biomechanical Study Design

Building on the previously discussed requirements for biomechanical study design and the current understanding of mechanical factors relevant to bone healing, the following section introduces the experimental setups developed for this work. These designs were selected not only based on methodological criteria - such as validity, reproducibility, and clinical relevance - but also with close attention to key biomechanical and biological relationships described in the fracture healing literature. In particular, the relationship between IFM, implant stability, and the applied loading scenario - factors that are essential to the biomechanical understanding of bone-implant systems. A growing body of evidence shows that healing outcomes are influenced not only by implant design, but also by the direction and magnitude of the mechanical loads applied during the healing process.

The objective of the studies presented in this work is to systematically investigate key biomechanical factors and assess their significance in the interaction between bone and implant. Particular emphasis is placed on measuring implant strain and IFM under defined loading conditions. The following studies form the experimental foundation for the publications included in this work.

## 4.1 In Vitro Study

The in vitro studies focus on the investigation of bone-implant systems composed of human cadaveric bones with induced fractures and corresponding treatments. Subsequent testing involves applying anatomically oriented and subject-specific loading scenarios to simulate physiologically relevant conditions.

Experimental evaluation is performed using digital image correlation (DIC), a non-contact optical measurement technique that enables full-field measurement of displacements, strains, and deformations on the surface of a specimen [58]. In this case, an artificial speckle pattern is applied to the specimen surface to facilitate tracking. By utilizing a multi-camera system, 3D measurements can be obtained, providing full-field data with depth information. To calibrate the system, a checkerboard-patterned calibration plate is positioned within the field of view of all cameras. Each camera captures images of the plate, and the calibration points are automatically detected in each image. These image coordinates are then used to calculate the extrinsic parameters, the spatial position and orientation, of each camera relative to the setup (see Figure 12 A). The resulting parameters are stored in a calibration file, which is later used during 3D data processing and analysis. The cameras capture a series of images throughout the loading process.

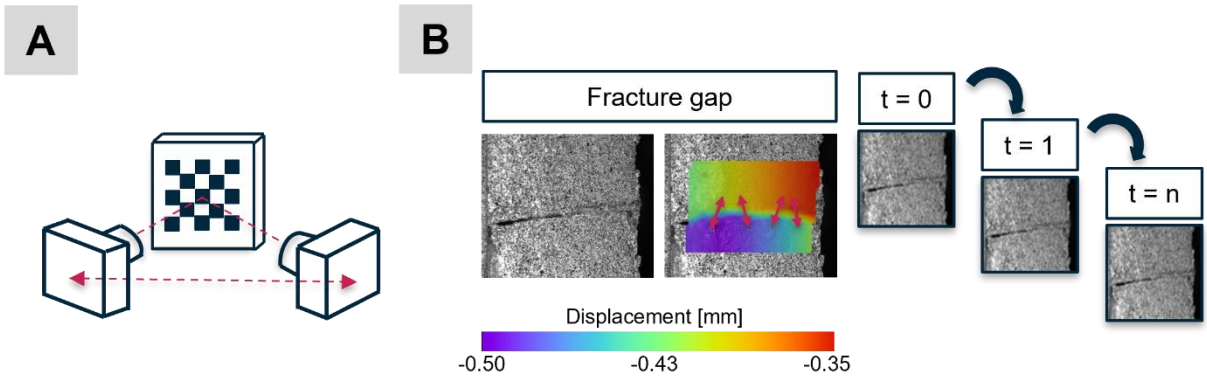


*Figure 12: A: Calibration process using multiple cameras, B: Principle of pattern recognition shown on fracture gap displacements during maximal force application.*

Image analysis is based on the principle of pattern recognition, specifically the correlation of speckle patterns across image frames. The initial image of the undeformed specimen serves as a reference, and subsequent frames are compared to this baseline to determine local shape changes and displacements. By tracking the evolution of the speckle pattern, the surface contour can be reconstructed, and displacement fields calculated (see Figure 12 B). Accordingly, surface strain can be determined by combining information on shape and displacement [59].

In the present studies the 3D-DIC software ISTRA4D™ (Dantec Dynamics, Skovlunde, Denmark) is applied for camera control, image acquisition and evaluation.

Strain gauges: In addition to, or as an alternative to other measurement methods, strain gauges can be used to assess deformation. The location of the gauge determines the specific region of strain measurement and provides localized insight into mechanical behavior.

The AO Foundation has developed a device known as the AO Fracture Monitor, designed to enable real-time, in vivo monitoring of fracture healing [60]. Measurement data are transmitted via Bluetooth to a smartphone and subsequently uploaded to a secure cloud-based platform for storage and further analysis (see Figure 13 A). The sensor is embedded within a compact housing that is affixed to the osteosynthesis plate, positioned directly above the fracture gap (see Figure 13 B). This approach enables continuous monitoring of the healing process close to the fracture gap. Additionally, real-time data recording allows for personalized recommendations, helping to actively support and improve patient recovery. Figure 13 C shows the sensor signal during a gait cycle measuring the relative change in strain.

The AO Fracture Monitor has been used in vitro in parts of the experimental work of the present studies to define the correlation between surface strain of the implant and IFM (Paper 2).

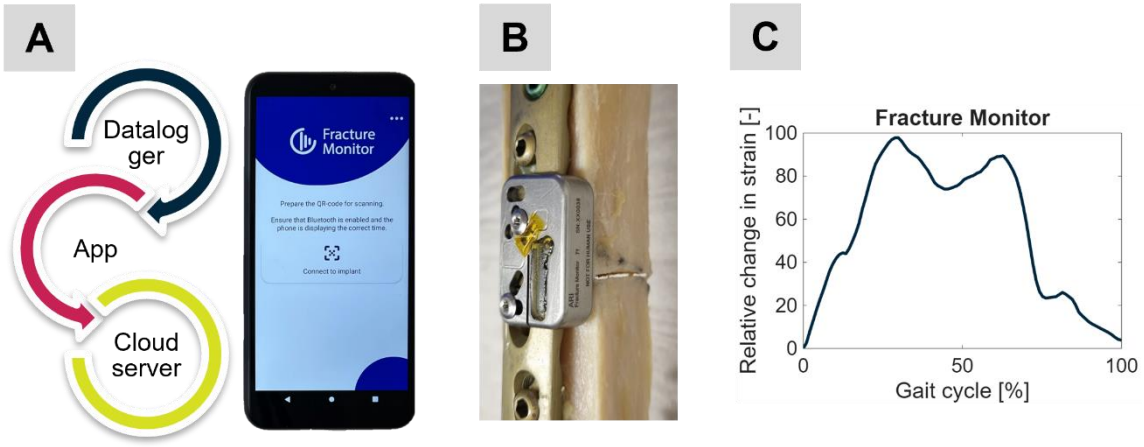


*Figure 13: A: The AO Fracture Monitor system consists of a datalogger, an app on a smart phone for data collection and a cloud server for data storage, B: AO Fracture Monitor mounted on a plate osteosynthesis above the fracture gap, C: Fracture Monitor signal measuring relative change in strain during a gait cycle.*

Following workflow was developed specifically for this study and has proven effective in addressing the research objectives:

1. Preprocess:
   a. Specimen preparation: Cadaveric specimens from body donations were preserved using a nitrite pickling salt solution method following the protocol established by Weigner [61]. Following dissection, the bone was isolated and thoroughly cleaned of residual soft tissue (see Figure 14 A). A fracture consistent with the AO classification system was then induced, followed by fixation using a plate osteosynthesis (see Figure 14 B).

   b. CT scanning of the bone-implant system: To support FE modelling and establish a density-modulus relationship, the treated bone was scanned with a CT scanner (Somatom Definition AS64, Siemens Healthineers, Erlangen, Germany), including a six-rod bone density calibration phantom (QRM-BDC/6, QRM GmbH Moehrendorf, Germany) (see Figure 14 C).

   c. Pre-test setup and calibration: Prior to testing, a black-and-white speckle pattern is applied to the bone and implant surface to facilitate DIC (see Figure 14 D). The bone-implant system is then mounted in a custom-built testing device. A specialized clamping system is used to securely hold the specimen in place, conforming to the complex contours of the epiphyseal regions. When using a multi-camera DIC setup, system calibration is required. This process defines the stereoscopic configuration and generates a calibration file necessary for subsequent 3D analysis.

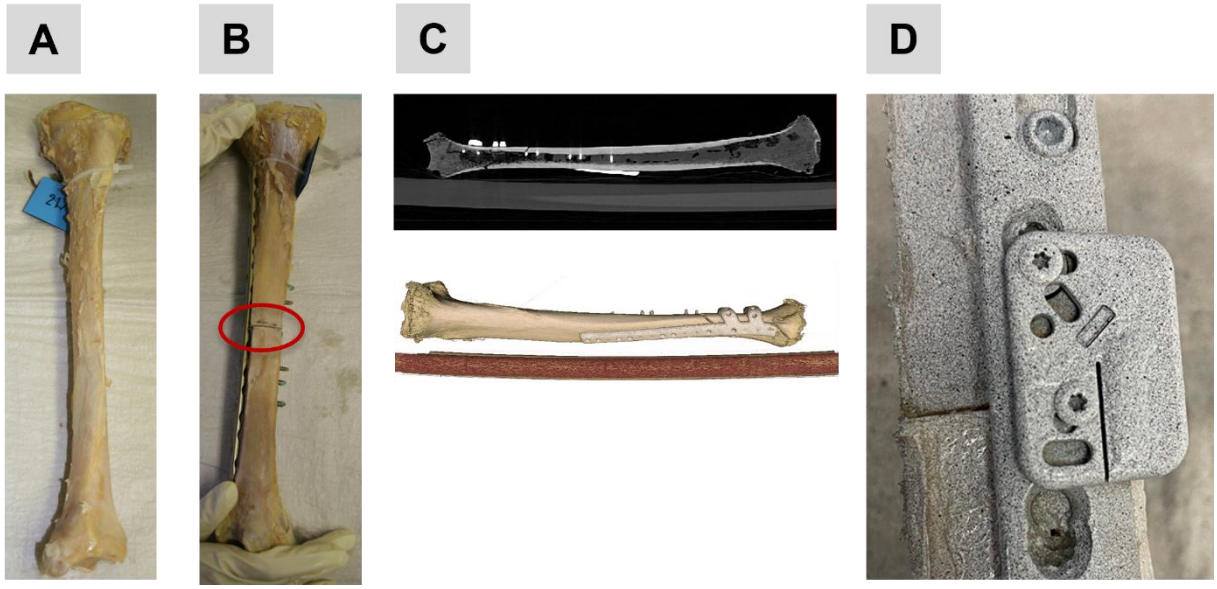


*Figure 14: A: Human tibia from body donation, B: Fractured and treated human tibia, C: CT-scan including bone density calibration phantom and 3D representation derived from CT scan, D: Speckled specimen with mounted AO Fracture Monitor on a plate osteosynthesis.*

2. Mechanical testing:
   The experiment is conducted on a custom-designed and built testing device. A special clamping design was used to match the bone's shape perfectly (see Figure 15 A). The system enables the application of direction-specific forces along all three translational axes. This allows a realistic replication of physiological loading conditions, such as those encountered during gait. Forces applied according to the anatomical axes (see Figure 15 C). Additionally, a camera system (see Figure 15 B) is directed at the region of interest (see Figure 16 A) and continuously records pattern changes during the experiment. Explanation of the testing device in detail see Paper 1. Figure 15 D shows the alignment of the tibia with anatomical axis during the experimental work.

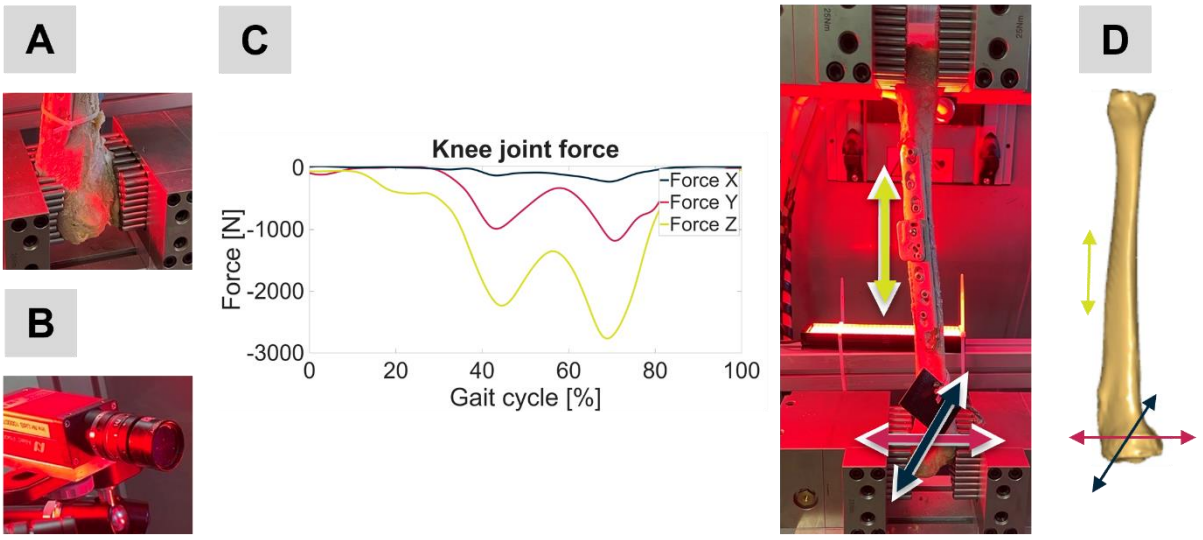


*Figure 15: A: Clamped specimen in mold clamping system, B: Cameras investigating mechanical testing, C: Knee joint force with respect to anatomical axes showing on clamped specimen inserted into the testing device, D: Alignment with anatomical axis of the tibia during the experiment. Skeletal bone was modeled with Anybody™ (AnyBody™ Technology A/S Aalborg, Denmark).*

3. Postprocess:
   DIC measurements were processed to evaluate implant stability (strain on implant surface) and quantify IFM, providing insight into the mechanical behavior of the fixation construct under simulated physiological loading. The data were analyzed using ISTRA 4D™ software (Dantec Dynamics, Skovlunde, Denmark) (see Figure 16 B).

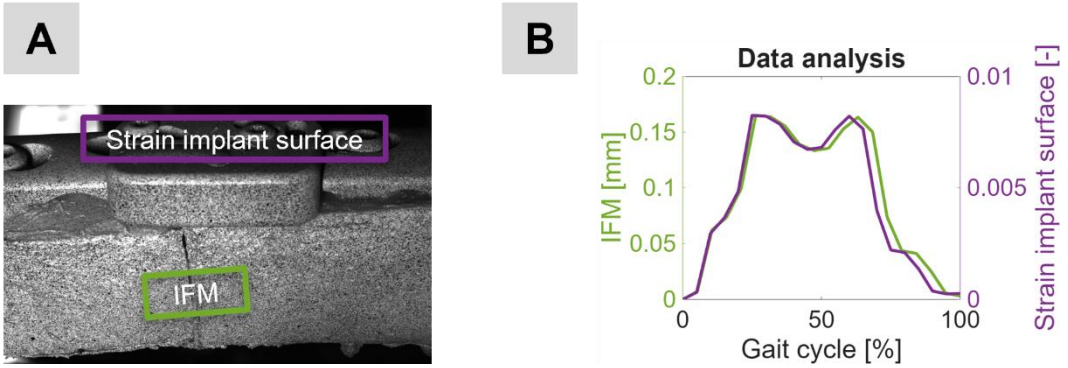


*Figure 16: A: Region of interest (strain of the implant surface, interfragmentary movement (IFM)), B: Data analysis according to the region of interests (strain of the implant surface, interfragmentary movement (IFM)).*

## 4.2 In Silico Study

Bone is commonly modeled as a linear elastic and anisotropic material under physiological loading conditions [62]. The assumption of linear elasticity is valid for small strains typically observed during everyday activities such as walking.

The segmented CT data of the bone serve as the basis for generating the geometric model. By incorporating a bone density calibration phantom during scanning, a subject-specific density-modulus relationship can be established (see Figure 17). To account for the inhomogeneity nature of bone, 25 material classes are defined, allowing each element to be assigned an appropriate elastic modulus based on its grayscale value [63] (see chapter 2.2 Geometry and Mechanical Properties of Bone). This approach ensures an anatomically accurate and subject-specific representation of both; bone geometry and density.

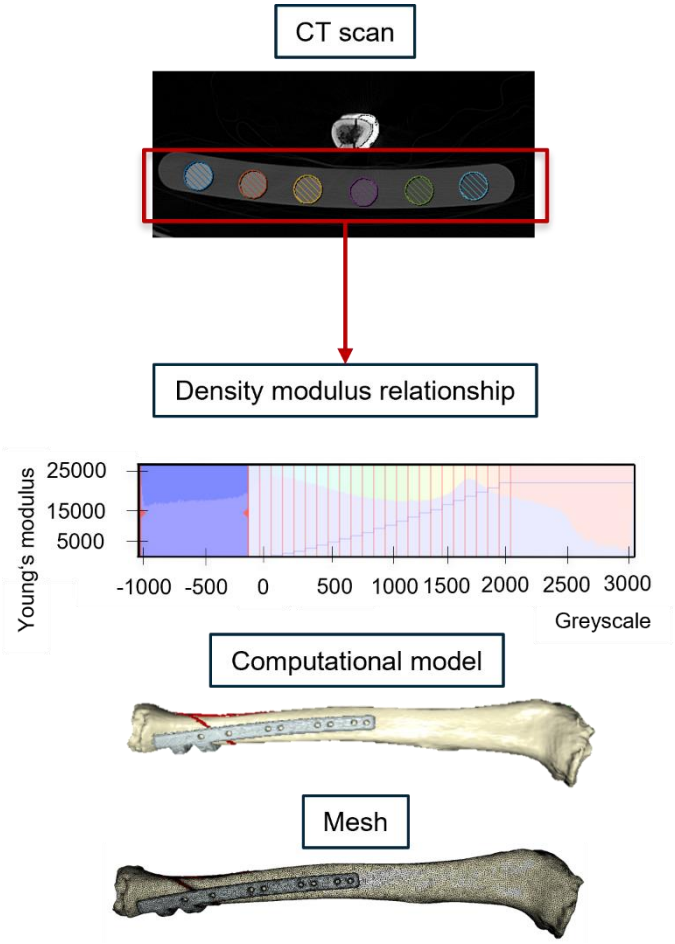


*Figure 17: Creating computational model from CT scan including subject-specific material properties calculated with the help of a bone density calibration phantom.*

Material properties for the implant [64] and fracture [65] were chosen as homogenous parameters from literature. To apply physiologically realistic boundary conditions and loading - comparable to those used in experimental testing - nodes in the epiphyseal regions are grouped into node sets.

Finally, the model is meshed using quadratic tetrahedral finite elements. Linear elastic assumptions were applied throughout the simulation. Geometry processing and material assignment are carried out using Simpleware™ (Synopsys, Mountain View, CA, USA).

The FE simulations were done in Abaqus™ (Dassault Systemes, Velizy-Villacoublay, France). Before applying the joint forces and loads, the meshed bone model was aligned so that the

coordinate axes of the simulation corresponded to the anatomical axes from the experiment. This ensured that all load vectors were applied in the correct anatomical directions. The alignment of the bone is analogous to the experiment (see Figure 15 D). To replicate physiological loading conditions from the experiment, a force function is implemented within the simulation. Joint forces are applied according to their anatomical direction using force tables that divide the loading scenario into discrete steps (see Figure 18 B). Using the example of an tibial fracture, the x and y force components were applied on the knee side (proximal epiphysis) and the z direction was fixed. According to the experiment, the z-force component was applied to the distal epiphysis and the x- and y- components were blocked (see Figure 18 A). This approach enables systematic iteration through a complete loading curve that represents an entire gait cycle. By modeling the loading conditions in this manner, the simulation provides a physiologically realistic representation of mechanical behavior, allowing for detailed analysis of IFM and implant loading.

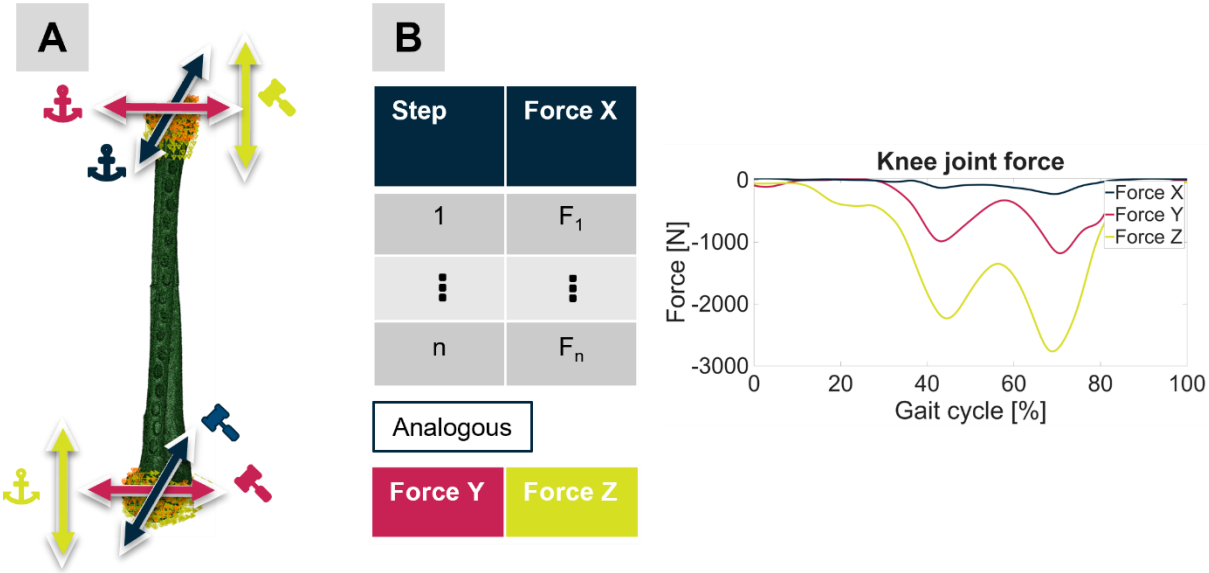


*Figure 18: A: Force application to the node sets at the proximal epiphysis (z-component is fixed, force application to x- and y component) and at distal epiphysis (x-and y-component are fixed, force application to z component). The alignment of the bone is analogous to the experiment (see Figure 15 D), B: Force curves are divided into discrete steps according to anatomical axes (blue = x-component, pink = y-component, yellow = z-component).*

Postprocessing analysis includes investigating the implant's behavior and the IFM. In order to validate the simulation results, the corresponding areas of interest were selected according to the experiment.

By applying the load incrementally, the stress distribution within the implant and its effects on the fracture gap can be evaluated at every point throughout the gait cycle. Figure 19 A illustrates the analysis at the peak load during gait, showing both the stress distribution in the implant and the corresponding healing window within the fracture gap.

Analyzing the IFM, points of the FE mesh were selected and their coordinates and displacements were determined. Upcoming strains were calculated from these data.

To interpret the results, the fracture region is visualized using the healing window. Individual elements within the fracture zone are color-coded based on their local strain levels. Red areas indicate too much movement, while yellow regions suggest strain values that are maybe too much movement, both of which inhibit bone formation.

Similarly, light blue areas represent insufficient movement, and dark blue indicates a complete lack of mechanical stimulation (no movement). Only elements within the green range fall inside the “perfect healing window,” where mechanical conditions are optimal for bone regeneration (Paper 2).

To validate the virtual analysis a correlation between experiment and simulation results were proven, concerning the applied knee joint force to the strain across the fracture (see Figure 19 B).

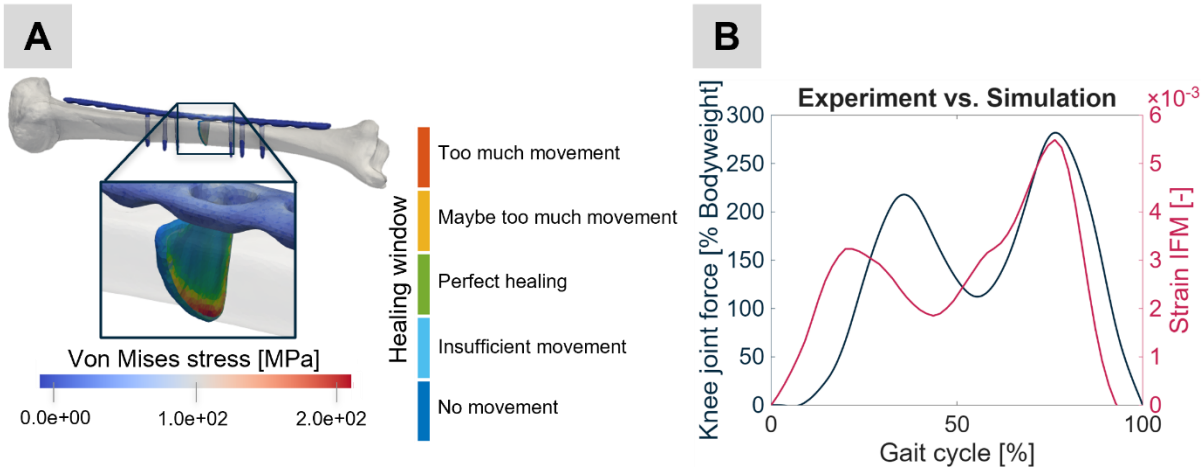


*Figure 19: A: Data analysis showing implant stress distribution with fracture behavior using the healing-window classification for the maximum force peak during gait, B: Validation showing correlation between the measured knee joint force from the experiment and the computational data, concerning the applied knee joint force to the strain across the fracture gap (interfragmentary movement (IFM)).*

# 5. Discussion

The papers presented in this work aimed to investigate the mechanical behavior of bone-implant systems under clinically relevant loading conditions. A standardized experimental (Paper 1) and computational workflow was established to evaluate biomechanical parameters critical to fracture healing, particularly implant stability and IFM.

This workflow was subsequently applied to explore potential correlations between these parameters. A strong relationship was observed between implant surface strain and IFM in in vitro experiments. Moreover, the studies demonstrated that IFM can be predicted from uniaxial strain measurements obtained via the AO Fracture Monitor. These findings were further validated through in silico simulations, confirming the validity of the correlations across both experimental and computational domains (Paper 2).

In further investigations, the performance of a novel implant concept, the biphasic plate, was evaluated. The analysis combined in vitro, in silico, and in vivo methods to assess the mechanical behavior of the bone-implant system under physiological loading. Experimental data were used to validate the computational models, which were then applied to patient-specific scenarios, highlighting the translational relevance of the approach (Paper 3).

The final paper focused on the impact of model complexity on computational outcomes (Paper 4). As discussed in the preceding chapters, the predictive accuracy of in silico models is highly dependent on input parameters. This study systematically examined how varying levels of model detail affect mechanical predictions, emphasizing the importance of careful model definition, parameter selection, and validation to ensure meaningful simulation results.

Translating biomechanical insights into clinical practice is essential for realizing the full potential of experimental and computational research. Mechanical parameters can only contribute meaningfully to patient outcomes if they are effectively integrated into real-world treatment scenarios. Moreover, biomechanical models offer the opportunity to link multiple simulation frameworks, enabling the development of more comprehensive and dynamic representations of physiological processes.

This chapter examines various approaches for translating biomechanical research into clinical practice and related application areas. The content is organized along the continuum of the clinical care process: beginning with the preoperative phase, which includes preoperative simulations and treatment comparisons and the postoperative phase, which addresses healing assessment and revision risk prediction.

## 5.1 Preoperative Phase

In the early phase of surgical planning, biomechanical models can be used to support the targeted preparation of operative procedures. The generation of 3D representations of the fracture site enables clinicians to visualize the pathology prior to surgery and systematically evaluate different treatment options.

Physical 3D-printed models provide a hands-on approach to surgical planning and contribute to more effective preoperative simulations. Studies have shown that the use of such models can significantly reduce operative time, blood loss, and the number of intraoperative fluoroscopic images required [66].

Additionally, implant and screw positions can be assessed preoperatively to evaluate their influence on the mechanical stability of the osteosynthesis [67]. These simulations play a

critical role in identifying potential risks, such as screw placement or regions of elevated stress, thereby enabling more precise and patient-specific surgical planning.

Advanced models featuring interactive visualizations are already being used in procedures such as knee surgery. By incorporating motion data, these models enhance the understanding of biomechanical behavior during joint loading [68].

For medical trainees in particular, such models provide significant educational value. Based on patient-specific motion and imaging data, virtual reality-based training systems have been developed to simulate surgical procedures in a realistic environment. However, in the field of orthopedics, such simulation tools are still limited in availability [69], with the knee joint, especially in the context of arthroscopy, being the most extensively studied application to date [70].

The integration of patient-specific data enables individualized preoperative planning that accounts for anatomical variation and supports the selection of a tailored surgical strategy. Moreover, in patients with specific conditions, such as metastatic bone disease, biomechanical simulations can be used to predict fracture risk and identify likely fracture locations [71].

## 5.2 Postoperative Phase

In the postoperative phase, a range of methods is available to support and monitor the healing process. Technologies such as motion capture systems and sensor-equipped insoles enable load-based simulations that can provide valuable insights into patient-specific recovery. These tools allow for the early identification of implant failure or the risk of nonunion, potentially preventing complications before they occur [72].

Combining insights from in vitro and in silico studies with continuous patient monitoring opens new avenues for developing advanced therapeutic strategies [73]. This integrative approach also supports the formulation of personalized recommendations tailored to an individual's healing trajectory [42]. These recommendations can take supportive and precautionary forms, encouraging beneficial behaviors. Possible statements could then be as follows: "Gradual weight-bearing from week three promotes bone healing," or warning against high-risk actions like "Early full weight-bearing increases the risk of nonunion by 25 %."

Beyond individualized predictions, FE simulations also offer broader clinical insights. For instance, recent findings indicate that stabilization of fibular fractures is recommended when an associated tibial fracture is present at the same level [74].

## 5.3 Further Biomechanical Applications

Beyond direct clinical translation, experimental and computational methods offer substantial potential for broader applications in research and development. A key area of use is in the design and optimization of novel orthopedic implants. In the early stages of development, simulations can be used to evaluate a wide range of geometries and materials - long before investing in expensive prototypes or launching preclinical studies.

For example, consider the development of a next-generation plate osteosynthesis system made from a semi-rigid material. This design aims to address limitations of traditional plates by reducing stress shielding and lowering the risk of delayed healing. By exploring such concepts through simulation, researchers can gain critical insights into implant performance early in the design process [75].

Modular modeling approaches allow for the flexible replacement of individual components - such as implants, screws, fracture types, and stages of healing - to analyze a range of treatment strategies.

The insights gained from these simulations are essential for the design of next-generation smart implants, which are expected to incorporate sensor and actuator technologies to actively support the healing process. In silico and in vitro studies play a central role in identifying the key parameters required for such systems [76]. They also help define important thresholds, e.g. the displacement needed to generate a mechanical stimulus capable of promoting bone regeneration [77].

Expanding biomechanical models beyond the bone-implant system - by incorporating soft tissue structures or muscle activity - offers the potential for more physiologically accurate representations of complex mechanical interactions within the musculoskeletal system. To enable the flexible integration of such models, standardized frameworks for data exchange are essential. Given that many models are based on patient-specific imaging data, it is first necessary to clarify whether sharing these datasets is feasible from a technical and data privacy standpoint. Furthermore, the appropriate format and level of detail required for model exchange must be defined.

Different types of models can be categorized based on their intended application but generally include core components such as geometry, FE meshes, material properties, and precomputed field variables such as displacement, stress, or strain.

To extend these models, appropriate loading scenarios must be defined and solved using high-performance computing platforms (e.g., Abaqus™). This approach allows individual models to be expanded and integrated, enabling the simulation of more comprehensive and complex biomechanical systems [78].

These examples underscore the importance of validating in silico results against existing literature or experimental data. Robust validation is essential to ensure that the findings are not only theoretically sound but also applicable in practice. This is especially relevant in translational contexts, where biomechanical models inform clinical decision-making, therapeutic planning, or the design of osteosynthesis systems.

The broad range of potential applications highlights reinforces the fact that the credibility of simulation-based approaches depends directly on their transparency and validity. Aligning simulations with experimental or clinical data is not only a means of quality control. It is essential for building trust in biomechanically informed models as a complementary tool in orthopedic and trauma care.

# 6. Limitation and Outlook

The preceding chapters established the foundational knowledge required to contextualize the individual studies presented in this work. Following an overview of fundamental biomechanical principles - including anatomical terminology, bone geometry and structure, fracture classifications, and treatment modalities - the mechanical aspects of fracture healing were examined in detail. Particular emphasis was placed on two key parameters: implant stability and IFM. Both are critical to the mechanical environment influencing bone regeneration.

The chapter on biomechanical study design addressed important criteria for conducting robust investigations. These include the definition of appropriate and quantifiable outcome measures, as well as the reliability, validity, and clinical relevance of the chosen methodology.

In addition, the specific requirements for computational modeling of medical devices were outlined, encompassing aspects such as model generation, constitutive laws, boundary conditions, and validation strategies.

Methodological considerations also included a comparison of experimental approaches (in vivo, in vitro, and in silico) highlighting their respective advantages and limitations. Central to all approaches is the definition of physiologically relevant loading conditions, which must reflect the clinical scenario under investigation and align with the study's objectives.

Building on this foundation, the specific study design applied across the included investigations was introduced and justified in the context of the overall research framework.

Despite the realistic representation of biomechanical conditions, this study is subject to methodological and system-related limitations that must be considered when interpreting the results.

One notable limitation of the presented studies concerns the relatively small size of the study populations. This aspect becomes particularly relevant when investigating individualized scenarios, where patient-specific geometries, loading conditions, or implant configurations can strongly influence the biomechanical outcome. As a result, it becomes challenging to derive broadly generalizable conclusions from single-case or low-sample-size analyses. Nevertheless, when multiple datasets are available - especially for similar fracture types or comparable clinical configurations - it is possible to identify consistent patterns or trends. These recurring findings may not allow for definitive generalization but provide valuable insights into typical biomechanical behaviors and can guide further hypothesis-driven research or clinical decision-making.

Moreover, such experimentally observed trends can be further substantiated through in silico studies, which allow for the systematic evaluation of larger virtual cohorts. By varying input parameters across a wider range of conditions, computational-based studies offer the opportunity to assess the validity of observed effects and to explore their sensitivity under controlled physiologically relevant scenarios.

In summary, cadaveric in vitro models remain one of the most realistic approaches for investigating the mechanical behavior of bone-implant systems. They allow for controlled, reproducible testing under conditions that closely approximate the anatomical reality. In the present studies, the absence of soft tissue enabled the application of digital image correlation techniques; however, it also led to limitations in structural stability that soft tissues would otherwise provide.

These models are well suited for focused mechanical investigations. They can be used to simulate specific healing trajectories by applying scaffolds with varying material properties. However, they inherently lack biological components. Critical factors like soft tissue interactions, dynamic muscle activity, and the physiological progression of healing are not represented, limiting the extent to which these models can replicate in vivo conditions. As a result, findings from in vitro studies must be interpreted with caution, particularly when used to validate computational models that incorporate biologically active elements.

Additional limitations stem from the boundary conditions used in this study. Applied loads - such as knee joint forces - were derived from motion capture data and scaled to match the body weight of the body donor. While this approach provides physiologically relevant loading conditions, the resulting loads are still approximations and may not fully reflect the individual biomechanics of each donor.

Small variations may also result from the clamping process. The irregular geometry of human bone presents greater challenges compared to standardized industrial samples. To address this, custom clamping blocks composed of multiple adjustable pins were used to conform as closely as possible to the bone's surface. Even so, proper bone alignment is critical to ensure that force components are applied along the correct anatomical axes.

When using long plate osteosynthesis constructs, care must be taken to prevent direct contact between the implant and the loading fixtures. Such contact can introduce artifacts and lead to inaccuracies in stiffness measurements.

Nevertheless, meaningful insights into key biomechanical parameters can be gained through this workflow, provided that the research question is clearly defined.

To date, experimental investigations of bone-implant systems have been limited to load applications along the three anatomical axes. As a result, the current three-axes test setup restricts the evaluation to normal and shear forces.

A next-generation testing device is currently in development and will enable motion along six degrees of freedom (three translational and three rotational axes). This advancement will allow for more comprehensive analyses based on complex loading conditions derived from motion capture data. With six independently actuated axes, it will be possible to expand beyond previous load scenarios to include the effects of torsional and bending moments on bone-implant systems.

The addition of three rotational axes enables the experimental investigation of upper limb motion patterns. While fracture healing in the lower extremity is often assessed using gait analysis, the progression of healing in upper extremity fractures is more closely linked to specific joint movements.

In the case of radius fractures, extension and flexion or pronation and supination are commonly cited as key functional motions. Supination refers to the outward rotation of the forearm, turning the thumb laterally, whereas pronation describes the opposite motion, in which the thumb rotates medially.

These kinematic patterns play a critical role during the healing phases of radius fractures. As such, biomechanical simulations should aim to replicate these motions accurately and be validated through experimental studies wherever possible.

# 7. Conclusion

In conclusion, a clearly defined research question combined with physiologically relevant loading conditions enables realistic experimental investigations and meaningful simulation of bone-implant systems. The integrated use of in vivo, in vitro, and in silico approaches allows for the formulation of validated and transferable findings. This interdisciplinary framework not only strengthens the scientific rigor of biomechanical studies but also facilitates the translation of insights across study types. Ultimately, such an approach holds the potential to contribute to more informed treatment strategies and to support long-term improvements in patient outcomes.

# Ethical Statement

The body donations in the studies came either from Science Care or from Saarland University. Regarding body donations from Science Care, all matters related to body donation are fully managed by Science Care itself. The institute of Forensic Medicine, Saarland University Hospital, received and stored the samples and performed after the experiments the on-site cremation.

Regarding human specimens from body donations from Saarland University, written informed consent for participation was not required from the participants or the participants' legal guardians/ next of kin in accordance with the national legislation and institutional requirements.

The ethics committee of Saarland Medical Board has approved the studies using human cadaveric specimens (Aerztekammer des Saarlandes, Germany, application number 146/21 and Aerztekammer des Saarlandes, Germany, application number 195/24).

All studies were conducted in accordance with the local legislation and institutional requirements.

The patients/participants provided their written informed consent to participate in this study. Written informed consent was obtained from the individual(s) for the publication of any potentially identifiable images or data included in this article. The study was conducted under the Declaration of Helsinki and approved by the Ethics Committees of the University of Tuebingen (Protocol codes 317/2022BO2). Informed consent was obtained from all subjects involved in the study.

# 8. References


[1] M. Rupp, C. Biehl, F. Budak, T. Ehlert, and A. Heppner, ‘Originalarbeit: Inzidenz von Frakturen in der Erwachsenenpopulation in Deutschland’, Dtsch Arztebl Int, vol. 118, no. 40, pp. 665–669, 2021, doi: 10.3238/arztebl.m2021.0238.

[2] T. A. Einhorn and L. C. Gerstenfeld, ‘Fracture healing: Mechanisms and interventions’, *Nat Rev Rheumatol*, vol. 11, pp. 45–54, 2015, doi: 10.1038/nrrheum.2014.164.

[3] K. Reiland, B. Haastert, W. Arend, et al., ‘Epidemiology of distal radius fractures in Germany – incidence rates and trends based on inpatient and outpatient data’, *Osteoporos Int*, vol. 35, pp. 317–326, 2024, doi: 10.1007/s00198-023-06904-6.

[4] C. M. Court-Brown, S. Rimmer, U. Prakash, and M. M. McQueen, ‘The epidemiology of open long bone fractures’, *Injury*, vol. 29, no. 7, pp. 529–534, 1998, doi: 10.1016/S0020-1383(98)00125-9.

[5] Statistisches Bundesamt, ‘Diagnosedaten der Krankenhäuser ab 2000 (Fälle, Sterbefälle, Berechnungs- und Belegungstage, durchschnittliche Verweildauer). Gliederungsmerkmale: Jahre, Behandlungsort, Alter, Geschlecht, Verweildauer, ICD10-3-Steller’, accessed Feb. 20, 2025. [Online]. https://www.gbe-bund.de/gbe/isgbe.information?p_uid=gast&p_aid=89916324&p_sprache=D&p_thema_id=247&p_thema_id2=1&p_thema_id3=&p_thema_id4=.

[6] G. M. Calori, E. Mazza, M. Colombo, C. Ripamonti, and L. Tagliabue, ‘Treatment of long bone non-unions with polytherapy: Indications and clinical results’, *Injury*, vol. 42, no. 6, pp. 587–590, 2011, doi: 10.1016/j.injury.2011.03.046.

[7] N. Walter, K. Hierl, C. Brochhausen, V. Alt, and M. Rupp, ‘The epidemiology and direct healthcare costs of aseptic nonunions in Germany – a descriptive report’, *Bone Joint Res*, vol. 11, no. 8, pp. 541–547, 2022, doi: 10.1302/2046-3758.118.BJR-2021-0238.R3.

[8] P. Andrzejowski and P. V. Giannoudis, ‘The “diamond concept” for long bone non-union management’, *J Orthop Traumatol*, vol. 20, no. 1, p. 21, 2019, doi: 10.1186/s10195-019-0528-0.

[9] C. L. Ekegren, E. R. Edwards, R. de Steiger, and B. J. Gabbe, ‘Incidence, costs and predictors of non-union, delayed union and mal-union following long bone fracture’, *Int J Environ Res Public Health*, vol. 15, no. 12, p. 2845, 2018, doi: 10.3390/ijerph15122845.

[10] M. Rupp, C. Biehl, M. Budak, U. Thormann, C. Heiss, and V. Alt, ‘Diaphyseal long bone nonunions – types, aetiology, economics, and treatment recommendations’, *Int Orthop (SICOT)*, vol. 42, no. 2, pp. 247–258, 2018, doi: 10.1007/s00264-017-3734-5.

[11] J. A. Nicholson, N. Makaram, A. Simpson, and J. F. Keating, ‘Fracture nonunion in long bones: A literature review of risk factors and surgical management’, *Injury*, vol. 52, suppl. 2, pp. S3–S11, 2021, doi: 10.1016/j.injury.2020.11.029.

[12] L. Claes, ‘Mechanobiologie der Frakturheilung Teil 1: Grundlagen [Mechanobiology of fracture healing part 1: Principles]’, *Unfallchirurg*, vol. 120, no. 1, pp. 14–22, 2017, doi: 10.1007/s00113-016-0280-3.

[13] K. Kaspar, H. Schell, P. Seebeck, M. S. Thompson, M. Schütz, N. P. Haas, and G. N. Duda, ‘Angle stable locking reduces interfragmentary movements and promotes healing

after unreamed nailing: Study of a displaced osteotomy model in sheep tibiae', *J Bone Joint Surg Am*, vol. 87, no. 9, pp. 2028–2037, 2005, doi: 10.2106/JBJS.D.02268.

[14] M. Klaus, Der Mofu-Baukasten: *Ein Lehrbuch für das Studium und den Unterricht der motorisch-funktionellen Behandlungsverfahren in der Ergotherapie*, 3rd ed., Dortmund, Germany: Verlag modernes lernen Borgmann GmbH & Co. KG, 2024, ISBN 978-3-8080-0850-8.

[15] B. Clarke, 'Normal bone anatomy and physiology', *Clin J Am Soc Nephrol*, vol. 3, suppl. 3, pp. S131–S139, 2008, doi: 10.2215/CJN.04151206.

[16] I. Guha, X. Zhang, C. S. Rajapakse, G. Chang, and P. K. Saha, 'Finite element analysis of trabecular bone microstructure using CT imaging and continuum mechanical modeling', *Med Phys*, vol. 49, no. 6, pp. 3886–3899, 2022, doi: 10.1002/mp.15629.

[17] J. H. Keyak, I. Y. Lee, and H. B. Skinner, 'Correlations between orthogonal mechanical properties and density of trabecular bone: Use of different densitometric measures', *J Biomed Mater Res*, vol. 28, no. 11, pp. 1329–1336, 1994, doi: 10.1002/jbm.820281111.

[18] N. K. Knowles, J. M. Reeves, and L. M. Ferreira, 'Quantitative computed tomography (QCT) derived bone mineral density (BMD) in finite element studies: A review of the literature', *J Exp Orthop*, vol. 3, no. 1, p. 36, 2016, doi: 10.1186/s40634-016-0072-2.

[19] B. Helgason, E. Perilli, E. Schileo, F. Taddei, S. Brynjólfsson, and M. Viceconti, 'Mathematical relationships between bone density and mechanical properties: A literature review', Clin Biomech (Bristol), vol. 23, no. 2, pp. 135–146, 2008, doi: 10.1016/j.clinbiomech.2007.08.024.

[20] C. M. Les, J. H. Keyak, S. M. Stover, K. T. Taylor, and A. J. Kaneps, 'Estimation of material properties in the equine metacarpus with use of quantitative computed tomography', *J Orthop Res*, vol. 12, no. 6, pp. 822–833, 1994, doi: 10.1002/jor.1100120610.

[21] W. B. Edwards and K. L. Troy, 'Finite element prediction of surface strain and fracture strength at the distal radius', *Med Eng Phys*, vol. 34, no. 3, pp. 290–298, 2012, doi: 10.1016/j.medengphy.2011.07.016.

[22] J. Y. Rho, M. C. Hobatho, and R. B. Ashman, 'Relations of mechanical properties to density and CT numbers in human bone', *Med Eng Phys*, vol. 17, no. 5, pp. 347–355, 1995, doi: 10.1016/1350-4533(95)97314-f.

[23] A. J. Wirth, J. Goldhahn, C. Flaig, P. Arbenz, R. Müller, and G. H. van Lenthe, 'Implant stability is affected by local bone microstructural quality', *Bone*, vol. 49, no. 3, pp. 473–478, 2011, doi: 10.1016/j.bone.2011.05.001.

[24] M. E. Müller, P. Koch, S. Nazarian, and J. Schatzker, 'Tibia/Fibula = 4', in *The Comprehensive Classification of Fractures of Long Bones*, Springer, Berlin, Heidelberg, 1990, doi: 10.1007/978-3-642-61261-9_7.

[25] A. John, R. Nappoly, and V. Daniel, 'Reduction techniques for intramedullary nailing of subtrochanteric femur fractures: A narrative review', *J Orthop Orthop Surg*, vol. 6, no. 3, pp. 12–18, 2025, doi: 10.29245/2767-5130/2025/3.1234.

[26] Y. Förster, C. Rentsch, W. Schneiders, R. Bernhardt, J. C. Simon, H. Worch, and S. Rammelt, 'Surface modification of implants in long bone', *Biomatter*, vol. 2, no. 3, pp. 149–157, 2012, doi: 10.4161/biom.21563.

[27] G. R. Rechter, R. T. Anthony, J. Rennard, J. F. Kellam, and S. J. Warner, ‘The impact of early axial interfragmentary motion on the fracture healing environment: A scoping review’, *Injury*, vol. 55, no. 12, p. 111917, 2024, doi: 10.1016/j.injury.2024.111917.

[28] S. M. Perren, ‘Evolution of the internal fixation of long bone fractures: The scientific basis of biological internal fixation – choosing a new balance between stability and biology’, *J Bone Joint Surg Br*, vol. 84, no. 8, pp. 1093–1110, 2002, doi: 10.1302/0301-620X.84B8.13752.

[29] A. L. Foster, T. F. Moriarty, C. Zalavras, M. Morgenstern, A. Jaiprakash, R. Crawford, M.-A. Burch, W. Boot, K. Tetsworth, T. Miclau, P. Ochsner, M. A. Schuetz, R. G. Richards, and W.-J. Metsemakers, ‘The influence of biomechanical stability on bone healing and fracture-related infection: The legacy of Stephan Perren’, *Injury*, vol. 52, no. 1, pp. 43–52, 2021, doi: 10.1016/j.injury.2020.06.044.

[30] R. Marsell and T. A. Einhorn, ‘The biology of fracture healing’, *Injury*, vol. 42, no. 6, pp. 551–555, 2011, doi: 10.1016/j.injury.2011.03.031.

[31] P. V. Giannoudis, T. A. Einhorn, and D. Marsh, ‘Fracture healing: The diamond concept’, Injury, vol. 38, suppl. 4, pp. S3–S6, 2007, doi: 10.1016/S0020-1383(08)70003-2.

[32] L. Claes, ‘Mechanobiologie der Frakturheilung Teil 2: Bedeutung für die Osteosynthese [Mechanobiology of fracture healing part 2: Relevance for internal fixation of fractures]’, *Unfallchirurg*, vol. 120, pp. 23–31, 2017, doi: 10.1007/s00113-016-0281-2.

[33] P. Augat, M. W. Hast, G. Schemitsch, M. Heyland, A. Trepczynski, E. Borgiani, G. Russow, S. Märdian, G. N. Duda, M. Hollensteiner, M. Bottlang, and E. H. Schemitsch, ‘Biomechanical models: Key considerations in study design’, *OTA Int*, vol. 4, no. 2 (suppl.), p. e099, 2021, doi: 10.1097/OI9.0000000000000099.

[34] U.S. Food and Drug Administration (FDA), *Reporting of Computational Modeling Studies in Medical Device Submissions*, Center for Devices and Radiological Health, Rockville, MD, Rep. FDA-2013-D-1530, Sept. 2016.

[35] J. Wolff, *Das Gesetz der Transformation der Knochen*, Berlin, Germany: Verlag von August Hirschwald, 1892.

[36] M. Miska, S. Findeisen, M. Tanner, B. Biglari, S. Studier-Fischer, P. A. Grützner, G. Schmidmaier, and A. Moghaddam, ‘Treatment of nonunions in fractures of the humeral shaft according to the diamond concept’, *Bone Joint J*, vol. 98-B, no. 1, pp. 81–87, 2016, doi: 10.1302/0301-620X.98B1.35682.

[37] L. E. Claes, C. A. Heigele, C. Neidlinger-Wilke, D. Kaspar, W. Seidl, K. J. Margevicius, and P. Augat, ‘Effects of mechanical factors on the fracture healing process’, *Clin Orthop Relat Res*, no. 355 (suppl.), pp. S132–S147, 1998, doi: 10.1097/00003086-199810001-00015.

[38] D. R. Epari, J. P. Kassi, H. Schell, and G. N. Duda, ‘Timely fracture-healing requires optimization of axial fixation stability’, J Bone Joint Surg Am, vol. 89, no. 7, pp. 1575–1585, 2007, doi: 10.2106/JBJS.F.00247.

[39] ASTM International, *Specification and Test Methods for Metallic Medical Bone Screws*, West Conshohocken, PA: ASTM International, 1977, doi: 10.1520/F0543.

[40] N. Garijo, N. Verdonschot, K. Engelborghs, J. M. García-Aznar, and M. A. Pérez, ‘Subject-specific musculoskeletal loading of the tibia: Computational load estimation’, *J*

*Mech Behav Biomed Mater*, vol. 65, pp. 334–343, 2017, doi: 10.1016/j.jmbbm.2016.08.026.

[41] J. D. Agneskirchner, D. Freiling, C. Hurschler, and P. Lobenhoffer, 'Primary stability of four different implants for opening wedge high tibial osteotomy', *Knee Surg Sports Traumatol Arthrosc*, vol. 14, no. 3, pp. 291–300, 2006, doi: 10.1007/s00167-005-0690-1.

[42] A. Andres, M. Roland, K. Wickert, B. Ganse, T. Pohlemann, M. Orth, and S. Diebels, 'Individual postoperative and preoperative workflow for patients with fractures of the lower extremities', *Clin Biomech (Bristol)*, p. 106503, 2025, doi: 10.1016/j.clinbiomech.2025.106503.

[43] G. Bergmann and P. Damm (eds.), *OrthoLoad*, Julius Wolff Institute, Berlin Institute of Health at Charité – Universitätsmedizin Berlin, 2008. Accessed: Aug. 26, 2025. [Online]. Available: https://orthoload.com/database/]

[44] A. Andres, M. Roland, K. Wickert, S. Diebels, D. Truhn, T. Histing, and B. Braun, 'Predicting the effect of individual weight-bearing on tibial load and fracture healing after tibial plateau fractures – introduction of a biomechanical simulation model', *Front Bioeng Biotechnol*, vol. 13, 2025, doi: 10.3389/fbioe.2025.1659029.

[45] K. M. Steele, M. S. Demers, M. H. Schwartz, and S. L. Delp, 'Compressive tibiofemoral force during crouch gait', *Gait Posture*, vol. 35, no. 4, pp. 556–560, 2012, doi: 10.1016/j.gaitpost.2011.11.023.

[46] M. Roberts, D. Mongeon, and F. Prince, 'Biomechanical parameters for gait analysis: A systematic review of healthy human gait', *Phys Ther Rehabil*, vol. 4, no. 1, p. 6, 2017, doi: 10.7243/2055-2386-4-6.

[47] K. Götz-Neumann, *Gehen verstehen: Ganganalyse in der Physiotherapie*, 4th ed., Stuttgart, Germany: Georg Thieme Verlag, 2006, ISBN 978-3-13-132374-3.

[48] J. Perry and J. M. Burnfield, *Gait Analysis: Normal and Pathological Function*, 2nd ed., Boca Raton, FL: CRC Press, 2024, originally published 2010 by SLACK Incorporated, ISBN 978-1-55642-766-4, doi: 10.1201/9781003525592.

[49] B. Gervais, A. Vadean, M. Brochu, and M. Raison, 'Influence of the load modelling during gait on the stress distribution in a femoral implant', *Multibody Syst Dyn*, vol. 44, no. 1, pp. 93–105, 2018, doi: 10.1007/s11044-018-9621-z.

[50] F. Linde and H. C. Sørensen, 'The effect of different storage methods on the mechanical properties of trabecular bone', *J Biomech*, vol. 26, no. 10, pp. 1249–1252, 1993, doi: 10.1016/0021-9290(93)90072-m.

[51] S. Unger, M. Blauth, and W. Schmoelz, 'Effects of three different preservation methods on the mechanical properties of human and bovine cortical bone', *Bone*, vol. 47, no. 6, pp. 1048–1053, 2010, doi: 10.1016/j.bone.2010.08.012.

[52] A. R. Kemper, C. McNally, E. A. Kennedy, S. J. Manoogian, and S. M. Duma, 'The material properties of human tibia cortical bone in tension and compression: Implications for the tibia index', in *Proceedings of the 20th International Technical Conference on the Enhanced Safety of Vehicles (ESV)*, Paper No. 07-0470, 2007.

[53] C. H. Turner and D. B. Burr, 'Basic biomechanical measurements of bone: A tutorial', *Bone*, vol. 14, no. 4, pp. 595–608, 1993, doi: 10.1016/8756-3282(93)90081-k.

[54] C. H. Turner, S. C. Cowin, J. Y. Rho, R. B. Ashman, and J. C. Rice, ‘The fabric dependence of the orthotropic elastic constants of cancellous bone’, *J Biomech*, vol. 23, no. 6, pp. 549–561, 1990, doi: 10.1016/0021-9290(90)90048-8.

[55] L. Rincón-Kohli and P. K. Zysset, ‘Multi-axial mechanical properties of human trabecular bone’, *Biomech Model Mechanobiol*, vol. 8, no. 3, pp. 195–208, 2009, doi: 10.1007/s10237-008-0128-z.

[56] D. T. Reilly and A. H. Burstein, ‘The elastic and ultimate properties of compact bone tissue’, *J Biomech*, vol. 8, no. 6, pp. 393–405, 1975, doi: 10.1016/0021-9290(75)90075-5.

[57] P. Janczyk, J. Weigner, A. Luebke-Becker, S. Kaessmeyer, and J. Plendl, ‘Nitrite pickling salt as an alternative to formaldehyde for embalming in veterinary anatomy: A study based on histo- and microbiological analyses’, Ann Anat, vol. 193, no. 1, pp. 71–75, 2011, doi: 10.1016/j.aanat.2010.08.003.

[58] M. Palanca, G. Tozzi, and L. Cristofolini, ‘The use of digital image correlation in the biomechanical area: A review’, Int Biomech, vol. 3, no. 1, pp. 1–21, 2015, doi: 10.1080/23335432.2015.1117395.

[59] S. P. Väänänen, S. Amin Yavari, H. Weinans, A. A. Zadpoor, J. S. Jurvelin, and H. Isaksson, ‘Repeatability of digital image correlation for measurement of surface strains in composite long bones’, *J Biomech*, vol. 46, no. 11, pp. 1928–1932, 2013, doi: 10.1016/j.jbiomech.2013.05.021.

[60] M. Windolf, V. Varjas, D. Gehweiler, R. Schwyn, D. Arens, C. Constant, S. Zeiter, R. G. Richards, and M. Ernst, ‘Continuous implant load monitoring to assess bone healing status: Evidence from animal testing’, *Medicina (Kaunas)*, vol. 58, no. 7, p. 858, 2022, doi: 10.3390/medicina58070858.

[61] R. Klopfleisch, M. von Deetzen, A. T. Weiss, J. Weigner, F. Weigner, J. Plendl, and A. D. Gruber, ‘Weigner’s fixative – an alternative to formalin fixation for histology with improved preservation of nucleic acids’, *Vet Pathol*, vol. 50, no. 1, pp. 191–199, 2013, doi: 10.1177/0300985812441031.

[62] C. Kober, R. Sader, H.-F. Zeilhofer, S. Prohaska, S. Zachow, and P. Deuflhard, ‘Anisotrope Materialmodellierung für den menschlichen Unterkiefer’, in Tagungsband des Workshops “Die Methode der Finiten Elemente in der Biomedizin, Biomechanik und angrenzenden Gebieten”, Universitätsklinikum/Universitätsrechenzentrum Ulm, 23.–24. Juli 2001, ZIB-Report 01-31, Okt. 2001. [Online]. Available: https://webdoc.sub.gwdg.de/ebook/e/2003/zib_2/reports/ZR-01-31.pdf.

[63] P. M. Cattaneo, M. Dalstra, and L. H. Frich, ‘A three-dimensional finite element model from computed tomography data: A semi-automated method’, *Proc Inst Mech Eng H*, vol. 215, no. 2, pp. 203–213, 2001, doi: 10.1243/0954411011533760.

[64] M. A. Imam and A. C. Fraker, ‘Titanium alloys as implant materials’, in *Medical Applications of Titanium and Its Alloys: The Material and Biological Issues*, S. A. Brown and J. E. Lemons, Eds., ASTM International, 1996, pp. 3–16.

[65] L. E. Claes and C. A. Heigele, ‘Magnitudes of local stress and strain along bony surfaces predict the course and type of fracture healing’, *J Biomech*, vol. 32, no. 3, pp. 255–266, 1999, doi: 10.1016/S0021-9290(98)00153-5.

[66] S. Shen, P. Wang, X. Li, X. Han, and H. Tan, ‘Pre-operative simulation using a three-dimensional printing model for surgical treatment of old and complex tibial plateau fractures’, Sci Rep, vol. 10, no. 1, p. 6044, 2020, doi: 10.1038/s41598-020-63219-w.

[67] J. W. A. Fletcher, M. Windolf, R. G. Richards, B. Gueorguiev, and P. Varga, ‘Screw configuration in proximal humerus plating has a significant impact on fixation failure risk predicted by finite element models’, *J Shoulder Elbow Surg*, vol. 28, no. 9, pp. 1816–1823, 2019, doi: 10.1016/j.jse.2019.02.013.

[68] J. X. Chen, H. Wechsler, J. M. Pullen, Y. Zhu, and E. B. MacMahon, ‘Knee surgery assistance: Patient model construction, motion simulation, and biomechanical visualization’, *IEEE Trans Biomed Eng*, vol. 48, no. 9, pp. 1042–1052, 2001, doi: 10.1109/10.942595.

[69] W. I. Willaert, R. Aggarwal, I. Van Herzeele, N. J. Cheshire, and F. E. Vermassen, ‘Recent advancements in medical simulation: Patient-specific virtual reality simulation’, *World J Surg*, vol. 36, no. 7, pp. 1703–1712, 2012, doi: 10.1007/s00268-012-1489-0.

[70] G. Cate, J. Barnes, S. Cherney, J. Stambough, D. Bumpass, C. L. Barnes, and K. J. Dickinson, ‘Current status of virtual reality simulation education for orthopedic residents: The need for a change in focus’, *Glob Surg Educ*, vol. 2, p. 46, 2023, doi: 10.1007/s44186-023-00120-w.

[71] A. Sternheim, F. Traub, N. Trabelsi, et al., ‘When and where do patients with bone metastases actually break their femurs?’, *Bone Joint J*, vol. 102-B, no. 5, pp. 638–645, 2020, doi: 10.1302/0301-620X.102B5.BJJ-2019-1328.R2.

[72] B. J. Braun, M. Orth, S. Diebels, K. Wickert, A. Andres, J. Gawlitza, A. Bücker, T. Pohlemann, and M. Roland, ‘Individualized determination of the mechanical fracture environment after tibial exchange nailing: A simulation-based feasibility study’, *Front Surg*, vol. 8, p. 749209, 2021, doi: 10.3389/fsurg.2021.749209.

[73] H. Isaksson, ‘Recent advances in mechanobiological modeling of bone regeneration’, Mech Res Commun, vol. 42, pp. 22–31, 2012, doi: 10.1016/j.mechrescom.2011.11.006.

[74] M. Orth, B. Ganse, A. Andres, K. Wickert, E. Warmerdam, M. Müller, S. Diebels, M. Roland, and T. Pohlemann, ‘Simulation-based prediction of bone healing and treatment recommendations for lower leg fractures: Effects of motion, weight-bearing and fibular mechanics’, *Front Bioeng Biotechnol*, vol. 11, p. 1067845, 2023, doi: 10.3389/fbioe.2023.1067845.

[75] A. Gee, H. Bougherara, E. H. Schemitsch, and R. Zdero, ‘Biomechanical design using in-vitro finite element modeling of distal femur fracture plates made from semi-rigid materials versus traditional metals for post-operative toe-touch weight-bearing’, Med Eng Phys, vol. 87, pp. 95–103, 2021, doi: 10.1016/j.medengphy.2020.11.015.

[76] B. Ganse, M. Orth, M. Roland, S. Diebels, P. Motzki, S. Seelecke, S.-M. Kirsch, F. Welsch, A. Andres, K. Wickert, B. J. Braun, and T. Pohlemann, ‘Concepts and clinical aspects of active implants for the treatment of bone fractures’, *Acta Biomater*, vol. 146, pp. 1–9, 2022, doi: 10.1016/j.actbio.2022.05.001.

[77] M. Roland, S. Diebels, K. Wickert, T. Pohlemann, and B. Ganse, ‘Finite element simulations of smart fracture plates capable of cyclic shortening and lengthening: Which stroke for which fracture?’, *Front Bioeng Biotechnol*, vol. 12, p. 1420047, 2024, doi: 10.3389/fbioe.2024.1420047.

[78] A. Erdemir, P. J. Hunter, G. A. Holzapfel, L. M. Loew, J. Middleton, C. R. Jacobs, P. Nithiarasu, R. Löhner, G. Wei, B. A. Winkelstein, V. H. Barocas, F. Guilak, J. P. Ku, J. L. Hicks, S. L. Delp, M. Sacks, J. A. Weiss, G. A. Ateshian, S. A. Maas, A. D. McCulloch, and G. C. Y. Peng, 'Perspectives on sharing models and related resources in computational biomechanics research', *J Biomech Eng*, vol. 140, no. 2, p. 024701, 2018, doi: 10.1115/1.4038768.

# 9. Publications

## 9.1 Publications included in the thesis

Paper 1:

**K. Wickert,** A. Andres, M. Roland, R. Leibinger, D. Kerner, F. Frenzel, F. Ramsthaler, S. Diebels and T. Tjardes, ‘Simulating Physiological Conditions: A Novel Testing Device for Bone–Implant Interfragmentary Movement‘, *under consideration/ review at a peer-reviewed journal owned by a major scientific publisher.*

Paper 2:

**K. Wickert**, M. Roland, A. Andres, S. Diebels, B. Ganse, D. Kerner, F. Frenzel, T. Tschernig, M. Ernst, M. Windolf, M. Müller, T. Pohlemann, and M. Orth, ‘Experimental and virtual testing of bone-implant systems equipped with the AO Fracture Monitor with regard to interfragmentary movement’, *Front Bioeng Biotechnol*, vol. 12, 2024, doi: 10.3389/fbioe.2024.1370837.

Paper 3:

A. Andres, **K. Wickert,** M. Roland, M. Orth, B. Braun, T. Histing, S. Diebels and T. Pohlemann, ‘Integrated Study of the Distal Femur Biphasic Plate: Exploring In Vivo, In Vitro, and In Silico Methodologies‘, submitted to *Frontiers in Bioengineering and Biotechnology.*

Paper 4:

**K. Wickert,** A. Andres, M. Roland, D. Crepulja, B. Braun, T. Histing, R. Leibinger, F. Reinauer and S. Diebels, ‘CT-, 3D-Scan and Manufacturer-Based Implant Models: A Comparative Finite Element Study on Implant Geometry and Interfragmentary Movement in Distal Radius Fracture Fixation‘, in progress.

### 9.1.1 Simulating Physiological Conditions: A Novel Testing Device for Bone–Implant Interfragmentary Movement (Paper 1)

Authors:

**K. Wickert,** A. Andres, M. Roland, R. Leibinger, D. Kerner, F. Frenzel, F. Ramsthaler, S. Diebels and T. Tjardes

Publication status:

*Under consideration/ review at a peer-reviewed journal owned by a major scientific publisher*

# Simulating Physiological Conditions: A Novel Testing Device for Bone–Implant Interfragmentary Movement

Kerstin Wickert [1,*], Annchristin Andres [1], Michael Roland [1], Ralf Leibinger [2], Dorothea Kerner [3], Felix Frenzel [3], Frank Ramsthaler [4], Stefan Diebels [1], Thorsten Tjardes [5]

1. Applied Mechanics, Saarland University, Saarbrücken, Germany
2. KLS Martin SE & Co. KG, Tuttlingen, Germany
3. Clinic of Diagnostic and Interventional Radiology, Saarland University Hospital, Homburg, Germany
4. Institute of Legal Medicine, Saarland University, Homburg, Germany
5. Department of Trauma Surgery, Orthopedic Surgery and Septic-Reconstructive Surgery, Hospital of the German Armed Forces, Berlin

*** Correspondence:**

Kerstin Wickert

Applied Mechanics
Saarland University
Campus A4 2, 1. OG
D-66123 Saarbrücken
Germany

phone: +49 681 302 2168
fax: +49 681 302 3992
email: kerstin.wickert@uni-saarland.de

# Abstract

*Background*

Enhancing bone healing requires identifying the factors that hinder the process. Once these factors are known, strategies can be developed to minimize disruptions and promote optimal bone recovery. Investigating the fracture site under realistic loading scenarios is essential for understanding and optimizing the healing process.

*Methods*

A testing device was developed and built to realistically simulate different loading scenarios on the human tibia. For this purpose, the treated tibia was clamped and subjected to scaled knee joint forces representative of a forward step. Implant stability and interfragmentary movement were assessed using force sensors and a camera system. A computed tomography scan, including a six-rod calibration phantom for bone density, was performed on the treated tibia to run a subject-specific biomechanical finite element simulation.

*Findings*

Forces and moments acting on the tibia during the gait cycle were determined using complementary measurement techniques. The biomechanical simulations were validated against the experimental data, allowing further analysis of micromovements within the fracture gap. This approach provides a basis for future patient-specific predictions during the healing process.

*Interpretation*

By understanding how individual knee joint forces affect implant stability and interfragmentary movement, this knowledge can be leveraged to improve bone healing outcomes.



# Keywords:

distal tibia fracture, gait simulation, subject-specific finite element analysis, personalized osteosynthesis, implant stability, interfragmentary movement, experimental biomechanics, human cadaveric specimen

# Introduction

Tibial fractures are among the most frequent and challenging orthopedic injuries, often associated with complications and an increased risk of non-union or pseudoarthrosis (Tian et al., 2020). The tibia, as a major weight-bearing bone, is critical for mobility and structural integrity. However, impaired healing of tibial fractures remains a significant clinical problem, with approximately 10% of all long bone fractures failing to heal properly (Einhorn & Gerstenfeld, 2015). Such cases frequently require prolonged treatment and sometimes revision surgery, underscoring the need for improved treatment strategies.

Fracture healing involves both biological and mechanical aspects. Modern implants address these factors through advances in implant design and surgical technique. More recently, personalized implants, tailored to the individual anatomy, aim to support fracture healing by actively interacting with the processes of fracture healing (Safali et al., 2023; Ganse et al., 2022; Roland et al., 2024). This approach to fracture care requires the integration of knowledge and methods from biomechanics, orthopedic trauma surgery, fracture biology, and computational modeling.

Biomechanical simulation of bone-implant systems and fracture healing allows for faster and more cost-effective predictions compared with clinical trials (Roland et al., 2023). Simulation technologies are well established in other industries, such as automotive and aerospace, where they are integral to product development and testing (Luan, 2024). Similarly, finite element (FE) simulations have a longstanding role in medical research (Sun et al., 2023). However, simulations must be grounded in experimental data to ensure validity. Only with experimentally derived material properties and boundary conditions can the mechanical behavior of bones and bone-implant systems be reliably simulated.

From a mechanical perspective, implant stability is central (Coray et al., 2016). Fracture healing depends on the strain-state of the callus: optimal strain promotes healing, whereas excessive or insufficient strain delays or prevents consolidation (Claes, 2017). Implant design must therefore account for these thresholds, which influence both implant longevity and the local micromechanical environment within the fracture gap.

Several experimental testing devices have been developed to investigate these factors, ranging from simple wear tests (Walker et al., 1996) to complex joint simulators (Henke et al., 2024). Testing modalities such as axial compression, bending, and torsion are commonly used to approximate physiological loading conditions on bone specimens (Turner & Burr, 1993). Advances in testing technology including servo-hydraulic machines and custom fixtures, have improved the ability to replicate in vivo mechanics (Sharir et al., 2008). Imaging methods such as digital image correlation (DIC) provide further insight into bone deformation and failure mechanisms (Bay et al., 1999). However, many manufacturer-driven tests remain limited to standardized protocols, which often fail to represent the complex and dynamic loading scenarios of daily activities such as walking or rehabilitation.

Physiological bone healing is supported by axial displacements, while torsional movements can disturb or even prevent union (Park & Augat, 2004). To address these limitations, we developed a testing device capable of applying force-driven scenarios that replicate the loading conditions of a gait cycle. The device enables the systematic investigation of bone-implant systems and interfragmentary movement (IFM), regardless of fracture type or osteosynthesis technique. Ultimately, this approach

provides a framework for experimentally validated simulations and the exploration of physiologically relevant implant behavior during routine activities.

# Methods

## Study Model

Tibial fractures were selected as the model system for developing and validating the testing device (Figure 1 C), as they represent one of the most challenging fracture types, often associated with complications and pseudoarthrosis (Tian et al., 2020).

## Loading Scenario: Gait Cycle

The loading scenario was based on the gait cycle, defined as the interval between two successive ground contacts of the same foot. It consists of two main phases: stance phase (touchdown, rolling, and toe-off) and swing phase (acceleration, mid-swing, and deceleration) (see Figure 3E).

During gait, displacement of the body's center of gravity produces multidimensional loading on the tibia (Götz-Neumann, 2006). The internal loading thus consists of both forces and moments (Wehner et al., 2009); consequently, pure axial testing alone is insufficient. The device architecture was therefore designed to apply not only axial forces during ground contact but also the changes in all three force components across the gait phases.

In clinical practice, patients often use crutches during rehabilitation, which alters the load distribution by reducing weight transfer through the injured leg (Rasouli & Reed, 2020). This modifies the mechanical environment at the fracture site. To replicate different rehabilitation conditions, the device control software allowed adjustment of the applied forces, simulating both full and partial weight-bearing scenarios.

Loading data was obtained from the Orthoload database, which includes in vivo forces measured in patients with instrumented implants (Orthoload database, 2025). According to these data, axial load on the tibial plateau during normal walking reaches approximately three times body weight (Steele et al., 2012; Wehner et al., 2009). Radial forces, though smaller (approximately 0.2 times body weight), are also relevant and were included. For partial weight-bearing with crutches, the applied loads were scaled according to donor or patient weight and literature data (Eickhoff et al., 2022; Merkle et al., 2023). Figure 1 A shows one representative step from the eight-step input file, with force components plotted along body axes (see Figure 1 B).

## Testing Device Components

### *Force Application*

The input file from Orthoload provides data on knee joint forces corresponding to the body axes: transverse (x), sagittal (y), and longitudinal (z). These forces are applied to the respective body axes on the clamped bone using linear motors (ESR Pollmeier GmbH, Ober-Ramstadt, Germany). The longitudinal force application (linear motor axis with primary part of F=1900/4000N and a stroke of 252mm) is directed at the distal end segment of the tibia (see Figure 1C, label a), while the transverse and sagittal force applications (linear motor axis with primary part of F=1000/2000N and a stroke of 60mm) on the tibial plateau are achieved through a cross-table mechanism (see Figure 1C, label e). The use of linear motors ensures precise force transmission and allows tight control and adjustment of forces. For the simulation a body donor weighing 90 kg was considered. This results in axial forces of approximately 2,700 N and radial forces of about 200 N to accurately simulate tibial loading.

### *Clamping System*

Secure fixation was achieved using an adaptable pin-based clamping system (Silver Clamp X-Clamp, MATRIX GmbH, Ostfildern, Germany), which conforms to complex freeform geometries such as the proximal tibia. This design allows stable fixation with minimal clamping force (Figure 1C, label c).

### *Sensors*

Six-axis force and moment sensors (K6D80, ME-Meßsysteme GmbH, Henningsdorf, Germany) with corresponding measuring amplifiers (GSV-8DS, ME-Meßsysteme GmbH, Henningsdorf, Germany) were positioned near the clamping points (Figure 1C, labels b). Sensor redundancy permitted cross-validation of measurements, ensuring robustness.

### *Monitoring of interfragmentary motion*

The experiment evaluation primarily uses the DIC (Istra4D V4.10, Dantec Dynamics, Skovlunde, Denmark) method (Palanca et al., 2016) which is a camera-based, non-contact measurement approach that allows precise quantification of deformations and movements of objects through image analysis. The images prior to and after deformation, i.e. loading of the bone, are compared. Initially, reference and target images are captured. By dividing these images into small regions of interest (subsets), pixel correlation was computed. Based on these correlations' displacements and strains in the respective regions of interest are computed. Therefore, four cameras (AV Manta G-507B, Stemmer Imaging, Puchheim, Germany) with DIC related lenses (COMPUTAR M1224-MPW2, Stemmer Imaging, Puchheim, Germany) are strategically positioned around the specimen via articulated arms (Magic Arm, Manfrotto, Cassola, Italy). The field of view of each pair of cameras is combined, enabling three-dimensional image correlation. In this configuration, two cameras are directed toward one side, capturing the fracture gap and its fixation, while the other two cameras focus on the opposite side of the fracture gap facilitating the measurement of a substantial part of the fracture while observing the implant throughout the gait cycle.

## Experimental Workflow

A cadaveric human tibia (female donor, age 74 years, weight 82 kg, no skeletal disease or knee arthroplasty) was used. The cadaveric specimen used in this study was acquired as tibial plateau to toe tip – left by Science Care (Science Care, Phoenix AZ, US) after successful and verified tissue request process as part of the German Federal Ministry of Science, Technology and Space, BMFTR, (former German Federal Ministry of Science and Education, BMBF) funded project "IIP-Extrem" (FKZ: 13GW0124). All matters related to body donation (e.g. a statement confirming that informed consent was obtained from the donar and/or their legal guardian(s) or next of kin) are fully managed by Science Care. The specimen was shipped to and stored at the Institute of Forensic Medicine, Saarland University Hospital, which also performed the on-site cremation after the experiments were completed. The study was conducted in accordance with the local legislation and institutional requirements. Currently, the workflow of this study is approved by the Saarland Medical Board (Saarländische Ärztekammer, Kennzeichen 195/24). The workflow included five steps:

### *i) Fracture Generation*

A distal tibia fracture (AO/OTA 43-A1) was induced using a custom device applying combined axial preload and torsion. Detailed device description and fracture data are provided in the Supplementary Material (see Figure 5 and Figure 6).

### *ii) Patient-specific implant design and treatment:*

The tibia fracture was reduced and fixed using a subject-specific implant tailored to both the geometry of the fracture and the anatomy of the tibia, allowing for an optimal anatomical adaptation and

mechanical stability. The design of the implant and its manufacturing process as well as the treatment process are provided in the Supplementary Material.

### *iii) Data acquisition for 3D model generation*

After reduction and fixation of the fracture a computed tomography (CT) scan (Somatom Definition AS64, Siemens Healthineers, Erlangen, Germany), including a six-rod bone density calibration phantom (QRM-BDC/6, six rods, QRM GmbH, Mohrendorf, Germany), was acquired. The specimen was placed longitudinally on the CT gantry with the phantom underneath. The scanner settings were: tube voltage: 120 kVp, tube current: 95 mA, collimation of 64 × 0.6 mm and a pitch factor of 0.8. Postprocessing included reconstruction of axial slices with a slice thickness of 3 mm (increment of 2 mm) and 0.6 mm (increment of 0.4 mm) applying a bone reconstruction kernel (B70s) and a soft tissue reconstruction kernel (B31s) respectively.

### *iv) Specimen preparation and experimental execution*

To facilitate the evaluation via DIC, the specimen was covered with a speckle pattern of white and then black paint spray (see Figure 2A). Knee joint forces equivalent of partial weight bearing, according to the donor's body weight, were then applied to the bone-implant system.

### *v) Evaluation of IFM and implant surface strain*

DIC was used to determine surface displacements and subsequent strains. The use of the multi-camera system enabled a 3D DIC evaluation. Through the initial calibration of the four cameras, the information for the stereoscopic setup, like orientation, was determined. The DIC results were then merged with the data from the force sensors and the specified force curves, as given by the testing device, for combined analysis.

## Simulation

Computational model of the bone-implant system relies on the segmentation of the image stack from the CT scan (see Figure 4A), as described previously described (Braun et al. (2021), Orth et al. (2023), Wickert et al. (2024)). Bone density values were determined by correlating the densitometric relationships with the segmented bone with the segmented masks of the calibration phantom. Then histograms of grayscale values versus voxel counts were generated, with curve maxima serving as reference points for mapping CT data in Hounsfield Units (HU) to equivalent mineral density values. These values are then used to calculate ash density (Eberle et al., 2013) and apparent density (Edwards et al., 2013). Material parameters are calculated using the density-modulus relationship (Rho et al., 1995), resulting in 25 material classes with HU-based boundaries (Cattaneo et al., 2001), while homogeneous material parameters for the implant and fracture gap (Claes & Heigele, 1999) were implemented in the model as given in the literature. The exact material parameters for the implant used in this study are a company secret but are within the range of values found in the literature (Imam & Fraker, 1996; Froes & Qian, 2018).

A finite element mesh was generated for the Abaqus environment (Dassault Systemes, Velizy-Villacoublay, France) using quadratic tetrahedral elements (C3D10). The model was aligned to correctly apply force values along the corresponding axes, and boundary conditions were applied analogously to the experimental setup. Knee joint forces from the second forward step of the input dataset were applied along their respective axes. Axial forces were applied to the tibia specimen via the longitudinal movement, while transverse and sagittal forces were applied to the tibial plateau with longitudinal movement restricted. To minimize computational complexity while maintaining accuracy, only force values from a single forward step were applied. Simulated results were compared to experimental data by comparing the simulation step with the mean of eight experimental steps.

# Results

## Experimental Results

The specimen was subjected to 30% of the knee joint forces associated with a forward step, representing partial weight bearing. Figure 2A shows the selected points within the fracture gap and on the implant surface, including start and end points. Total displacement across the fracture gap and bone-implant system as a whole, measured at the time of peak axial force during the first step, is shown relative to the reference image obtained before loading.

Temporal changes in line length across the fracture are illustrated in Figure 2B. Line 1 runs parallel to the longitudinal bone axis, while Line 2 crosses the gap transversely to assess displacement. Tracking both lines during the experiment revealed greater variation in Line 2, which can be attributed to the substantial longitudinal force applied. Consequently, the transversely oriented fracture exhibited greater movement compared with the parallel orientation. Minimal length changes were observed on the implant surface due to its higher stiffness (Figure 2C). These results highlight the influence of fracture orientation relative to the longitudinal axis. The experiment simulated the postoperative condition with an empty fracture gap, ensuring that no additional mechanical confounders were present. Furthermore, the characteristic double-peaked curves of the input data, corresponding to the eight steps, were clearly visible.

## Simulation Results

Experimental data were used to validate the simulation by comparing surface strains and IFM results with simulation outcomes. In addition, von Mises stress of the implant was analyzed as a measure of fixation stability.

Figure 3 compares experimental and simulation results. Strains within the fracture gap were assessed at two positions: (A) fracture parallel to the longitudinal axis and (B) transverse to the gap. Implant surface strain is shown in (C). The eight experimental steps were averaged into a mean representative step, with shaded areas indicating one standard deviation. All three graphs display strain as a function of the gait cycle. Another finding from the simulation is the implant's stability under load during a forward step. Figure 4B illustrates the von Mises stress distribution on the implant, reaching 140 MPa at the point of maximum force application.

# Discussion

Successful fracture healing depends on the balanced interplay between the biological and mechanical microenvironment within the fracture gap. The extent of IFM permitted by an osteosynthesis defines the mechanical environment, specifically, the magnitude of strain to which osteocytes are subjected during weight bearing. Routine clinical imaging techniques, which are central to postoperative evaluation and follow-up, do not provide systematic access to the fracture gap itself. Given the fact that loading patterns of the fracture gap must fit a narrow corridor to sustainably support fracture healing (Claes et al., 1998), an understanding of loading dynamics is essential to understand the biological and mechanical validity of an osteosynthesis, i.e. a bone implant system. However, most existing testing systems rely on cyclic monoaxial loading, thereby neglecting torsional and shear forces that are integral to physiologic loading.

To address this gap, we developed and validated a testing device capable of applying dynamic, multidimensional loading to a bone-implant system, combined with specimen-specific FE analysis. The testing device integrates linear modules along the x-, y-, and z-axes with a cross-table mechanism, thereby enabling simulation of everyday activities such as walking or stair climbing. While uniaxial experiments are useful for assessing stability and failure thresholds, they cannot capture IFM under physiological conditions. By contrast, this device places emphasis on the clinically relevant interface, i.e., the fracture gap.

Importantly, the device also enables validation of FE simulations. Nonetheless, careful alignment of regions of interest is essential when comparing simulations to experimental data, as discrepancies may arise from differences in node selection or measurement points. In addition, although the simulation closely replicates experimental conditions, the fracture gap was assigned a material property in the model, whereas in the experiment the gap remained “empty,” reflecting the immediate postoperative state. Another challenge lies in replicating clamping conditions: the specimen was aligned with respect to the axes for force application, but translation of these constraints into the model by selecting corresponding nodes and applying boundary conditions is necessarily approximate and does not exactly match real-world conditions.

A limitation of this study is that a generic gait curve was applied. Although human gait curves are broadly similar, they are not identical, and thus the applied curve may not perfectly match the donor specimen. To minimize this bias, input data were scaled to the donor’s body weight. The close agreement between experimental and simulation results, even with this limitation, supports the validity of the approach (see Figure 3 A-D).

Another source of potential bias is that experiment, simulation, and evaluation were performed by the same research team. Future studies should consider methodological separation of these steps, as proposed by Trabelsi and colleagues (Trabelsi et al., 2011), to strengthen reproducibility.

Gait and partial weight bearing are inherently three-dimensional processes. The testing device presented here decomposes these processes into their mechanical components and enables controlled application in the time domain. This ensures that magnitude, direction, and timing of loading remain consistent with physiological conditions. In this study, exemplified by a 30% body weight partial-weight-bearing step.

The complex loading curve observed during weight bearing in both longitudinal and orthogonal directions translated into a square-wave, like strain pattern in the fracture gap. Both longitudinal and orthogonal IFM exhibited this configuration, with strain magnitudes differing by two orders of magnitude. As expected, strains parallel to the loading axis were higher than those measured

orthogonal to the gap. In addition, strain measured across the implant surface closely mirrored the gait cycle loading pattern, particularly during the stance phase (see Figure 3 E).

Taken together, these results demonstrate that the device allows for differentiated, real-time analysis of strain distributions across the fracture gap. Since strain magnitude and pattern are known to influence cellular gene expression and the osteogenic potential of stromal cells, the presented setup provides a powerful link between the micro-scale (cellular behavior) and the macro-scale (implant mechanics) of fracture healing.

## Conclusion

This study presents a workflow for experimental research using human cadaveric specimens to investigate bone–implant systems. Beyond validating finite element simulations, the overarching aim is to apply the insights gained to improve fracture healing. By inducing fractures in donated human tibiae, stabilizing them with osteosynthesis, and testing them under realistic and individualized loading scenarios, this approach enables new investigations into implant stability and interfragmentary movement.

The workflow demonstrates the potential to optimize conventional testing methods and provide deeper insights into the biomechanics of fracture healing. Further refinement is needed to better align gait curves with both the testing device and the in silico simulations, which is expected to improve the accuracy of computational predictions. Future studies will focus on different fracture types and their implications for treatment strategies and healing outcomes (Wickert et al., 2024).

## Data availability

The original contributions presented in the study are included in the article/ supplementary material; further inquiries can be directed to the corresponding author.

## Funding

This work was funded by the German Federal Ministry of Research, Technology and Space (BMFTR), previously German Federal Ministry Education and Research (BMBF) under the grant “FKZ: 13GW0124”.

## Author Contributions

KW Methodology, Formal Analysis, Investigation, Visualization, Writing – Original Draft, Writing – Review and Editing

AA Writing – Review and Editing

MR Formal Analysis, Investigation, Supervision, Funding acquisition, Visualization, Writing – Original Draft, Writing – Review and Editing

RL Resources, Writing – Original Draft, Writing – Review and Editing

DK Data curation, Visualization, Writing – Review and Editing

FF Data curation, Visualization, Writing – Review and Editing

FR Conceptualization, Resources, Writing – Review and Editing

SD Conceptualization, Supervision, Funding acquisition, Writing – Review and Editing

TT Conceptualization, Resources, Supervision, Funding acquisition, Writing – Original Draft, Writing – Review and Editing

## Competing interests

The author RL is an employee of KLS Martin SE & Co. KG, and therefore, he has received/will receive benefits for personal or professional use from KLS Martin SE & Co. KG related directly or indirectly to the subject of this manuscript.

## Ethics Statement

The cadaveric specimen used in this study was acquired as tibial plateau to toe tip – left by Science Care (Science Care, Phoenix AZ, US) after successful and verified tissue request process as part of the German Federal Ministry of Science, Technology and Space, BMFTR, (former German Federal Ministry of Science and Education, BMBF) funded project “IIP-Extrem” (FKZ: 13GW0124). All matters related to body donation (e.g. a statement confirming that informed consent was obtained from the donar and/or their legal guardian(s) or next of kin) are fully managed by Science Care. The specimen was shipped to and stored at the Institute of Forensic Medicine, Saarland University Hospital, which also performed the on-site cremation after the experiments were completed. The study was conducted in

accordance with the local legislation and institutional requirements. Currently, the workflow of this study is approved by the Saarland Medical Board (Saarländische Ärztekammer, Kennzeichen 195/24).

# References


Bay, B.K., Smith, T.S., Fyhrie, D.P. & Saad, M. (1999) Digital volume correlation: Three-dimensional strain mapping using X-ray tomography. *Experimental Mechanics* **39**: 217-226. Doi: 10.1007/BF02323555

Bergmann, G., Bender, A., Dymke, J., Duda, G. & Damm, P. (2014) Standardized loads acting in knee implants. *PLoS One* **9**(1), 1. Doi: 10.1371/journal.pone.0086035

Braun, B.J., Orth, M., Diebels, S., Wickert, K., Andres, A., Gawlitza, J., Bücker, A., Pohlemann, T., & Roland, M. (2021) Individualized Determination of the Mechanical Fracture Environment After Tibial Exchange Nailing - A Simulation-Based Feasibility Study. *Frontiers in Surgery* **8**: 1-9. Doi: 10.3389/fsurg.2021.749209

Cattaneo, P.M., Dalstra, M., & Frich, L.H. (2001) A three-dimensional finite element model from computed tomography data: A semi-automated method. *Proceedings of the Institution of Mechanical Engineers, Part H: Journal of Engineering in Medicine* **215**(2): 203-213. Doi: 10.1243/0954411011533760

Claes, L. E. et al. Effects of mechanical factors on the fracture healing process. *Clin. Orthop. Relat. Res.* **355** (Suppl.), S132–S147 (1998).

Claes, L.E., & Heigele, C.A. (1999) Magnitudes of local stress and strain along bony surfaces predict the course and type of fracture healing. *Journal of Biomechanics* 32(3): 255-266. Doi: 10.1016/S0021-9290(98)00153-5

Claes, L. Mechanobiologie der Frakturheilung Teil 2. Unfallchirurg 120, 23–31 (2017). https://doi.org/10.1007/s00113-016-0281-2

Coray, R., Zeltner, M., & Özcan, M. (2016) Fracture strength of implant abutments after fatigue testing: A systematic review and a meta-analysis. *Journal of the Mechanical Behavior of Biomedical Materials*, *62*, 333-346. https://doi.org/10.1016/j.jmbbm.2016.05.011

Eberle, S., Göttlinger, M., & Augat, P. (2013) An investigation to determine if a single validated density-elasticity relationship can be used for subject specific finite element analyses of human long bones. *Medical Engineering and Physics* **35**(7): 875-883. Doi: 10.1016/j.medengphy.2012.08.022

Edwards, W.B., Schnitzer, T.J., & Troy, K.L. (2013) Torsional stiffness and strength of the proximal tibia are better predicted by finite element models than DXA or QCT. *Journal of Biomechanics*, **46**(10): 1655-1662. Doi: 10.1016/j.jbiomech.2013.04.016

Eickhoff, A.M., Cintean, R., Fiedler, C. Gebhard, F., Schütze, K. & Richter, P.H. (2022) Analysis of partial weight bearing after surgical treatment in patients with injuries of the lower extremity. Archives of Orthopaedic and Trauma Surgery **142**: 77-81. Doi: 10.1007/s00402-020-03588-z

Einhorn, T.A., & Gerstenfeld, L.C. (2015) Fracture healing: Mechanisms and interventions. *Nature Reviews Rheumatology* **11**(1): 45-54. Doi: 10.1038/nrrheum.2014.164

Froes, F.H. & Qian, M. (2018) Titanium in medical and dental applications. Woodhead Publishing Doi: 1016/ C2016-0-03591-X.

Ganse, B., Orth, M., Roland, M., Diebels, S., Motzki, P., Seelecke, S., Kirsch, S.M., Welsch, F., Andres, A., Wickert, K., Braun, B.J. & Pohlemann T. (2022) Concepts and Clinical Aspects of Active Implants for the Treatment of Bone Fractures. *Acta Biomaterialia* **146**:1-9. Doi: 10.1016/j.actbio.2022.05.001

Götz-Neumann, K. (2006) Gehen verstehen Ganganalyse in der Physiotherapie. Georg Thieme Verlag.

Henke, P., Ruehrmund, L., Bader, R. & Kebbach, M. (2024) Exploration of the Advanced VIVOTM Joint Simulator: An In-Depth Analysis of Opportunities and Limitations Demonstrated by the Artificial Knee Joint. *Bioengineering* **11**(2):178. Doi: 10.3390/bioengineering11020178.

Imam, M.A. & Fraker, A.C. (1996) Titanium alloys as implant materials. *In: Brown S., Lemons J., Editors. Medical Applications of Titanium and Its Alloys: The Material and Biological Issues. West Conshohicken, PA: ASTM International*, 3-16.

Luan, T. (2024) A Comprehensive Review of Simulation Technology: Development, Methods, Applications, Challenges and Future Trends. *International Journal of Emerging Technologies and Advanced Applications* **1**:9-14. Doi: 10.62677/IJETAA.2405119.

Merkle, T.P., Hofmann, N., Knop, C. & Da Silva, T. (2023) Can elderly individuals perform partial weight bearing on their lower limbs? A prospective cohort study using ambulatory real-time biofeedback. *Journal of Orthopaedic Surgery and Research* **18**(1):324. Doi: 10.1186/s13018-023-03807-4

Orth, M., Ganse, B., Andres, A., Wickert, K., Warmerdam, E., Müller, M., Diebels, S., Roland, M., & Pohlemann, T. (2023) Simulation-based prediction of bone healing and treatment recommendations for lower leg fractures: Effects of motion, weight-bearing and fibular mechanics. *Frontiers in Bioengineering and Biotechnology* **11**. Doi: 10.3389/fbioe.2023.1067845

Orthoload database. (2025) Input data testing device. Retrieved August 27, 2025, from https://orthoload.com/database/?implantId=1322&activityId=1521&activityIndentationLevel=1&parameterId=1&parameterIndentationLevel=-1&patientId=k8l&fileId=k8l_191211_1_107p&fileType=t&selectBox=file

Palanca, M., Tozzi, G., & Cristofolini, L. (2015) The use of digital image correlation in the biomechanical area: a review. *International Biomechanics* **3**(1): 1-21. Doi: 10.1080/23335432.2015.1117395

Park, S.H., & Augat, P. (2004) Shear movement at the fracture site delays healing in a diaphyseal fracture model. *Journal of Orthopaedic Research* **22**(5): 1156-1157. Doi: 10.1016/j.orthres.2004.02.003

Rasouli, F. & Reed, K.B. (2020) Walking assistance using crutches: A state of the art review. Journal of Biomechanics **98**:109489. Doi: 10.1016/j.jbiomech.2019.109489.

Rho, J.Y., Hobatho, M.C., & Ashman, R.B. (1995) Relations of mechanical properties to density and CT numbers in human bone. *Medical Engineering and Physics* **17**(5): 347-355. Doi: 10.1016/1350-4533(95)97314-F

Roland, M., Diebels, S., Orth, M. *et al.* Reappraisal of clinical trauma trials: the critical impact of anthropometric parameters on fracture gap micro-mechanics—observations from a simulation-based study. *Sci Rep* **13**, 20450 (2023). https://doi.org/10.1038/s41598-023-47910-2

Roland, M., Diebels, S., Wickert, K., Pohlemann, T. & Ganse, B. (2024) Finite element simulations of smart fracture plates capable of cyclic shortening and lengthening: which stroke for which fracture? Frontiers in Bioengineering and Biotechnology **12**:1420047. Doi: 10.3389/fbioe.2024.1420047.

Safali, S., Berk, T., Makelov, B., Acar, M.A., Gueorguiev, B., & Pape, H.C. (2023) The Possibilities of Personalized 3D Printed Implants - A Case Series Study. *Medicina (Lithuania)* **59**(2): 1-12. Doi: 10.3390/medicina59020249

Sharir, A., Barak, M.M. & Shahar, R. (2008) Whole bone mechanics and mechanical testing. *The Veterinary Journal* **177**(1):8-17. Doi: 10.1016/j.tvjl.2007.09.012.

Steele, K.M., De Mers, M.S., Schwartz, M.H., & Delp, S.L. (2012) Compressive tibiofemoral force during crouch gait. *Gait and Posture* **35**(4): 556-560. Doi: 10.1016/j.gaitpost.2011.11.023

Sun, T., He, X. & Li, Z. (2023) Digital twin in healthcare: Recent updates and challenges. *Digital Health* **9**:1-13. Doi: 10.1177/20552076221149651.

Tian, R., Zheng, F., Zhao, W., Zhang, Y., Yuan, J., Zhang, B., & Li, L. (2020) Prevalence and influencing factors of nonunion in patients with tibial fracture: Systematic review and meta-analysis. *Journal of Orthopaedic Surgery and Research* **15:377** Doi: 10.1186/s13018-020-01904-2

Trabelsi, N., Yosibash, Z., Wutte, C., Augat, P. & Eberle, S. (2011) Patient-specific finite element analysis of the human femur--a double-blinded biomechanical validation. *Journal of Biomechanics* **44**(9):1666-1672. Doi: 10.1016/j.jbiomech.2011.03.024

Turner, C.H. & Burr, D.B. (1993) Basic biomechanical measurements of bone: a tutorial. *Bone*. **14**(4):595-608. Doi: 10.1016/8756-3282(93)90081-k.

Walker, P.S., Blunn, G.W. & Lilley, P.A. (1996) Wear testing of materials and surfaces for total knee replacement. *Journal of Biomedical Materials Research* **33**:159-175. Doi: 10.1002/(SICI)1097-4636(199623)33:3<159::AID-JBM6>3.0.CO;2-P

Wehner, T., Claes, L., & Simon, U. (2009) Internal loads in the human tibia during gait. *Clinical Biomechanics* **24**(3): 299-302. Doi: 10.1016/j.clinbiomech.2008.12.007

Wickert, K., Roland, M., Andres, A., Diebels, S., Ganse, B., Kerner, D., Frenzel, F., Tschernig, T., Ernst, M., Windolf, M., Müller, M., Pohlemann, T., & Orth, M. (2024) Experimental and virtual testing of bone-implant systems equipped with the AO Fracture Monitor with regard to interfragmentary movement. *Frontiers in Bioengineering and Biotechnology*, *12*. Doi: 10.3389/fbioe.2024.1370837

# Figures

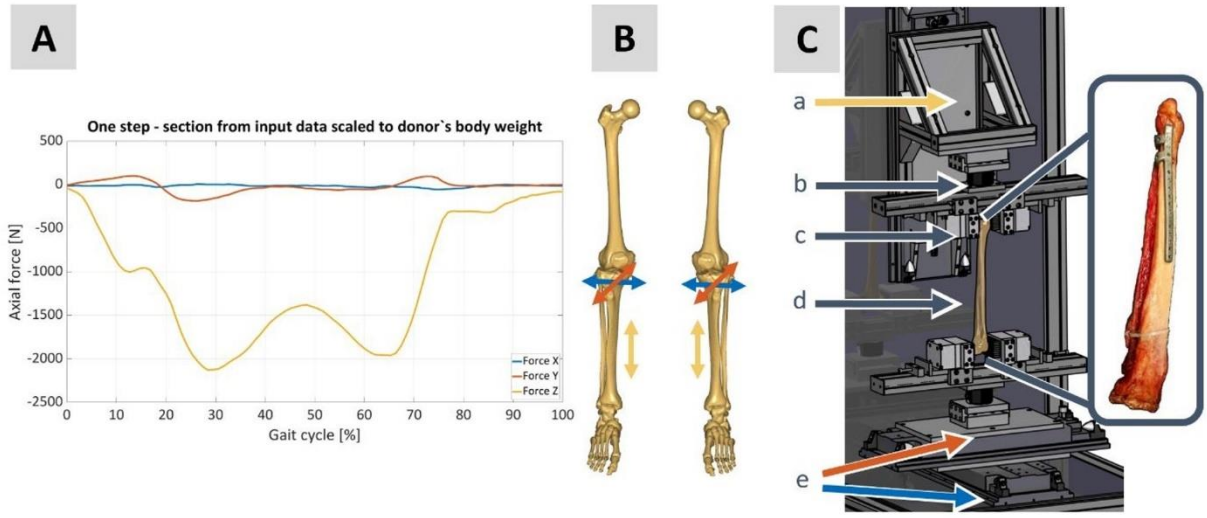


*Figure 1: A: Knee joint forces relative to the body axes during a forward step serve as the input dataset for the test scenario, B: Arrows mark the individual axes (x, y and z) of the knee joint force curves from A using the tibia as an example, C: Testing device with tibia (d), clamped in special clamping system (c). Forces applied over carve insertion: horizontally (a) and vertically (e) and measuring sensors (b).*

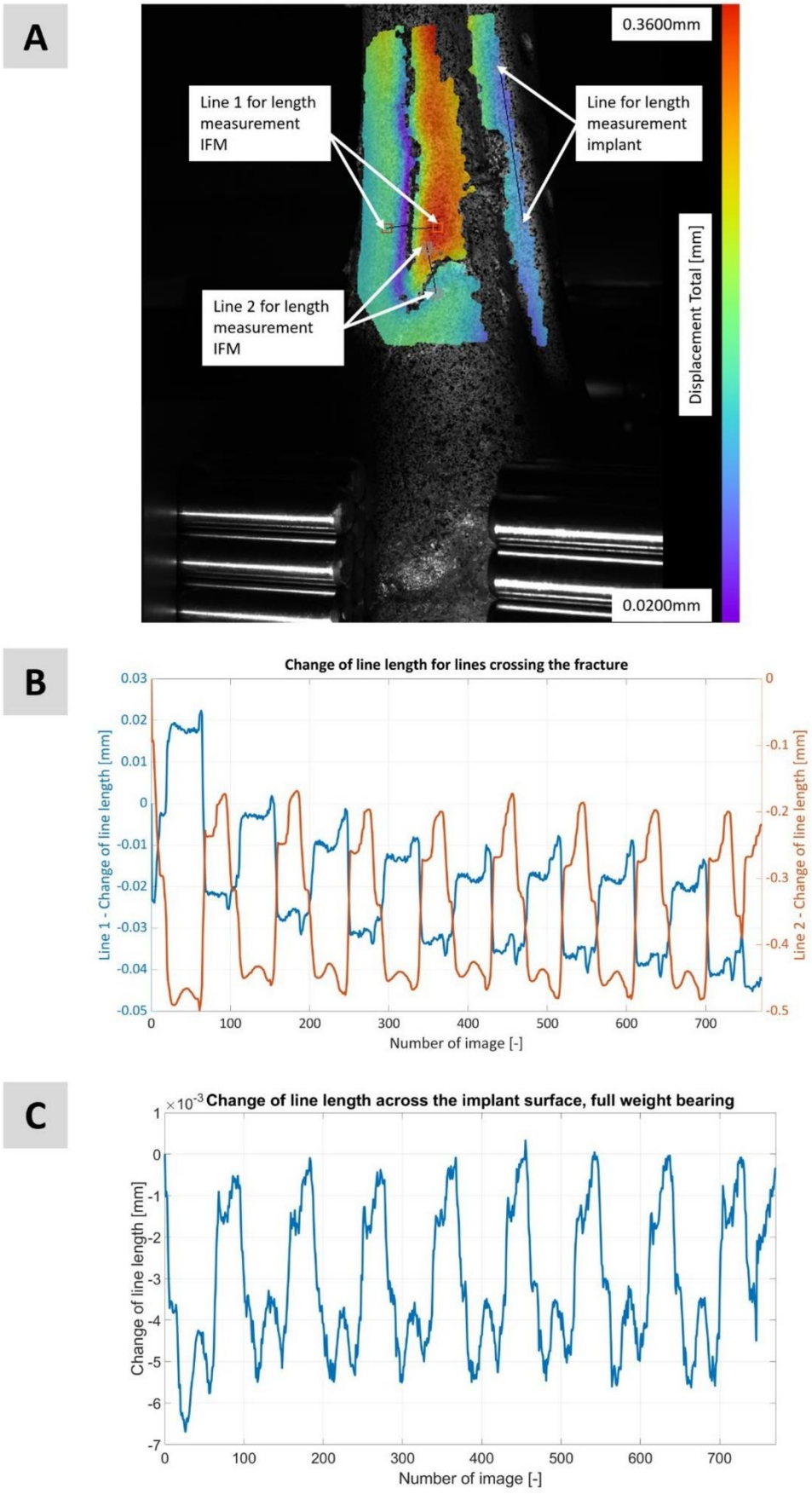


*Figure 2: A: DIC image including fracture and implant, B: change of line length for lines crossing the fracture (see a) Line1 and Line2), C: change of line length crossing implant surface (see a) line implant).*

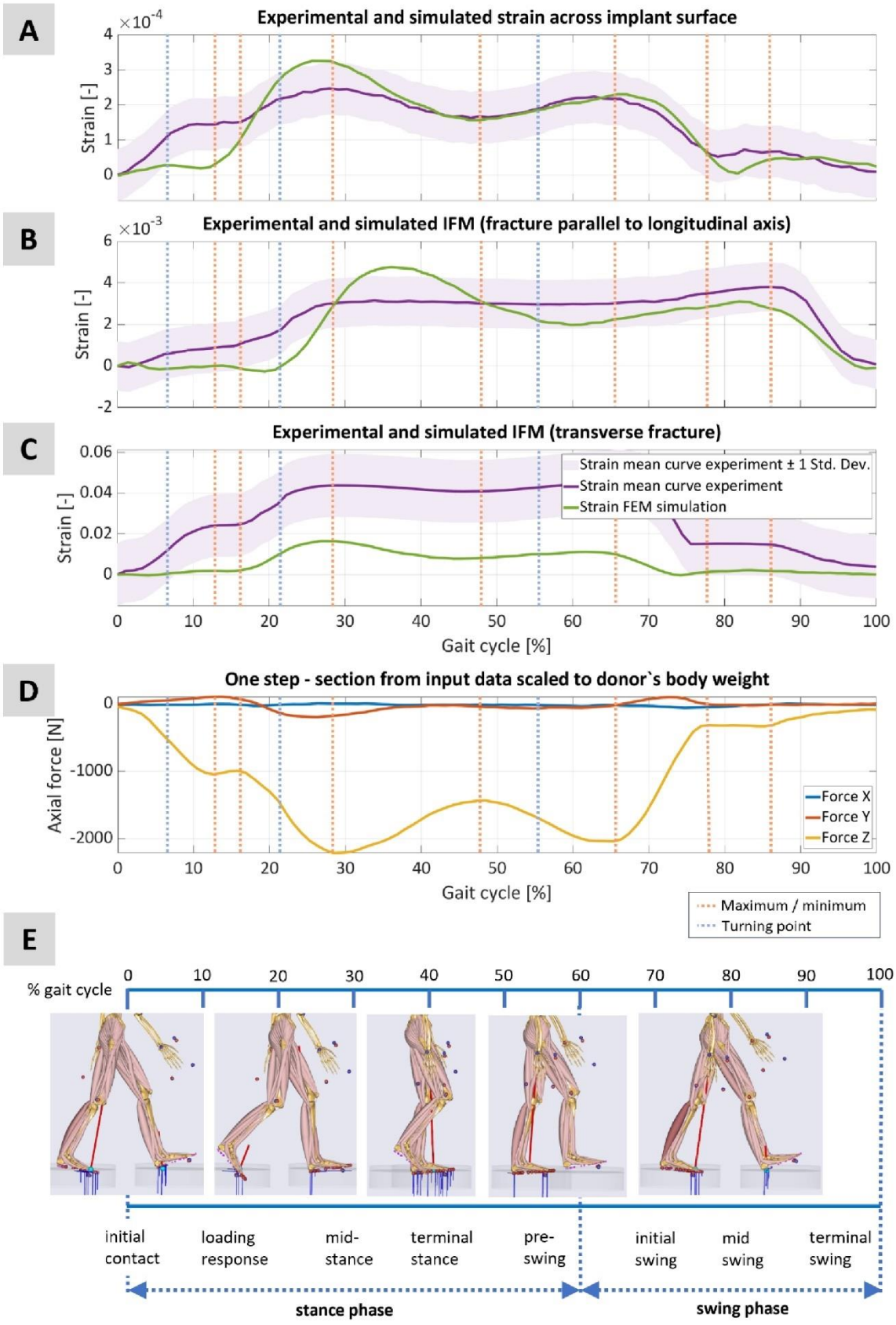


*Figure 3: Comparison of experimental and simulated strains concerning A: Strain across the implant surface, B: the IFM (fracture parallel to the longitudinal axis), C: Transverse IFM, with regard to D: the input file of the testing device (one step forward) (also see Figure 1A) and E: the corresponding gait cycle.*

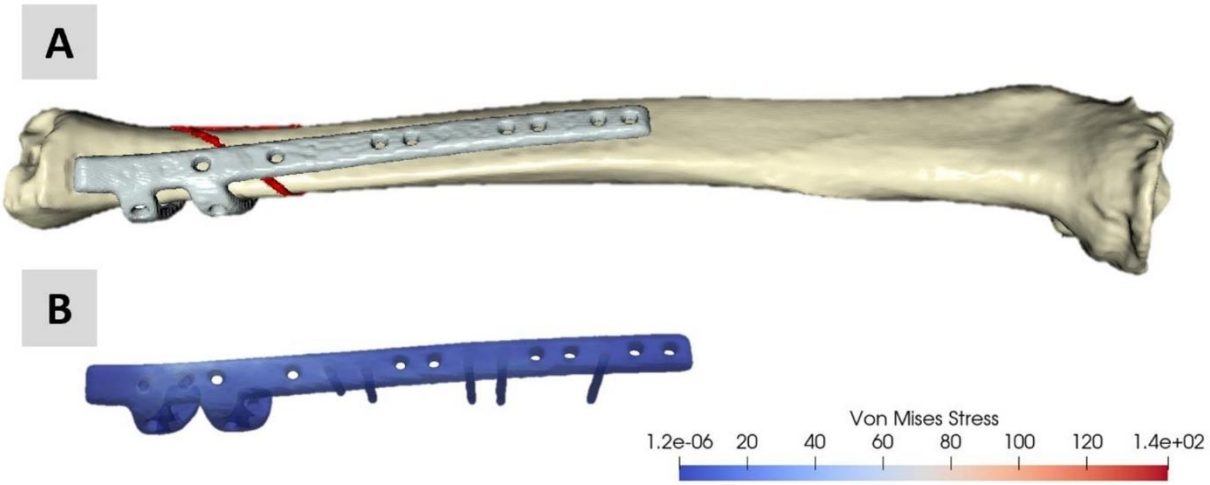


*Figure 4: A Computational model as input for the FE-Simulation consists of tibia, fracture and implant, B: Von Mises Stress at maximum knee joint force during a step forward.*

# Supplementary Material

## *In-vitro* fracture generation

The fracture generation was performed with human cadaveric specimens of the lower limb via an *in-vitro* experiment. To enable a correct grip of the clamping system, the soft tissue envelope at the ankle and the knee was removed.

The testing device is shown in Figure 5 and the fracture generation works as follows: (1) the specimen is clamped into the testing device via a flexible clamping system for complex geometries (Silver Clamp X-Clamp, MATRIX GmbH, Ostfildern, Germany), (2) in a preprocessing step, the angle α can be set in the range from 0° to about 45° degrees by positioning of the machine vises of the clamping system. The maximum adjustable value is related to the length of the specimen. Here the value was set to 0° in the experiment. (3) An axial loading can be applied on the side of the knee onto the tibial plateau with respect to a user chosen loading function. In this study, a linear loading function representing the body weight of the donor in combination with the forces acting on a knee during different activities was applied. According to the force values from the OrthoLoad database which includes *in-vivo* measurements of orthopedic implants in different clinical settings, cf. (Bergmann et al. 2014), a maximum force of 3260N was chosen to represent an injury caused by a high-energy event. All occurring forces and momentums are continuously measured with the two 6-axis sensors (K6D80, ME-Meßsysteme GmbH, Henningsdorf, Germany) and are plotted in Figure 6.

A stepper motor realizing an axial loading up to 5 kN to a specimen applies the loading function via a bellow coupling (Wittenstein alpha GmbH, Igersheim, Germany) and a precision ball screw spindle drive (Eisenmann und Hommes GmbH, Remscheid, Germany). With respect to the pre-set angle from step two, additional moments occur here, which place an additional load bearing on the specimen. After applying this preload scenario, (4) the specimen is rotated at the distal end by a second stepping motor with integrated control of the same type (KOCO Motion MDrive Plus² Motion Control, KOCO MOTION GmbH, Dauchingen, Germany). Here, the stepper motor is connected with a low-backlash planetary gearbox (Wittenstein alpha GmbH, Igersheim, Germany) and combined with a claw coupling to provide the motor with the necessary forward motion. This combination of a given preload with a rotation of the distal end of the tibia guarantees a complex distal fracture morphology, which would suggest the use of a personalized implant in clinical practice.

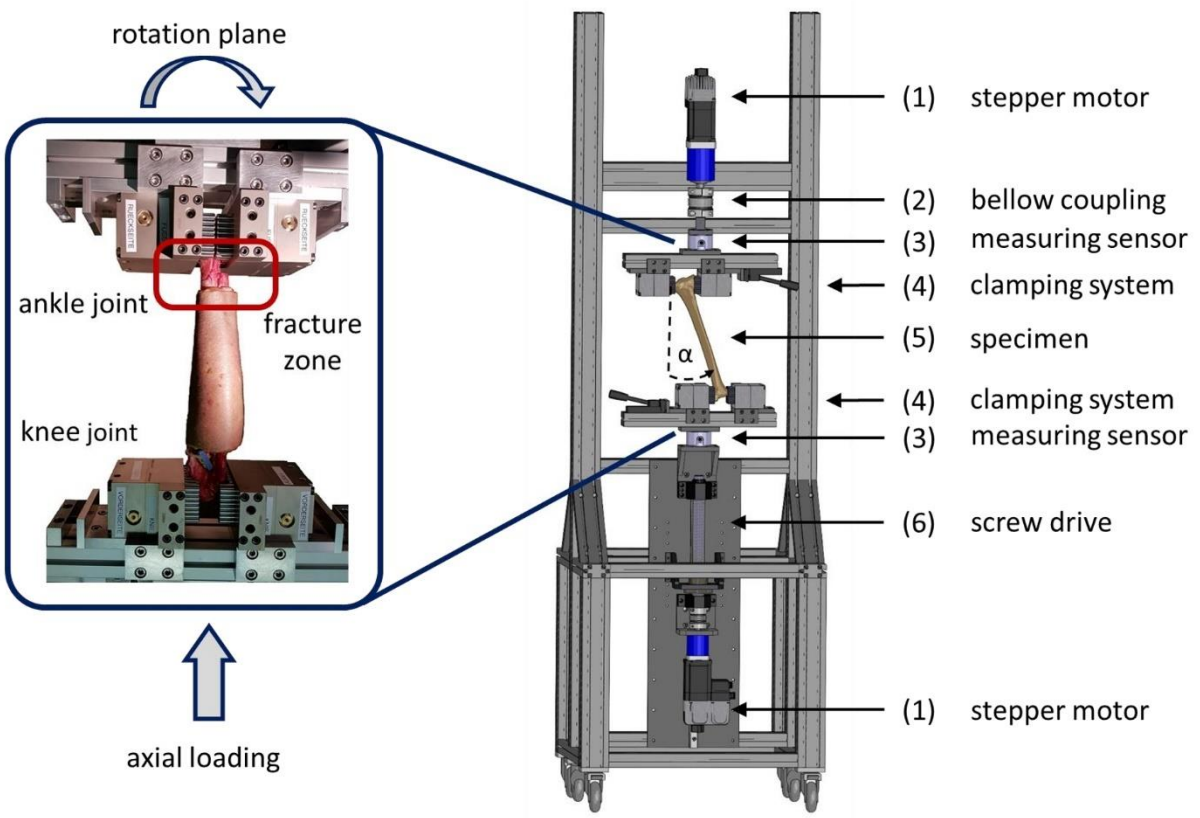


*Figure 5: Schematic representation of the fracture generation experiment. Computer assisted design (CAD) illustration of the testing device (right) with the essential parts and components. Photographic representation of a specimen during the experiment with sketched load and rotation axes (left). The fracture zone at the distal end of the tibia is marked in red.*

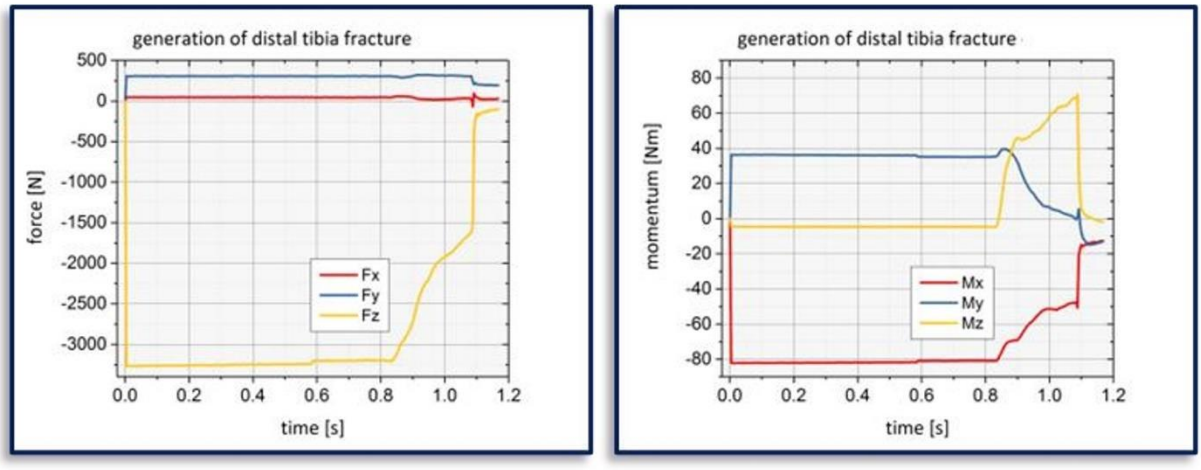


*Figure 6: Result of the fracture generation process. Force values over time with respect to the x-, y- and z-axis (left) and the corresponding momentum values over time (right). Here, the positive x-axis represents the anterior direction, the positive y-axis represents the lateral direction and the positive z-axis points into the axial direction of the tibia.*

## *Implant Design and manufacturing*

A tibia treatment using a patient-specific bone plate was not yet a standard indication at KLS Martin at the time the experiment was conducted. However, it was developed, simulated, and manufactured using the same planning and design routines that are typically standardized for patient-specific forearm treatments and mandibular reconstructions.

Established materials, suitable bone screws with locking threads, and their standardized manufacturing processes were used. This included a titanium alloy Ti-6Al-4V, selective laser melting (SLM) with milled threads for the individualized bone plate, and conventionally machined screws.

The experience gained in the IPS (Individual Patient Solution) field was purposefully applied to ensure that the plate-screw combination tested on the specimen corresponds to a real medical treatment scenario.

## 9.1.2 Experimental and virtual testing of bone-implant systems equipped with the AO Fracture Monitor with regard to interfragmentary movement (Paper 2)

Authors:

**K. Wickert**, M. Roland, A. Andres, S. Diebels, B. Ganse, D. Kerner, F. Frenzel, T. Tschernig, M. Ernst, M. Windolf, M. Müller, T. Pohlemann, and M. Orth

Publication status:

Published in *Frontiers in Bioengineering and Biotechnology*

Citation:

**K. Wickert**, M. Roland, A. Andres, S. Diebels, B. Ganse, D. Kerner, F. Frenzel, T. Tschernig, M. Ernst, M. Windolf, M. Müller, T. Pohlemann, and M. Orth, 'Experimental and virtual testing of bone-implant systems equipped with the AO Fracture Monitor with regard to interfragmentary movement', *Front Bioeng Biotechnol*, vol. 12, 2024, doi: 10.3389/fbioe.2024.1370837.

frontiers | Frontiers in Bioengineering and Biotechnology

TYPE Original Research
PUBLISHED 08 March 2024
DOI 10.3389/fbioe.2024.1370837



OPEN ACCESS

EDITED BY
Alexandros E. Tsouknidas,
University of Western Macedonia, Greece

REVIEWED BY
Meir T. Marmor,
University of California, San Francisco, United States
Hwa Bok Wee,
The Pennsylvania State University, United States

*CORRESPONDENCE
Kerstin Wickert,
kerstin.wickert@uni-saarland.de

RECEIVED 15 January 2024
ACCEPTED 21 February 2024
PUBLISHED 08 March 2024

CITATION
Wickert K, Roland M, Andres A, Diebels S, Ganse B, Kerner D, Frenzel F, Tschernig T, Ernst M, Windolf M, Müller M, Pohlemann T and Orth M (2024), Experimental and virtual testing of bone-implant systems equipped with the AO Fracture Monitor with regard to interfragmentary movement.
*Front. Bioeng. Biotechnol.* 12:1370837.
doi: 10.3389/fbioe.2024.1370837



# Experimental and virtual testing of bone-implant systems equipped with the AO Fracture Monitor with regard to interfragmentary movement

Kerstin Wickert[1]*, Michael Roland[1], Annchristin Andres[1], Stefan Diebels[1], Bergita Ganse[2], Dorothea Kerner[3], Felix Frenzel[3], Thomas Tschernig[4], Manuela Ernst[5], Markus Windolf[5], Max Müller[6], Tim Pohlemann[6] and Marcel Orth[6]

[1]Applied Mechanics, Saarland University, Saarbrücken, Germany, [2]Werner Siemens Endowed Chair of Innovative Implant Development (Fracture Healing), Saarland University, Homburg, Germany, [3]Clinic of Diagnostic and Interventional Radiology, Saarland University Hospital, Homburg, Germany, [4]Institute of Anatomy and Cell Biology, Saarland University, Homburg, Germany, [5]AO Research Institute Davos (ARI), Davos, Switzerland, [6]Department of Trauma, Hand and Reconstruction Surgery, Saarland University Hospital, Homburg, Germany

**Introduction:** The management of fractured bones is a key domain within orthopedic trauma surgery, with the prevention of delayed healing and non-unions forming a core challenge. This study evaluates the efficacy of the AO Fracture Monitor in conjunction with biomechanical simulations to better understand the local mechanics of fracture gaps, which is crucial for comprehending mechanotransduction, a key factor in bone healing. Through a series of experiments and corresponding simulations, the study tests four hypotheses to determine the relationship between physical measurements and the predictive power of biomechanical models.

**Methods:** Employing the AO Fracture Monitor and Digital Image Correlation techniques, the study demonstrates a significant correlation between the surface strain of implants and interfragmentary movements. This provides a foundation for utilizing one-dimensional AO Fracture Monitor measurements to predict three-dimensional fracture behavior, thereby linking mechanical loading with fracture gap dynamics. Moreover, the research establishes that finite element simulations of bone-implant systems can be effectively validated using experimental data, underpinning the accuracy of simulations in replicating physical behaviors.

**Results and Discussion:** The findings endorse the combined use of monitoring technologies and simulations to infer the local mechanical conditions at the fracture site, offering a potential leap in personalized therapy for bone healing. Clinically, this approach can enhance treatment outcomes by refining the assessment precision in trauma trials, fostering the early detection of healing disturbances, and guiding improvements in future implant design. Ultimately, this

study paves the way for more sophisticated patient monitoring and tailored interventions, promising to elevate the standard of care in orthopedic trauma surgery.

KEYWORDS

**experimental biomechanics, biomechanical simulation, bone healing, orthopedic trauma surgery, osteosynthesis, smart implant, patient monitoring**

# 1 Introduction

The treatment of tibial and fibular fractures has seen significant experimental and clinical progress in recent years. However, the rates of delayed bone healing and non-union remain high, posing a substantial challenge to healthcare systems globally (Zura et al., 2016; Dailey et al., 2018). Fractures are a common occurrence in any society, affecting individuals regardless of age, social, or societal status. The majority of these fractures require surgical intervention for stabilization, a practice that has dramatically improved healing outcomes and functional restoration over the past 6 decades (Tzioupis and Giannoudis, 2007; Calori and Giannoudis, 2011).

Despite these advancements, complications such as infection, delayed healing, and non-union can frequently compromise the expected results, leading to increased treatment time, numbers of surgical interventions, and healthcare costs (Augat et al., 2005). The World Health Organization (WHO) identifies trauma as a "major healthcare epidemic," contributing to 16% of the global disease burden. This is due, in part, to the high complication rates up to 10% (Fong et al., 2013) associated with fractures, particularly those of the tibia at the diaphyseal segment (Harris and Lyons, 2005), which are among the most common lower extremity fractures generating high treatment costs in case of non-unions (Dahabreh et al., 2007; Antonova et al., 2013).

The stability of the osteosynthesis plays a crucial role in the healing process. It directly influences interfragmentary movement (IFM), the relative motion between bone fragments (Claes, 2017). Understanding the mechanisms underlying the effects of IFM on fracture healing is of paramount importance in enhancing the treatment and management of fractures, ultimately leading to improved clinical outcomes. The AO Foundation has developed a medical device to record the relative loading of an implant that can be attached to a plate used to treat fractures (Windolf et al., 2022). Their goal is to enable clinical studies in human patients with continuous biomechanical recordings at the fracture site, as well as to improve clinical practice by offering live feedback on the healing progress.

The primary aim of the present study was to establish a link between the 1D continuous measurement signal from the AO Fracture Monitor and the 3D outcome of the corresponding biomechanical simulation regarding the local fracture mechanics within the bone-implant system. To investigate this, the following four hypotheses and methodological aims were formulated:

(1) Digital Image Correlation (DIC) outcomes and the IFM correlate in experiments on cadaveric bone-implant systems conducted in a specialized testing device.
(2) From the data recorded by the AO Fracture Monitor, it is possible to predict the DIC results for the IFM, connecting the implant loading with the fracture gap behavior.
(3) The quality of simulation results can be assessed using the IFM DIC data.
(4) A linear model can be determined for conversion of AO Fracture Monitor data to simulated IFM, transitioning from 1D to 3D.

# 2 Materials and methods

## 2.1 Specimen preparation, surgical procedure and imaging

The cadaveric specimens ($n$ = 3) came from body donations and were fixed with a nitrite pickling salt solution (Janczyk et al., 2011). The specimens were obtained from a male donor (left and right tibia), age of death 56 years, and from a female donor (left tibia), age of death 81 years. The cadaveric tibiae were used to induce osteotomies in the diaphyseal area of the bones. The osteotomies were performed using a regular clinical saw with a thickness of 0.9 mm (Colibri II, DePuy Synthes, Norderstedt, Germany) and were shaped as transverse fractures equivalent to a fracture type 42-A3 according to the AO classification (Müller et al., 1990). The osteotomized bones were then anatomically reduced and stabilized by limited contact-dynamic compression plates (LC-DCP) 4.5/5.0 mm (DePuy Synthes). The resulting gap size was measured between 0.0–0.9 mm in the area of the osteotomy. During osteosynthesis, the plates were first fixated to the bones using cortical screws to induce the dynamic compression (DC) effect according to AO principles (Buckley et al., 2018). Further plate fixations were performed by locking screws. The prepared specimen from the female donor is exemplified in Figure 1C. The three specimens are named as follows throughout this manuscript: $2131_1$ (male donor, left tibia), $2131_2$ (male donor, right tibia) and $2139_1$ (female donor, left tibia).

The geometric models for the biomechanical FE simulations are based on computed tomography (CT) scans conducted from each of the specimens, including a six-rod bone density calibration phantom (QRM-BDC/6, QRM GmbH Moehrendorf, Germany). All bone-implant systems were scanned with a commercially available CT scanner (Somatom Definition AS64, Siemens Healthineers, Erlangen, Germany). The bone-implant systems were placed longitudinally on the CT table with the phantom being positioned under it. Spiral CT acquisitions were performed using the following specifications: tube voltage: 120 kVp, tube current: 95 mA, collimation of 64 × 0.6 mm and a pitch factor

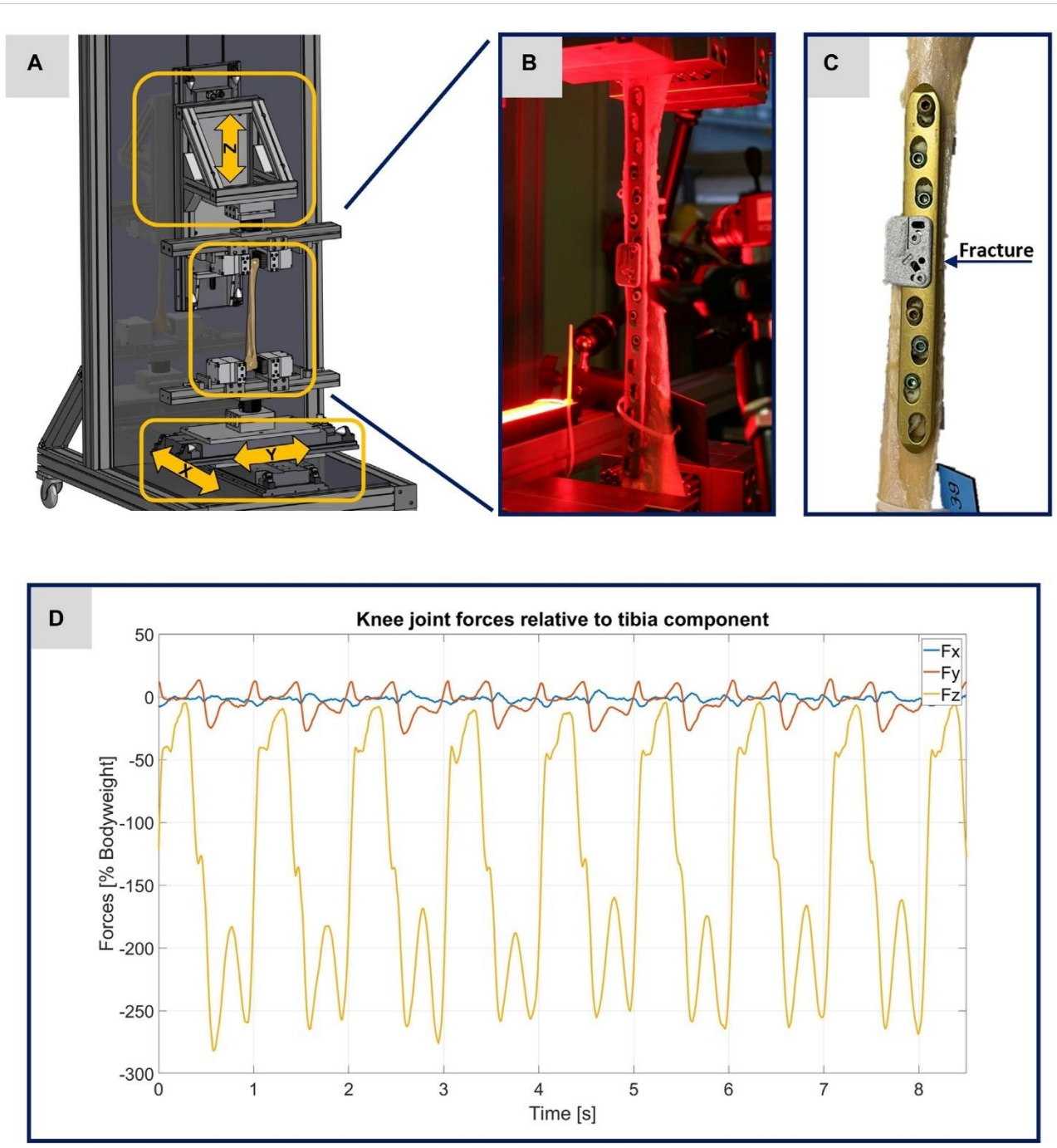


FIGURE 1
Illustration of the experimental setup. **(A)** Computer-aided design representation of the testing device. The three arrows show the direction of movement of the linear modules. **(B)** Photo of a specimen clamped in the testing device before the start of an experiment. **(C)** Photo of the specimen $2139_1$ as exemplary image of the treated tibiae. **(D)** Plot of the original data from the OrtholoadTM database representing the scalable input parameters for the testing device.

of 0.8. Further postprocessing included reconstruction of axial slices with a slice thickness of 3 mm (increment of 2 mm) and 0.6 mm (increment of 0.4 mm) applying a bone reconstruction kernel (B70s) and a soft tissue reconstruction kernel (B31s) respectively.

The AO Fracture Monitor is an active implantable medical device for continuous monitoring of bone fracture healing (Ernst et al., 2021a; Ernst et al., 2021b; Windolf et al., 2022). The AO Fracture Monitor will be attached to conventional bone plates (DePuy Synthes) via two adjacent empty screw holes on the fracture bridging plate segment. A strain gauge measures relative loading of the bone plate. The data are accessed via a Bluetooth connection with the accompanying Smartphone application at a sampling rate of 10 Hz. In normal use, the data are internally processed into relevant metrics and stored on the AO Fracture Monitor. Recorded data are transmitted automatically via Bluetooth

to the patient's smartphone once a day and accessible to the physician via a web application. During the experiments presented here, the data were also recorded at 10 Hz, but were not processed internally, but transferred directly via Bluetooth and smartphone for further downstream analysis.

Before performing the experiments, the AO Fracture Monitor was applied right above the fracture in each of the three specimens. For this purpose, two inserts were attached to the implant with a torque of 4 Nm. The AO Fracture Monitor was fixed in each case to the inserts with two screws (tightening torque 1.5 Nm). Typical placements of the AO Fracture Monitor are illustrated in Figures 1B, C.

For the evaluation of the experiments via DIC, it was necessary to apply a speckle pattern to the specimens. A white spray paint was used to create an even surface. Then a black spray paint was used to create an artificial speckle pattern. To achieve better results and reduce disturbing influences, red light filters were used for the cameras and the specimens were illuminated with red light, cf. Figure 1B.

## 2.2 Mechanical testing device and testing protocol

All experiments were performed using a specially designed testing device. The operational scope of this testing device is to precisely simulate different loading scenarios of treated human tibiae during walking, with the goal to enhance the comprehension of the interplay between bone and implant. To implement the requirements addressed here in the testing device, forces were applied longitudinally (in the $z$-direction) and transversely (in the x- and y-directions) to the bone axis using linear modules, as illustrated in Figure 1A. The maximum possible force applied along the bone axis is limited to 5 kN and the maximum possible stroke is set to 235 mm. Transverse force application is accomplished using two linear modules, responsible for bone displacement in the x- and y-directions, with maximum possible forces limited to 2 kN and maximum possible strokes to 60 mm. The specimens were held in place using an individual flexible mold clamping system, consisting of multiple pins that conformed perfectly to the complex shape of the bone (Silver Clamp X-Clamp, MATRIX GmbH, Ostfildern, Germany). The tibial plateau was secured in the lower clamp, pointed upwards, while the distal epiphysis was clamped to the upper clamp. This type of clamping facilitates the force application with regard to the selected linear modules and their control and regulation technology.

To guarantee the authenticity of the loading scenarios, input parameters from Orthoload™ were used, specifically the dataset from subject k8l_191,211_1_107p (male participant with a body weight of 755.0 N), which exemplifies knee forces during walking on a treadmill for eight steps (Orthoload database, 2023). Each specimen was subjected to two tests, one at full weight bearing representing a normal step forward, and another test at 50% of the forces representing a partial weight bearing scenario. Figure 1D shows the original data from the Orthoload database, which, scaled according to the specifications, were used as input parameters for the testing device.

Throughout the experiments, the testing device mapped the forces from the eight steps of the input file onto the donor bones with a machine velocity of also 10 Hz. During the experiments, a six-axis force sensor (K6D80, ME-Meßsysteme GmbH, Henningsdorf, Germany) was affixed to each mold clamping system for real-time monitoring of the forces exerted. This setup verified the application of force data from the scaled Orthoload™ file at a 10 Hz frequency.

For further experimental analysis, the recording was executed using a two-camera system calibrated for subsequent three-dimensional DIC, with real-time synchronization ensured by a trigger box (DAQhw-Triggereinheit, LIMESS Messtechnik und Software GmbH, Krefeld, Germany) linked to the CompactRIO (C-RIO, National Instruments, Austin, United States). This setup captured the dynamics of the implant surface, the AO Fracture Monitor, and the fracture gap, facilitating a comprehensive optical evaluation. Strain comparisons on the implant and AO Fracture Monitor surfaces, as well as the IFM, were analyzed using the ISTRA 4D 4.4.4.694 software (Dantec Dynamics, Skovlunde, Denmark). The standard deviation in DIC is 1 per thousand (0.001).

## 2.3 Simulation workflow

The geometric models used in this study are based on CT imaging. The dicom image stacks of the treated tibiae including the six-rod bone density calibration phantom were segmented into different masks (bone, implant, fracture, single rods) with an adaptive threshold procedure, supplemented by a morphological close filter with isotropic values, an island removal, a cavity fill, and a mask smoothing with a recursive Gaussian filter with anisotropic values resulting in a high segmentation quality without detectable problems. The segmentation procedure as well as the following meshing strategy were performed in the image processing and model generation software Simpleware™ ScanIP (Synopsys, Mountain View, CA, United States). The material parameters of the osteosynthesis (Young's Modulus: 108,000 MPa, Poisson ratio: 0.375, standard values for medical titanium alloys) (Imam and Fraker, 1996) and the fracture gap (Young's Modulus: 3 MPa, Poisson ratio: 0.4, values for initial connective tissue in fracture healing) (Claes and Heigele, 1999) were chosen from literature as homogeneous parameters.

The material properties of the three tibiae were carefully characterized and calibrated with respect to the data given by the calibration phantom. A four-step procedure was performed to transfer the grayscale values in Hounsfield units (HU) from the CT images to local bone properties. (1) A densitometric relationship defining a mapping to convert raw CT attenuation to bone mineral density (BMD) values was defined for each tibia. Therefore, histograms were generated for each rod of the calibration phantom, reflecting the corresponding grayscale values relative to their voxel count. These histogram curves were then smoothed using a robust local regression method. Curve maxima were used as calibration points for a least square fit, which defines the required mapping of CT data in HU to equivalent mineral density values. (2) In the second step, the ash density values were

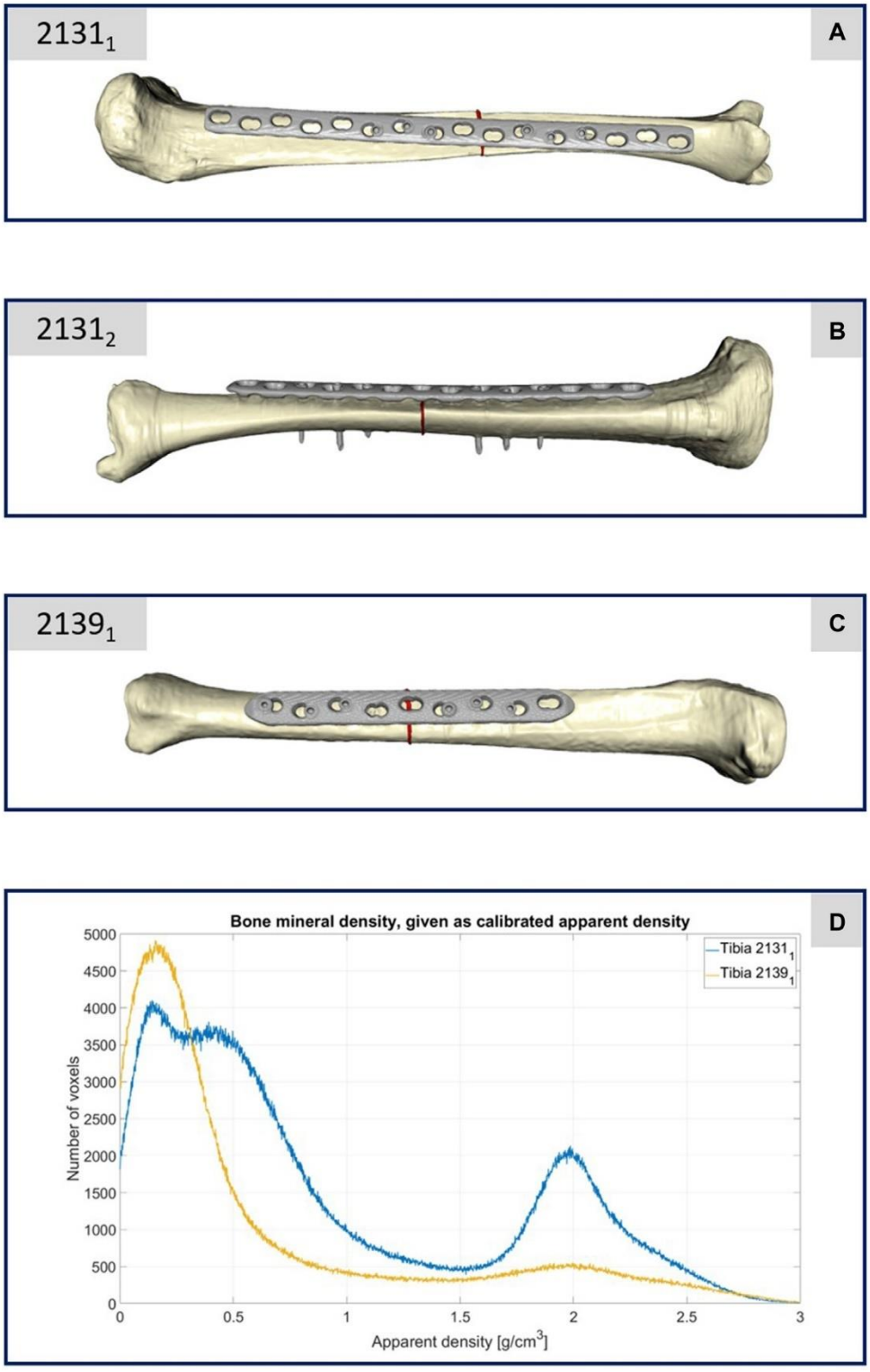


FIGURE 2
**(A–C)** Illustration of the computational models of the three different treated tibiae. **(D)** Plot of the bone mineral density of the two specimens $2131_1$ and $2139_1$ with respect to the apparent density and the corresponding number of CT voxels.

calculated from the equivalent mineral density values via the relationship for hydroxyapatite phantoms from (Eberle et al., 2013). (3) These values were then used to calculate the apparent density values with the conversion formula given in (Edwards et al., 2013). (4) The last step was the mapping to the material parameters via the density-modulus relationship introduced in (Rho et al., 1995).

TABLE 1 Number of mesh cells (quadratic tetrahedral elements of Abaqus type C3D10 with straight edges) per segmented mask.

| | | Specimen | | |
|---|---|---|---|---|
| | | $2131_1$ | $2131_2$ | $2139_1$ |
| Segmented mask | Implant | 179,125 | 201,067 | 149,101 |
| | Fracture | 56,895 | 87,649 | 71,855 |
| | Bone, all material cards | 964,391 | 1,088,442 | 657,814 |

In accordance with the work of (Cattaneo et al., 2001), a total of 25 different bone material cards were defined and stored in the computational meshes. All these computations were performed in Matlab (Matlab 2021b; MathWorks, MA United States). After the material assignment, the areas close to the joints (foot and knee) were also marked in the ScanIP software during the meshing in order to be able to apply the boundary conditions correctly in the simulation environment and thus be able to represent the clamping in the testing device realistically in the simulations. Figures 2A–C shows the generated computational models of the three specimens.

For the meshing strategy, quadratic tetrahedral finite elements of C3D10 type, characterized by straight edges, were chosen and the meshes were adaptively refined with respect to the implants and fracture areas resulting in numbers of mesh cells given in Table 1. All biomechanical FE simulations were performed in the finite element analysis and computer-aided engineering software suite Abaqus (Dassault Systemes, Velizy-Villacoublay, France). Once the three models were imported into Abaqus, the initial step was to align the bone-implant systems properly. The reference for alignment was established using the coordinate system provided by Orthoload™. To mimic the experimental conditions, the second forward step was simulated with careful consideration of the boundary conditions. The boundary conditions were implemented to accurately replicate the experimental setup. Specifically, the x- and y-components of the knee joint force were applied to the tibial plateau, while the z-component remained fixed. At the distal end, the z-component of the knee joint force was applied, while the components in the x- and y-directions were constrained. The simulation proceeded by systematically iterating through all the force values until all the force components of the forward step were effectively accounted for and simulated. This approach ensured a comprehensive analysis of the biomechanical response during the simulated step forward. By meticulously replicating the experimental conditions and considering the appropriate boundary conditions, the simulations provided a valuable opportunity to gain insights into the behavior and response of the bone-implant systems under different loading conditions representing full and partial weight bearing.

## 2.4 Statistical analyses and data processing

For hypothesis 1, we conducted Pearson correlation analyses to assess the relationship between the DIC measurements of the IFM and the implant across all eight experimental steps. Furthermore, we derived mean curves from the collective dataset and adjust these curves at the baseline of zero. Subsequently, we employed linear regression analysis to examine the predictive relationship, treating the implant data as independent variable and the IFM data as the dependent variable.

For hypothesis 2, we conducted a comparative analysis of the data from the AO Fracture Monitor and the corresponding IFM data from the DIC evaluation. The raw data from the eight steps were initially processed to compute their mean curves. This entailed averaging the values across all eight steps at each point in time, providing a representative trend for the collective behavior observed during the experiments. To ensure a common basis for comparison, the mean curves were interpolated across a standardized set of time points, facilitating an accurate correlation and regression analysis between the datasets. The interpolated mean curves were then adjusted to the origin to negate any initial offset and align the starting points of both datasets. Linear regression models were employed to predict the IFM values based on the AO Fracture Monitor data, utilizing the adjusted mean curves. The model's performances were quantified using the mean squared error (MSE) and the coefficient of determination ($R^2$), with a high $R^2$ value indicating a strong predictive capability of the model.

In order to investigate hypothesis 3 and thus to compare the simulation results with the experiments conducted, the following procedure was executed: (1) the displacement data, computed using the DIC analysis software ISTRA 4D, were saved alongside the initial or base lengths of the evaluation lines (refer to Figures 3–5). (2) Both the image data and the DIC results derived from them were calibrated in a manner similar to the AO Fracture Monitor results, considering the beginning of the experiment. (3) The length changes at each time point were computed and compared to the base lengths to ascertain the strains throughout the experiment's duration. (4) Analogous to the lines chosen in the DIC analysis, points were selected on the FE mesh surfaces, and both their coordinates and corresponding displacements were recorded. (5) The saved coordinates were utilized to establish the base lengths of the lines on the FE meshes. The associated displacements were then employed to calculate the changes in length and subsequently the strains. This process provided IFM curves from the simulations, which served as a virtual equivalent to the experimentally obtained IFM curves.

For the comparison of results, mean value curves were calculated from the experimental IFM curves over all eight steps and these were compared with the virtual IFM curves obtained from the simulation. For this purpose, the experimental IFM curves were interpolated to the same time points, since the simulations were performed with a slightly higher time resolution of the forward step than the DIC evaluation. Thereafter, the Euclidean distance and the MSE between the simulated and experimental curves were calculated for all experiments, as well as the Pearson correlation coefficient between the data of the curves.

To explore hypothesis 4, which postulates a correlation of the 1D signal from the AO Fracture Monitor and the simulated 3D local micro-mechanics within the fracture gap, a systematic approach was undertaken. The methodology entailed the computation of the stress and strain tensors at each integration point followed by averaging

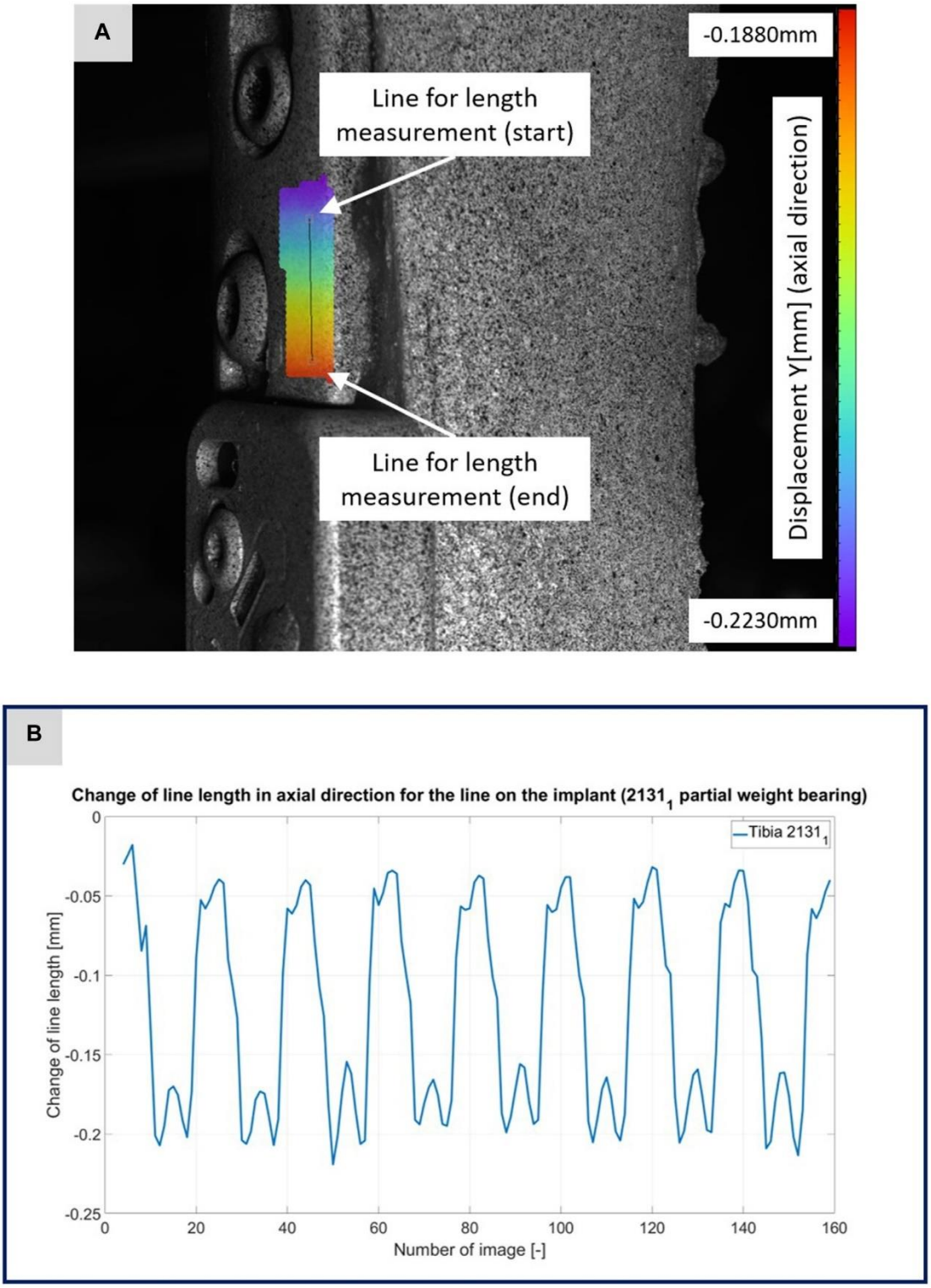


FIGURE 3
**(A)** Illustration of the DIC analysis for a line virtually placed on the implant for specimen $2131_1$. The color bar shows the displacement in axial direction with a minimum value of −0.2230 mm and a maximum value of −0.1880 mm. **(B)** The plotted curve shows the change of the line length over the experiment.

over every mesh cell. Subsequent to this, pertinent strain metrics such as octahedral shear strain and hydrostatic strain were derived, which are essential for the following 3D evaluation of the healing window, cf. (Claes and Heigele, 1999; Shefelbine et al., 2005). Furthermore, to facilitate a comparative analysis with the AO Fracture monitor's 1D output, the strain energy density was also computed. The strain energy density describes the amount of strain energy stored in a material per unit volume due to deformation and

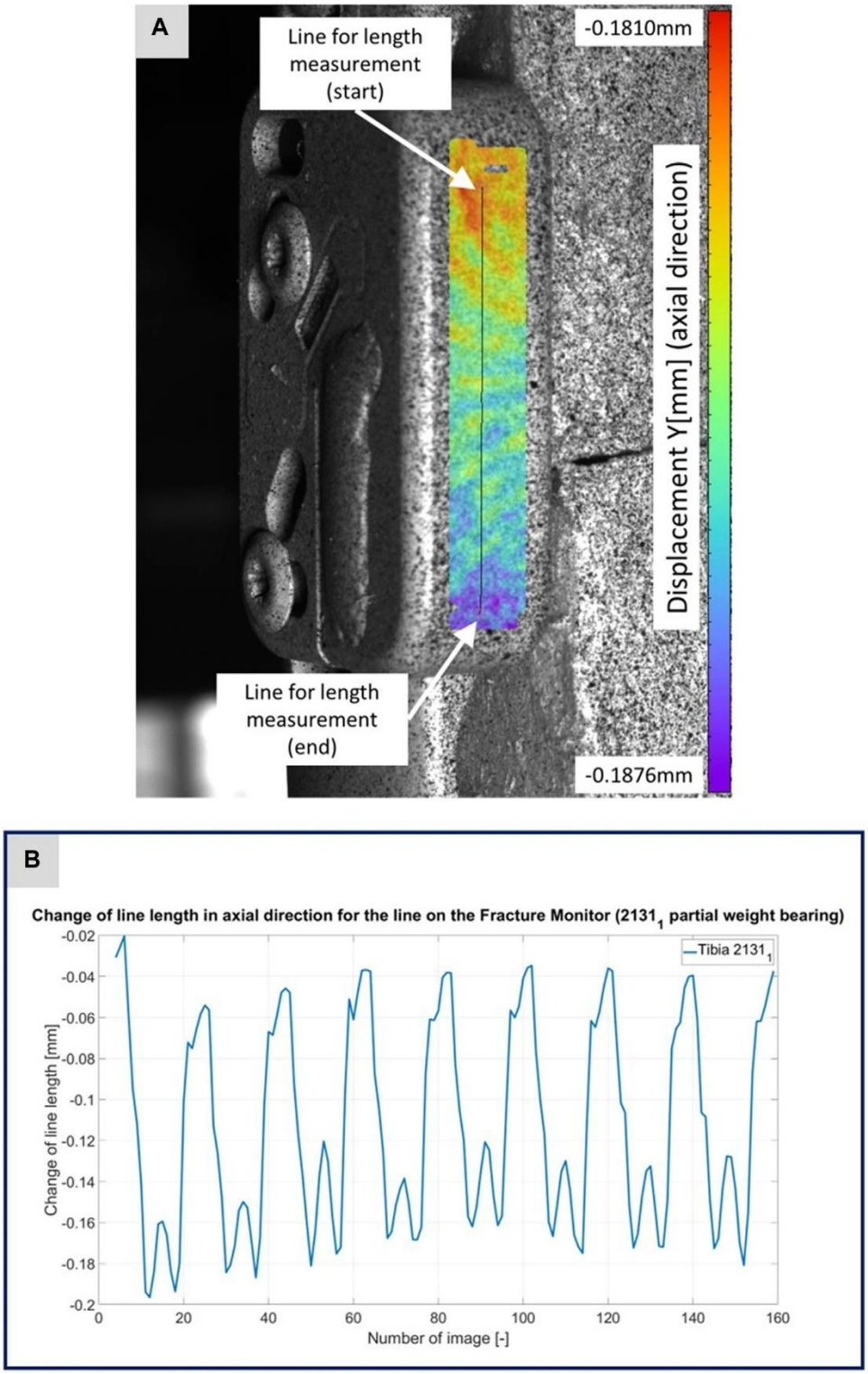


FIGURE 4
**(A)** Illustration of the DIC analysis for a line virtually placed on the Fracture Monitor for specimen $2131_1$. The color bar shows the displacement in axial direction with a minimum value of −0.1876 mm and a maximum value of 0.1810 mm. **(B)** The plotted curve shows the change of the line length over the experiment.

is a comparative measure offering benefits for analyzing bone-implant systems. It simplifies complex data from 3D simulations into a scalar value without losing crucial information and therefore acts as a unified metric that effectively captures multi-axial strain states. Statistical values, including sum, mean, median, maximum, interquartile range (IQR) and 90th percentile (90th PRC) of the

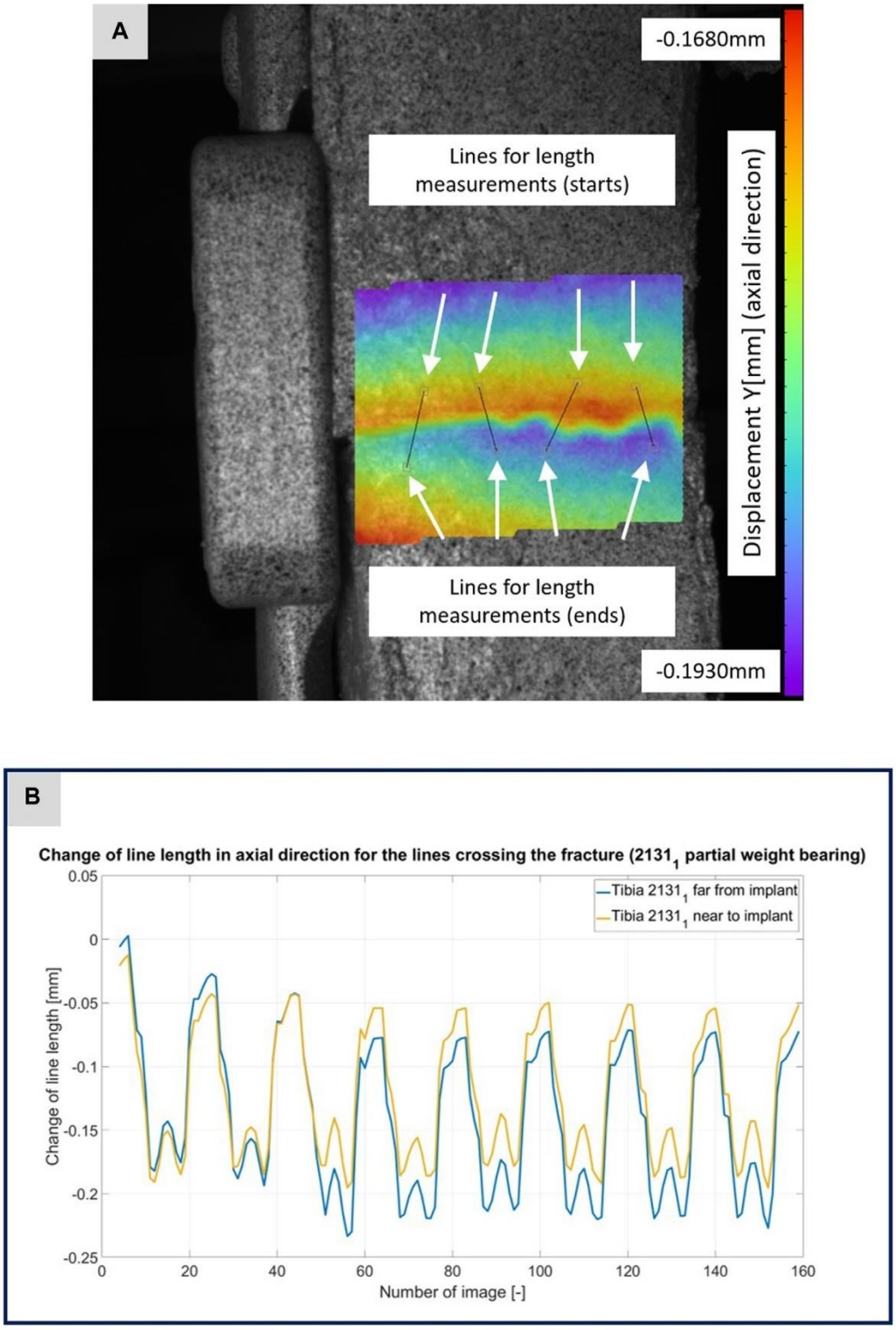


FIGURE 5
**(A)** Illustration of the DIC analysis for four lines virtually placed across the fracture gap for specimen 2131$_1$. The color bar shows the displacement in axial direction with a minimum value of −0.1930 mm and a maximum value of −0.1680 mm. **(B)** The plotted curves show the change of the line lengths over the experiment for the line near to implant and the line far from implant.

strain energy density, were computed across the fracture gap. These measures were then cross-correlated with the AO Fracture Monitor's mean value curves from the corresponding experiments. In addition, linear regressions were computed to predict the statistical values of the strain energy density from the AO Fracture Monitor mean curves.

TABLE 2 Correlation coefficients from a Pearson test for the DIC data evaluated for the implant and for the IFM. All correlations are significant at the 0.01 level.

| Step | Specimen | | | | |
|---|---|---|---|---|---|
| | $2131_1$ | | $2131_2$ | | $2139_1$ |
| | Full weight bearing | Partial weight bearing | Full weight bearing | Partial weight bearing | Partial weight bearing |
| 1 | 0.9899 | 0.9989 | 0.9592 | 0.9989 | 0.9980 |
| 2 | 0.9839 | 0.9902 | 0.9348 | 0.8887 | 0.8986 |
| 3 | 0.9948 | 0.9505 | 0.8548 | 0.9993 | 0.9965 |
| 4 | 0.9845 | 0.9995 | 0.9243 | 0.9996 | 0.9965 |
| 5 | 0.9918 | 0.9991 | 0.8548 | 0.9995 | 0.9969 |
| 6 | 0.9911 | 0.9991 | 0.8719 | 0.9997 | 0.9967 |
| 7 | 0.9835 | 0.9995 | 0.8932 | 0.9997 | 0.9975 |
| 8 | 0.9871 | 0.9989 | 0.8608 | 0.9996 | 0.9963 |

# 3 Results

## 3.1 Experimental results

Each specimen was subjected to the two described loading scenarios, representing the forces for a step forward with full weight bearing and with 50 percent of the forces describing a step forward with partial weight bearing. During the experiment under full weight bearing, one of the three specimens (specimen $2139_1$) failed and fractured inside the clamping system.

The CT scan data of this specimen confirmed its lower bone mineral density, as depicted in Figure 2D. This figure compares the bone mineral density as apparent density over the number of voxels between specimens $2139_1$ and $2131_1$, highlighting considerably reduced density in $2139_1$, particularly in areas typically dense in cortical bone. This discrepancy is attributed to the older age and different sex of the donors, with $2139_1$ being from an elderly female and $2131_1$ from a middle-aged male. Given the negligible difference in density between the male donor's limbs, only one was depicted in Figure 2D. Thus, specimen $2139_1$ underwent testing only with a decreased load, representing partial weight bearing.

Figures 3–5 illustrate the DIC analyses process. Figure 3 displays the axial displacement for a small section of the implant surface. The timing of this snapshot corresponds to the moment when the axial force specification reached its maximum during the second step in the input data. In addition to the displacement field, the temporal change in line length throughout the entire experiment was plotted as a curve (Figure 3B). This curve mirrors the progression of the force specification (input parameter of the testing device) as depicted in Figure 1D. The typical double-peak structure with its two maxima is visible in the curve. Figure 4 displays the axial displacement field on the lateral surface of the AO Fracture Monitor at the same time point. Analogous to Figure 3, the plot of the line length change over the entire course of the experiment also shows the double-peak curve for the eight steps from the input file. In contrast to the length change on the implant surface, there are larger differences in the data of the individual steps here. This could be due to the fact that the AO Fracture Monitor, as described, was screwed onto the implant, thereby creating a connection with a small amount of play between the force application and the measurement surface. Figure 5 presents the result of the length change of the same specimen $2131_1$ at the same time point as Figures 3, 4. The two plotted lines represent the length change near the implant and the length change of the line furthest from the implant, respectively. Again, the double-peak pattern is evident, analogous to the other results. However, it can be observed that the line length at the end of the experiment did not return as far towards the initial length as in the case of the implant. This could be due to the fact that the fracture gap was empty and not filled with a suitable material.

For hypothesis 1, Table 2 presents Pearson correlation coefficients that revealed a significant linear relationship at the 0.01 level between the DIC results for the implant and the IFM for all specimens. The consistently high coefficients across all steps, particularly under partial weight bearing conditions, indicate a strong adherence to the force application protocol. Specimen $2139_1$, tested only under a reduced load, showed significant correlation values exceeding 0.89, underscoring the reliability of the experimental design.

Based on the high correlation coefficients, the linear regressions between the mean curves of the DIC results were computed for all five experiments. For this purpose, the mean curves were adjusted with respect to the origin, which is due to the slightly different setup weight of the testing device, which partially (clamping, holder, etc.) loads on the specimen. Figure 6 illustrates this procedure exemplarily for specimen $2131_1$ as the other experiments and specimens show very similar results. All linear regression functions are listed in Table 3 and show a strong linear regression for each specimen under full and partial weight bearing conditions. Notably, specimen $2139_1$ under partial weight bearing presented the highest correlation ($R^2 = 0.9995$), indicating an almost perfect linear relationship. These regressions provide a reliable model for predicting the IFM based on implant surface strain data received by DIC evaluation. The slopes of the regression

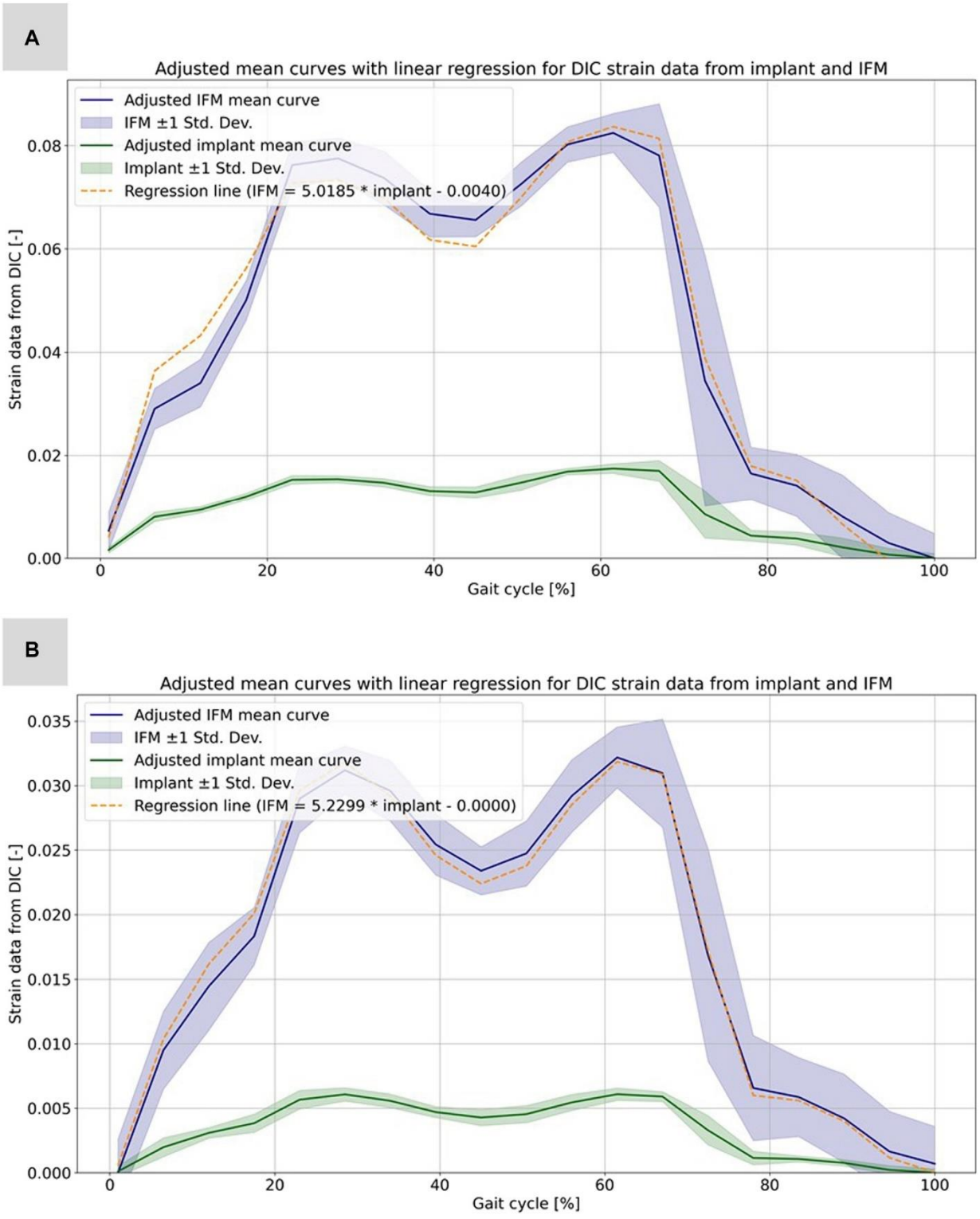


FIGURE 6
Illustration of the calculated strain data from the evaluation of the DIC data for the implant and the IFM for specimen $2131_1$. **(A)** Full weight bearing experiment: mean curves for the IFM and the implant data together with shaded error bars representing one standard deviation and the linear regression as dashed line. **(B)** Partial weight bearing: same curves over the full gait cycle.

lines vary only between 5.0185 and 5.6297 for the two specimens $2131_1$ and $2131_2$. This is expected, as both bones came from the same donor, were exposed to the same loading conditions and had similar fractures and treatments. Nonetheless, the substantial difference in the value of $2139_1$, which stands at 10.2688, precludes the possibility of making broad generalizations in this context.

TABLE 3 Functions of the linear regression (cf. Table 2) including the coefficient of determination $R^2$.

| Specimen | Loading | Linear regression | $R^2$ |
|---|---|---|---|
| $2131_1$ | Full weight bearing | IFM = 5.0185 * implant—0.0040 | 0.9799 |
| | Partial weight bearing | IFM = 5.2299 * implant—0.0000 | 0.9949 |
| $2131_2$ | Full weight bearing | IFM = 5.0689 * implant—0.0162 | 0.8504 |
| | Partial weight bearing | IFM = 5.6297 * implant—0.0002 | 0.9984 |
| 21391 | Partial weight bearing | IFM = 10.2688 * implant—0.0008 | 0.9995 |

TABLE 4 Results of the linear regression analysis for the AO Fracture Monitor data (FM) and the corresponding experimental IFM data. The table shows the correlation coefficient between the datasets, the mean square error, the coefficient of determination $R^2$, and the linear regression to compute the IFM from the corresponding FM data for all five experiments.

| Specimen | Loading | Correlation coefficient | MSE | $R^2$ | Linear regression |
|---|---|---|---|---|---|
| $2131_1$ | Full weight bearing | 0.8673 | 3.06e-05 | 0.9799 | IFM = 3.025e-04 * FM + 0.01321 |
| | Partial weight bearing | 0.8954 | 3.27e-05 | 0.9949 | IFM = 2.111e-04 * FM + 0.00452 |
| $2131_2$ | Full weight bearing | 0.9921 | 3.19e-05 | 0.8504 | IFM = 1.468e-03 * FM—0.08425 |
| | Partial weight bearing | 0.9887 | 1.96e-05 | 0.9984 | IFM = 9.476e-04 * FM + 0.01128 |
| 21391 | Partial weight bearing | 0.9901 | 1.14e-05 | 0.9995 | IFM = 5.227e-04 * FM + 0.00803 |

The experiments conducted with the AO Fracture Monitor delivered seamless signal monitoring throughout the entire process. Utilizing the live mode feature, the data was recorded in real time and could be accessed and followed on a smartphone through Bluetooth technology. Furthermore, the datasets were transmitted to a cloud server with a time stamp after every measurement, processed and sent back for analysis. For hypothesis 2, the regression analysis revealed significant linear relationships between AO Fracture Monitor and IFM datasets, as evidenced by the high correlation coefficients and the close fit of the regression models to the observed data, cf. Table 4. The analysis under full weight bearing conditions for specimen $2131_1$ showed a correlation coefficient of 0.8673 with an MSE of 3.06e-05 and an $R^2$ of 0.9799. Under partial weight bearing, the correlation coefficient improved to 0.8954, with a slightly higher MSE of 3.27e-05 and an improved $R^2$ of 0.9949.

For Specimen $2131_2$, the full weight bearing condition yielded a very high correlation coefficient of 0.9921, an MSE of 3.19e-05, and a lower $R^2$ of 0.8504 compared to partial weight bearing, which demonstrated a correlation coefficient of 0.9887, an MSE of 1.96e-05, and a very high $R^2$ of 0.9984, indicating a near-perfect fit. Specimen $2139_1$, which was only evaluated under partial weight bearing, exhibited a correlation coefficient of 0.9901, with the lowest MSE in the dataset at 1.14e-05, and the highest $R^2$ value of 0.9995, denoting an almost exact predictive relationship in the regression model. Figure 7 shows all five regressions. The relatively high quality of the predictions is particularly evident in Figures 7C, D. However, the values of the straight-line slopes for samples $2131_1$ and $2131_2$ are not as similar as for the linear regressions for the different DIC evaluations.

The idea of computing these linear regressions was to link the measurements of the IFM from DIC and the AO Fracture Monitor to provide a better understanding of the IFM in clinical patients where additional data to the AO Fracture Monitor signal is neither available nor measurable. Figure 7E shows exemplarily the AO Fracture Monitor data for specimen $2131_1$ for full and partial weight bearing.

The curves were adjusted to the origin, as the AO Fracture Monitor only measures relative changes and the implant load is subject to slight variations at the start of the experiments due to the setup weight of the testing device, which partially (clamping, holder, etc.) also loads on the specimen. Figure 7E clearly reproduces double-peak stance-phase curve, cf. Figure 1D of the knee joint forces. In addition, the difference between full and partial weight bearing is visible and is around 1.79, i.e., slightly less than the expected factor of 2, but of the same order of magnitude as for specimen $2131_2$.

## 3.2 Biomechanical simulation results

Figures 8A–E depicts the simulation results at the moment of peak axial loading during the forward step. This figure specifically highlights the von Mises stress distribution on the implant in each case, since these key indicators have a high informative value with regard to a possible implant failure. Notably, even at the zenith of axial loading during full weight bearing and naturally during reduced partial weight bearing, the stress values peak at only 200 GPa. These peak values are localized above the fracture during full weight bearing and remain well below the stress thresholds that might induce failure.

Figures 9A–E presents a comparison between the IFM derived from the DIC of the experiments (refer to Figure 5) and the results from the simulations. The blue curves depict the average IFM across all eight steps, with the band indicating the standard deviation from the experiments. In contrast, the orange curves represent the

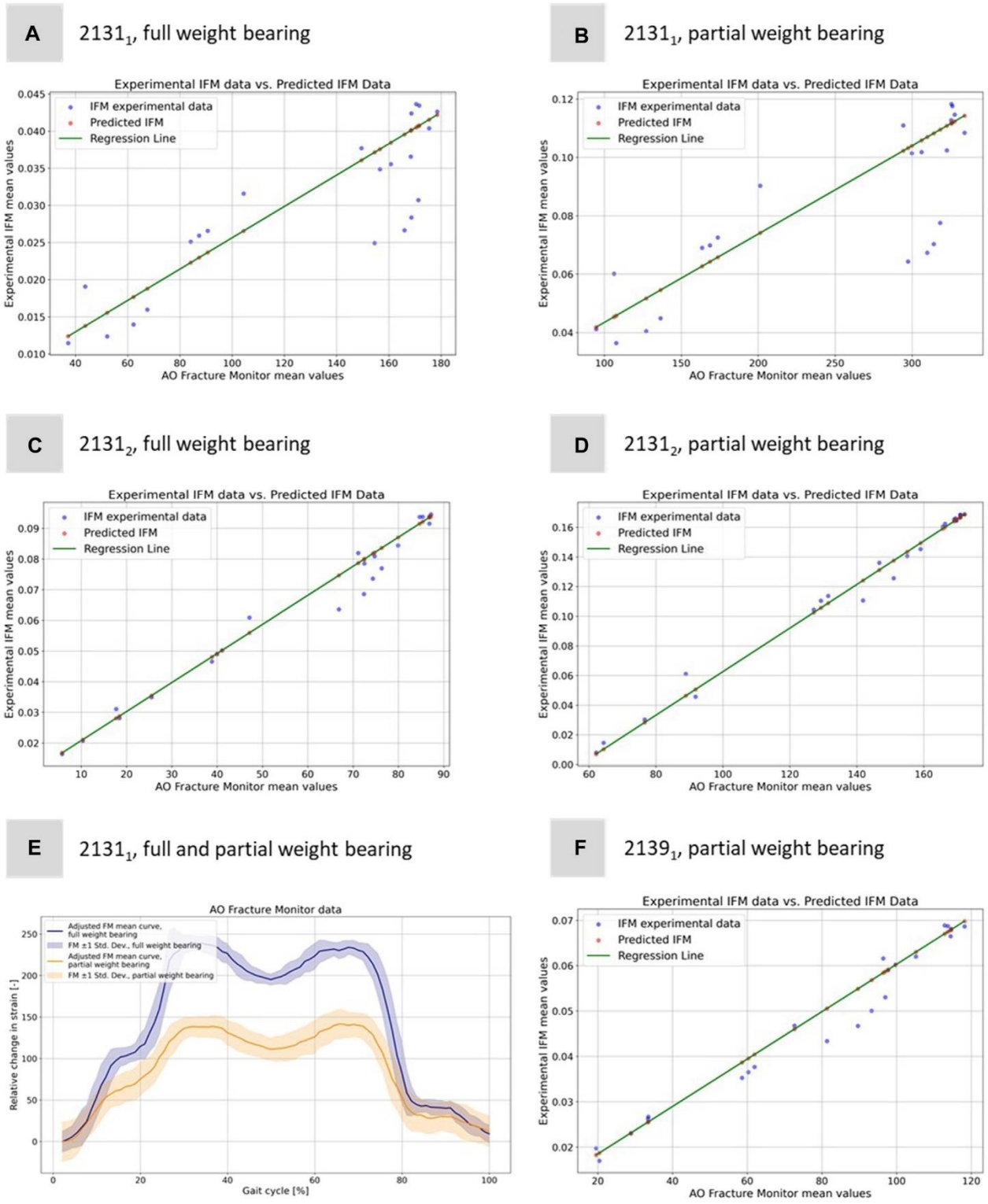


FIGURE 7
Illustration of the regression model to predict the experimental IFM data from the corresponding 1D AO Fracture Monitor data. Results for **(A)** specimen 2131$_1$ under full weight bearing, **(B)** specimen 2131$_1$ under partial weight bearing, **(C)** specimen 2131$_2$ under full weight bearing, **(D)** specimen 2131$_2$ under partial weight bearing, and **(F)** specimen 2139$_1$ under only partial weight bearing. **(E)** Exemplary adjusted AO Fracture Monitor data for specimen 2131$_1$ for full and partial weight bearing.

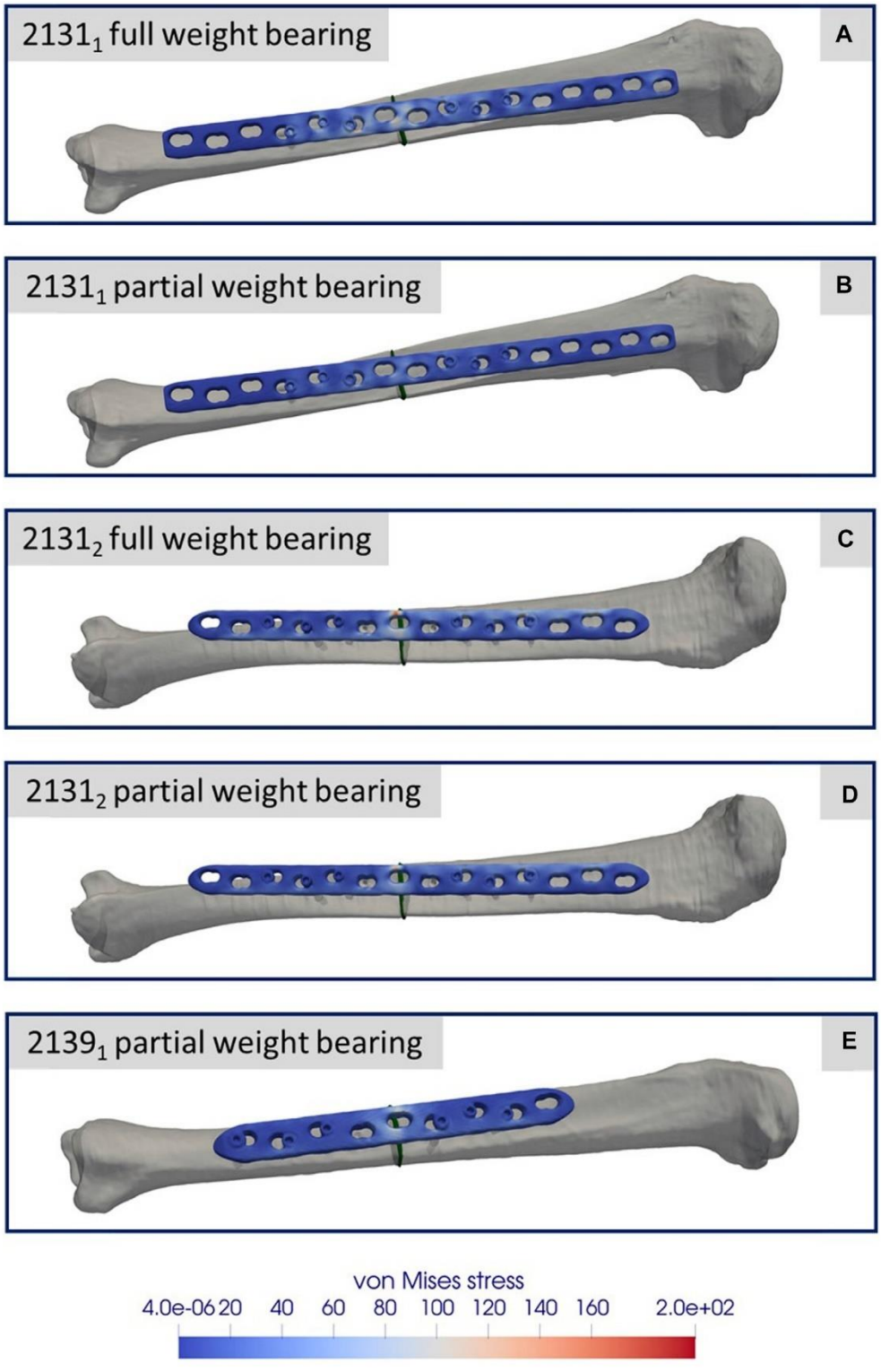


FIGURE 8
Simulation results for the three different specimens and the considered weight bearing cases **(A–E)**. All images show the von Mises stress distribution of the implant at the time point of the maximal axial force during a normal step forward.

simulation results. Specifically, in Figures 9A, B for specimen $2131_1$, the simulation values exceeded those of the experiments. This discrepancy might arise from minor differences in the specimen's orientation between the experiment and the simulation. While simulations ensure optimal alignment, clamping, and force transmission, experiments might introduce slight inaccuracies due to potential errors in these areas. However, the curves still closely resemble the experimental outcomes. For Figures 9C, D,

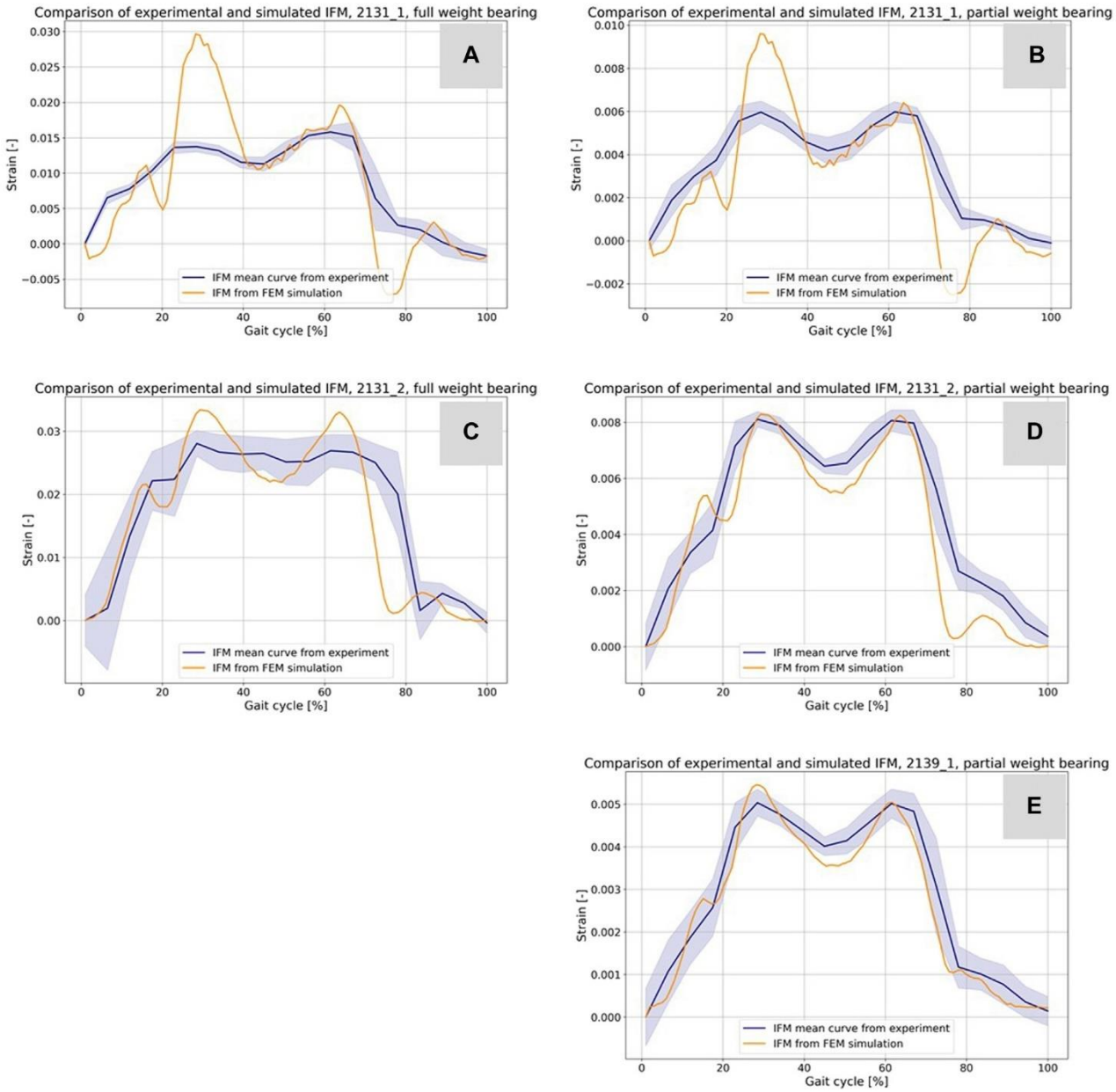


FIGURE 9
Comparison of the IFM from DIC of the experiments (cf. Figure 5) and the corresponding result based on the simulations **(A–E)**. The curves combined with a band representing the standard deviation show the experimental results and the orange curves show the counterpart from the simulations.

**TABLE 5 Results for the comparison of the virtual IFM curves from the simulations and the mean IFM curves from the experiments. The table shows the Euclidean distance and the MSE as distance measure between the curves of every experiment, illustrated in Figure 9, and the correlation coefficient from a Pearson test of the data from the curves.**

| Specimen | Loading | Euclidean distance | MSE | Correlation coefficient |
|---|---|---|---|---|
| $2131_1$ | Full weight bearing | 0.05785 | 3.38e-05 | 0.8401 |
| | Partial weight bearing | 0.01800 | 3.27e-06 | 0.8726 |
| $2131_2$ | Full weight bearing | 0.05898 | 3.51e-05 | 0.8727 |
| | Partial weight bearing | 0.01202 | 1.46e-06 | 0.9495 |
| $2139_1$ | Partial weight bearing | 0.00408 | 1.68e-07 | 0.9813 |

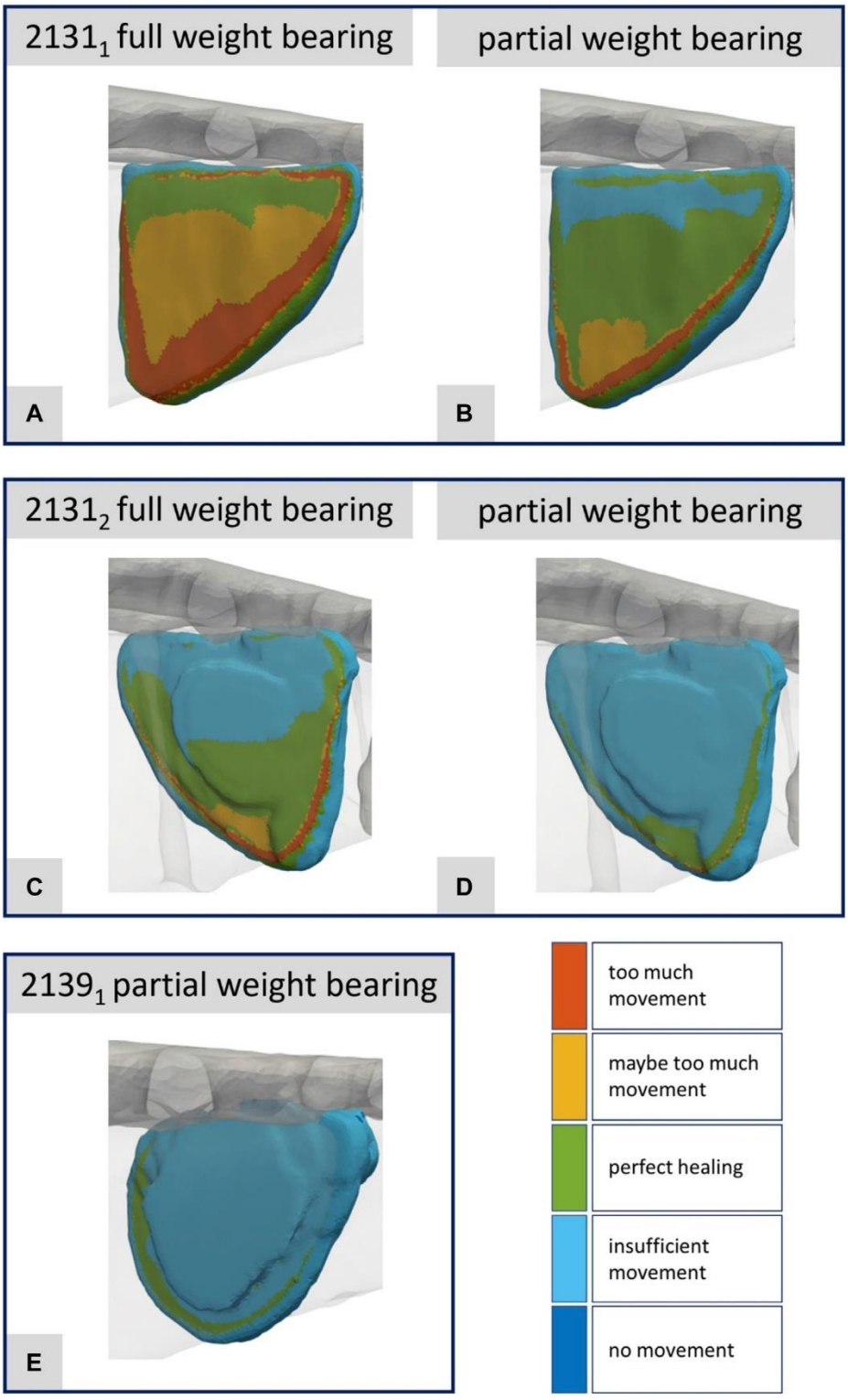


FIGURE 10
Illustration of the strain-based healing window for all fractures at the time point of the maximal axial force during a normal step forward **(A–E)**. Corresponds to Figures 8A–E.

concerning sample 2131$_2$, the simulation closely mirrors the experimental results. Moreover, Figure 9E for sample 2139$_1$ showcases an excellent match between experimental and simulation results.

Table 5 shows additional statistical values for the curves in Figure 10 and enables an evaluation of hypothesis 3. The data provided includes Euclidean distances, MSE, and Pearson correlation coefficients for all experiments. For specimen 2131$_1$

TABLE 6 Results for the evaluation of the 3D simulations reduced to the strain energy density inside the fracture gap and the 1D relative strain signal from the AO Fracture Monitor from the corresponding experiments.

| Specimen | Loading | Statistical value | Euclidean distance | MSE | $R^2$ | Correlation coefficient | Linear regression |
|---|---|---|---|---|---|---|---|
| $2131_1$ | Full weight bearing | 90th PRC | 0.0274 | 1.203e-06 | 0.6716 | 0.8204 | 4.8802e-05 * x—0.00086 |
| | | MEAN | 0.0102 | 1.191e-06 | 0.6728 | 0.8202 | 1.8358e-05 * x—0.00032 |
| | | IQR | 0.1030 | 8.408e-06 | 0.6716 | 0.8195 | 1.8399e-05 * x—0.00025 |
| | Partial weight bearing | 90th PRC | 0.0276 | 8.608e-06 | 0.6654 | 0.8157 | 8.7492e-05 * x—0.00141 |
| | | MEAN | 0.0104 | 1.218e-06 | 0.6654 | 0.8157 | 3.2921e-05 * x—0.00052 |
| | | IQR | 0.0104 | 1.215e-06 | 0.6683 | 0.8175 | 3.3096e-05 * x—0.00046 |
| $2131_2$ | Full weight bearing | 90th PRC | 0.0241 | 6.543e-06 | 0.7456 | 0.8635 | 1.1727e-04 * x—0.00229 |
| | | MEAN | 0.0090 | 9.184e-07 | 0.7478 | 0.8648 | 4.4191e-05 * x—0.00086 |
| | | IQR | 0.0089 | 8.849e-07 | 0.7585 | 0.8709 | 4.4644e-05 * x—0.00082 |
| | Partial weight bearing | 90th PRC | 0.0235 | 6.185e-06 | 0.7598 | 0.8715 | 1.6627e-04 * x—0.00213 |
| | | MEAN | 0.0088 | 8.746e-07 | 0.7598 | 0.8717 | 6.2574e-05 * x—0.00079 |
| | | IQR | 0.0088 | 8.754e-07 | 0.7611 | 0.8724 | 6.2822e-05 * x—0.00073 |
| $2139_1$ | Partial weight bearing | 90th PRC | 0.0199 | 4.464e-06 | 0.8264 | 0.9091 | 1.3691e-04 * x—0.00147 |
| | | MEAN | 0.0075 | 6.289e-07 | 0.8273 | 0.9096 | 5.1543e-05 * x—0.00055 |
| | | IQR | 0.0074 | 6.193e-07 | 0.8310 | 0.9116 | 5.1818e-05 * x −0.000488 |

under full weight bearing, the Euclidean distance is 0.05785 with an MSE of 3.38e-05 and a correlation coefficient of 0.8401, indicating a substantial positive correlation between the experimental and simulation data. The performance under partial weight bearing shows improved correlation at 0.8726 with reduced Euclidean distance and MSE, suggesting greater accuracy in the simulations under these conditions. Specimen $2131_2$ mirrors this trend, with even higher correlations under partial weight bearing, particularly a correlation coefficient of 0.9495, signifying a very close match between the simulated and experimental data. Specimen $2139_1$, tested only under partial weight bearing, shows an outstanding correlation of 0.9813, the highest among the samples, along with the lowest Euclidean distance and MSE values. These metrics collectively indicate a strong alignment between the simulated and experimental curves, especially under partial weight bearing, thus supporting hypothesis 3, which posits that the simulation model accurately predicts the behavior of the specimens under varying load conditions.

Figures 10A–E presents the corresponding data for the fracture gap with regard to the strain-based healing window as originally defined by Claes and Heigele (1999) and later by Shefelbine et al. (2005). The color-coded representation demarcates the different fracture regions: areas with too much movement or strain (red), areas likely experiencing too much movement or strain (yellow), and regions identified as beneficial for healing (green). One can clearly see the difference between full and partial weight bearing. For specimen $2131_1$ in particular, large areas change from too much movement to areas favorable for healing when the load input is reduced from full to partial weight bearing. This innovative fracture analysis approach was first showcased in Orth et al. (2023) drawing from a real clinical case and building upon concepts introduced by Braun et al. (2021).

To investigate hypothesis 4, Table 6 presents the evaluation results comparing 3D simulations, reduced to strain energy density within the fracture gap, to 1D relative strain signals from the experiments using the AO Fracture Monitor. For specimen $2131_1$, under full weight bearing, 90th PRC had a Euclidean distance of 0.0274 and an $R^2$ of 0.6716, with a correlation coefficient of 0.8204, suggesting a moderate to strong linear relationship as indicated by the regression function. The mean and IQR show similar levels of correlation. The same applies to the quantity's

maximum, median and sum, so that these have been omitted for the sake of clarity. Under partial weight bearing, the 90th PRC slightly increased to 0.0276 with a small reduction in correlation, whereas the mean and IQR values had minimal change. Specimen $2131_2$ showed a better fit in the full weight bearing condition with a PRC Euclidean distance of 0.0241 and a higher $R^2$ of 0.7456, and an even stronger correlation coefficient of 0.8635. The regression model for PRC indicates a strong predictive relationship. The mean and IQR also displayed strong correlations, with the IQR yielding the highest $R^2$ of 0.7585 under full weight bearing. Partial weight bearing conditions for this specimen also showed strong correlations, with $R^2$ values exceeding 0.7598 across statistical values.

For specimen $2139_1$, only partial weight bearing data is available, which shows the strongest correlations among the three specimens. The PRC Euclidean distance is 0.0199 with an $R^2$ of 0.8264 and a correlation coefficient of 0.9091. The mean and IQR similarly show strong correlations, with $R^2$ values above 0.8273 and tightly clustered regression coefficients. These results suggest that the strain energy density derived from 3D simulations correlates well with the 1D experimental strain signals, and the linear regression models provide a good predictive relationship between the simulated and experimental data.

## 4 Discussion

The present study confirmed a significant correlation between the surface strain data of the implant and the IFM as both were derived from the same experiments evaluated via DIC (hypothesis 1). It also established that the 1D measurements captured by the AO Fracture Monitor could predict the IFM measured by DIC, thus linking the implant loading to the behavior of the fracture gap (hypothesis 2). Additionally, the study showed that the simulation results could be reliably evaluated using the experimental DIC data for IFM, especially under partial weight bearing conditions (hypothesis 3). Finally, a strong connection was found between the AO Fracture Monitor's signals and the simulated IFM, which enabled a transition from 1D to 3D understanding via the strain energy density within the bone-implant system, with linear regression models providing a strong predictive relationship (hypothesis 4). These results, in turn, may be used for clinical application analyses of the AO Fracture Monitor in translational studies.

Both the experiments performed and the simulations based on them are subject to various limitations and few simplifications made. One simplification that had to be made is the use of knee forces from the Orthoload database. These represent the data of the selected patient (k8l) and are only a simplifying assumption as knee forces for the bone donors. In addition, the body weight of the donors was not known, so the body weight of the patient selected from the Orthoload database was adopted here as a simplification. In retrospect, this might have been chosen too high for sample $2139_1$ and could be the reason for the failure of the osteoporotic bone under high weight bearing conditions. Another difficulty that always arises in this type of experiment is the clamping of the specimens. Since bones as a biological and a natural grown structure have a relatively complex geometry compared to standard industrial specimens, a good clamping and alignment of the specimens is challenging. This potentially leads to minor errors in both axial alignment ($z$-axis) and in maintaining the x- and $y$-axes of the clamped bones. The corresponding bone areas are marked in the simulation and the boundary conditions are set there in analogy to the real test execution. Inaccuracies may occur due to the possible slightly offset of the angles caused by the alignment of the specimens and the perfectly aligned simulation models.

Another limitation is the load input to the bone-implant system from the clamping itself and the associated machine setup that occurs as a type of preload or bias and is reflected in the AO Fracture Monitor data because the AO Fracture Monitor cannot technically perform a calibration step after the specimens are installed. The manual calibration step of the AO Fracture Monitor was always done before the start of the particular testing protocols after the installation of the specimens and the alignment and calibration of the camera system. If it were technically possible to combine the calibration step of the AO Fracture Monitor and its data acquisition with the triggering of the testing device, the significance of the data and its subsequent use could be increased even further.

Within the evaluation of the DIC and the software used for this purpose, averaging processes take place that cannot be fully represented in the simulation evaluation. The goal to compare the results of the simulations with the results of the experiments as good as possible can be influenced by using analysis software and the processes running in it. The biomechanical FE simulations were limited to only one step and do not represent all eight steps used as input data in the testing device. This restriction was made because the amount of data for one step in the output database (ODB) files from Abaqus is already up to 100 Gigabyte, making the evaluation time and memory intensive. When simulating the entire input data, the ODB files then reach a size of 800 Gigabyte per specimen and load case, which exceeds the available computer capacity for the evaluation process.

We are aware that the conclusions are drawn from only a small number of experiments, and more experiments from a larger number of donors will have to be provided to further analyze and strengthen the results and associations. Nevertheless, the outcomes of this study suggest that patient-specific simulations in conjunction with the AO Fracture Monitor measurements provide a viable method for assessing the local mechanics within a fracture gap, which is pivotal for understanding mechanotransduction. This methodology can enrich clinical outcomes by enabling personalized healing strategies, refining prognostic accuracy in trauma trials, and offering a sophisticated approach for early detection and intervention in cases of healing complications. Moreover, it has the potential to guide the enhancement of the design of trauma implants, thus improving overall patient care in orthopedic trauma surgery.

## Data availability statement

The original contributions presented in the study are included in the article/supplementary material, further inquiries can be directed to the corresponding author.

## Ethics statement

The ethics committee of Saarland Medical Board has approved the present study using human cadaveric specimens (Aerztekammer des Saarlandes, Germany, application number 146/21). The studies were conducted in accordance with the local legislation and

institutional requirements. The human samples used in this study were acquired from Samples were obtained from body donations at Saarland University. Written informed consent for participation was not required from the participants or the participants' legal guardians/next of kin in accordance with the national legislation and institutional requirements.

## Author contributions

KW: Writing–original draft, Writing–review and editing, Conceptualization, Data curation, Formal Analysis, Investigation, Methodology, Visualization. MR: Conceptualization, Data curation, Formal Analysis, Investigation, Methodology, Visualization, Writing–original draft, Validation. AA: Formal Analysis, Investigation, Methodology, Writing–review and editing. SD: Conceptualization, Formal Analysis, Funding acquisition, Writing–review and editing. BG: Conceptualization, Formal Analysis, Funding acquisition, Writing–review and editing. DK: Data curation, Visualization, Writing–original draft. FF: Data curation, Visualization, Writing–review and editing. TT: Resources, Writing–review and editing, Writing–original draft. ME: Data curation, Writing–original draft, Resources. MW: Data curation, Writing–review and editing, Resources. MM: Formal Analysis, Methodology, Resources, Writing–review and editing, Investigation. TP: Formal Analysis, Funding acquisition, Writing–review and editing, Conceptualization. MO: Investigation, Formal Analysis, Methodology, Resources, Writing–original draft, Conceptualization.

## Funding

The author(s) declare that financial support was received for the research, authorship, and/or publication of this article. This study was funded by the Werner Siemens Stiftung under the grant "Smart Implants."

## Acknowledgments

The authors thank Katja Schäfer for Irina Scheck from the Institute of Anatomy and Cell Biology, Saarland University for their help during the specimen preparation. The authors would also like to thank the people who made the decision during their lifetime to donate themselves for science and teaching after their decease.

## Conflict of interest

TP is president and board member of the AO Foundation, Switzerland, and extended board member of the German Society of Orthopedic Trauma Surgery (DGU), the German Society of Orthopedic Surgery and Traumatology (DGOU), and the German Society of Surgery (DGCH). TP is also the speaker of the medical advisory board of the German Ministry of Defense.

The remaining authors declare that the research was conducted in the absence of any commercial or financial relationships that could be construed as a potential conflict of interest.

## Publisher's note



## References

Antonova, E., Le, T. K., Burge, R., and Mershon, J. (2013). Tibia shaft fractures: costly burden of nonunions. *BMC Musculoskelet. Disord.* 14, 42. doi:10.1186/1471-2474-14-42

Augat, P., Simon, U., Liedert, A., and Claes, L. (2005). Mechanics and mechano-biology of fracture healing in normal and osteoporotic bone. *Osteoporos. Int.* 16 (Suppl. 2), S36–S43. doi:10.1007/s00198-004-1728-9

Braun, B. J., Orth, M., Diebels, S., Wickert, K., Andres, A., Gawlitza, J., et al. (2021). Individualized determination of the mechanical fracture environment after tibial exchange nailing-A simulation-based feasibility study. *Front. Surg.* 8, 749209. doi:10.3389/fsurg.2021.749209

Buckley, R. E., Moran, C. G., and Apivatthakakul, T. (2018). "Section 3 Reduction, approaches, and fixation techniques," in *AO priniciples of frature management* (Georg Thieme, Stuttgart: Spinger). doi:10.1055/b-0038-160825

Calori, G. M., and Giannoudis, P. V. (2011). Enhancement of fracture healing with the diamond concept: the role of the biological chamber. *Inj. Int. J. Care Inj.* 42, 1191–1193. doi:10.1016/j.injury.2011.04.016

Cattaneo, P. M., Dalstra, M., and Frich, L. H. (2001). A three-dimensional finite element model from computed tomography data: a semi-automated method. *Proc. Inst. Mech. Eng. Part H. J. Eng. Med.* 215 (2), 203–212. doi:10.1243/0954411011533760

Claes, L. (2017). Mechanobiology of fracture healing part 2: relevance for internal fixation of fractures. *Unfallchirurg* 120 (1), 23–31. doi:10.1007/s00113-016-0281-2

Claes, L. E., and Heigele, C. A. (1999). Magnitudes of local stress and strain along bony surfaces predict the course and type of fracture healing. *J. Biomech.* 32 (3), 255–266. doi:10.1016/S0021-9290(98)00153-5

Dahabreh, Z., Dimitriou, R., and Giannoudis, P. V. (2007). Health economics: a cost analysis of treatment of persistent fracture non-unions using bone morphogenetic protein-7. *Inj. Int. J. Care Inj.* 38, 371–377. doi:10.1016/j.injury.2006.08.055

Dailey, H. L., Wu, K. A., Wu, P. S., McQueen, M. M., and Court-Brown, C. M. (2018). Tibial fracture nonunion and time to healing after reamed intramedullary nailing: risk factors based on a single-center review of 1003 patients. *J. Orthop. Trauma* 32, 263–269. doi:10.1097/BOT.0000000000001173

Eberle, S., Göttlinger, M., and Augat, P. (2013). An investigation to determine if a single validated density-elasticity relationship can be used for subject specific finite element analyses of human long bones. *Med. Eng. Phys.* 35 (7), 875–883. doi:10.1016/j.medengphy.2012.08.022

Edwards, W. B., Schnitzer, T. J., and Troy, K. L. (2013). Torsional stiffness and strength of the proximal tibia are better predicted by finite element models than DXA or QCT. *J. Biomech.* 46 (10), 1655–1662. doi:10.1016/j.jbiomech.2013.04.016

Ernst, M., Baumgartner, H., Döbele, S., Höntzsch, D., Pohlemann, T., and Windolf, M. (2021a). Clinical feasibility of fracture healing assessment through continuous monitoring of implant load. *J. Biomech.* 116, 110188. doi:10.1016/j.jbiomech.2020.110188

Ernst, M., Richards, R. G., and Windolf, M. (2021b). Smart implants in fracture care - only buzzword or real opportunity? *Injury* 52, S101–S105. doi:10.1016/j.injury.2020.09.026

Fong, K., Truong, V., Foote, C. J., Petrisor, B., Wiliams, D., Ristevski, B., et al. (2013). Predictors of nonunion and reoperation in patients with fractures of the tibia: an observational study. *BMC Musculoskelet. Disord.* 14, 103. doi:10.1186/1471-2474-14-103

Harris, I., and Lyons, M. (2005). Reoperation rate in diaphyseal tibia fractures. *ANZ J. Surg.* 75 (12), 1041–1044. doi:10.1111/j.1445-2197.2005.03618.x

Imam, M. A., and Fraker, A. C. (1996). "Titanium alloys as implant materials," in *Med. Appl. Titan. Its alloy. Mater. Biol. Issues*. Editors S. Brown and J. Lemons (West Conshohicken, PA: ASTM Int.), 3–16.

Janczyk, P., Weigner, J., Luebke-Becker, A., Kaessmeyer, S., and Plendl, J. (2011). Nitrite pickling salt as an alternative to formaldehyde for embalming in veterinary anatomy-A study based on histo- and microbiological analyses. *Ann. Anat.* 193 (1), 71–75. doi:10.1016/j.aanat.2010.08.003

Müller, M. E., Koch, P., Nazarian, S., and Schatzker, J. (1990). "Tibia/fibula = 4," in *The comprehensive classification of fractures of long bones* (Berlin, Heidelb: Springer). doi:10.1007/978-3-642-61261-9_7

Orth, M., Ganse, B., Andres, A., Wickert, K., Warmerdam, E., Müller, M., et al. (2023). Simulation-based prediction of bone healing and treatment recommendations for lower leg fractures: effects of motion, weight-bearing and fibular mechanics. *Front. Bioeng. Biotechnol.* 11, 1067845. doi:10.3389/fbioe.2023.1067845

Orthoload database (2023). Input data testing device. Available at: https://orthoload.com/database2017/?implantId=1322&activityId=1521&activityIndentationLevel=1&parameterId=1&parameterIndentationLevel=1&patientId=k8l&fileId=k8l_191211_1_107p&fileType=t&selectBox=file (Accessed July 21, 2023).

Rho, J. Y., and HobathoAshman, M. C. R. B. (1995). Relations of mechanical properties to density and CT numbers in human bone. *Med. Eng. Phys.* 17 (5), 347–355. doi:10.1016/1350-4533(95)97314-F

Shefelbine, S. J., Augat, P., Claes, L., and Simon, U. (2005). Trabecular bone fracture healing simulation with finite element analysis and fuzzy logic. *J. Biomech.* 38, 2440–2450. doi:10.1016/j.jbiomech.2004.10.019

Tzioupis, C., and Giannoudis, P. V. (2007). Prevalence of long-bone non-unions. *Injury* 38 (Suppl. 2), S3–S9. doi:10.1016/s0020-1383(07)80003-9

Windolf, M., Varjas, V., Gehweiler, D., Schwyn, R., Arens, D., Constant, C., et al. (2022). Continuous implant load monitoring to assess bone healing status - evidence from animal testing. *Med* 58, 858. doi:10.3390/medicina58070858

Zura, R., Xiong, Z., Einhorn, T., Watson, J. T., Ostrum, R. F., Prayson, M. J., et al. (2016). Epidemiology of fracture nonunion in 18 human bones. *JAMA Surg.* 151 (11), 1627755–e162812. doi:10.1001/jamasurg.2016.2775

## 9.1.3 Integrated Study of the Distal Femur Biphasic Plate: Exploring In Vivo, In Vitro, and In Silico Methodologies (Paper 3)

Authors:

A. Andres, **K. Wickert,** M. Roland, M. Orth, B. Braun, T. Histing, S. Diebels and T. Pohlemann

Publication status:

Submitted to *Frontiers in Bioengineering and Biotechnology*

# Integrated Study of the Distal Femur Biphasic Plate: Exploring In Vivo, In Vitro, and In Silico Methodologies

**Kerstin Wickert[1*], Annchristin Andres[1*], Michael Roland[1], Marcel Orth[2], Benedikt Braun[3], Tina Histing[3], Stefan Diebels[1], Tim Pohlemann[2]**

[1]Applied Mechanics, Saarland University, Saarbrücken, Germany, [2]Department of Trauma, Hand and Reconstruction Surgery, Universitatsklinikum des Saarlandes, Homburg, Germany, [3]University Hospital Tuebingen on Behalf of the Eberhard-Karls-University Tuebingen, Faculty of Medicine, BG Hospital Tuebingen, Eberhard Karls Universitat Tubingen, Tübingen, Germany

***Submitted to Journal:***
Frontiers in Bioengineering and Biotechnology

***Specialty Section:***
Biomechanics

***Article type:***
Original Research Article

***Manuscript ID:***
1720191

***Received on:***
07 Oct 2025

***Revised on:***
10 Oct 2025

***Journal website link:***
www.frontiersin.org

## Scope Statement

In this interdisciplinary study, our engineers, mathematicians, and surgeons/physicians collaborate to comprehensively explore the distal femur biphasic plate through a triad of methodologies: in vivo, in vitro, and in silico. By integrating human specimen experiments and computational approaches to assess this critical anatomical and functional area, we have gained insights to improve orthopedic interventions and digital health solutions. This work aligns perfectly with Frontiers in Bioengineering and Biotechnology mission to bridge technology and clinical practice. Our interdisciplinary team, which approaches questions from different angles and has already worked together successfully on various projects, can contribute to the study's results with its experience and expertise in the respective specialist area. The findings to analyze a plate from all these different perspectives significantly impact clinical studies and their outcomes by providing a more precise preliminary assessment of the factors influencing the mechanical properties of an implant.

## Conflict of interest statement

### The authors declare a potential conflict of interest and state it below

TP is president and board member of the AO Foundation, Switzerland, and extended board member of the German Society of Orthopaedic Trauma Surgery (DGU), the German Society of Orthopaedic Surgery and Traumatology (DGOU), and the German Society of Surgery (DGCH). TP is also the spokesman of the medical advisory board of the German Ministry of Defence. TP and Saarland University hold parts of the Biphasic Plate Patent (EP3331462B1).
The remaining authors declare that the research was conducted without commercial or financial relationships that could be constructed as a potential conflict of interest.



## Credit Author Statement

**Annchristin Andres**: Conceptualization, Data curation, Formal Analysis, Investigation, Methodology, Software, Visualization, Writing – original draft, Writing – review & editing. **Benedikt Braun**: Conceptualization, Investigation, Resources, Validation, Writing – review & editing. **Kerstin Wickert**: Conceptualization, Data curation, Formal Analysis, Investigation, Methodology, Software, Visualization, Writing – original draft, Writing – review & editing. **Michael Roland**: Investigation, Supervision, Writing – review & editing. **Marcel Orth**: Conceptualization, Investigation, Resources, Validation, Writing – review & editing. **Stefan Diebels**: Conceptualization, Formal Analysis, Funding acquisition, Supervision, Writing – review & editing. **Tina Histing**: Funding acquisition, Project administration, Writing – review & editing. **Tim Pohlemann**: Conceptualization, Funding acquisition, Project administration, Writing – review & editing.

## Keywords

biphasic plate, human cadaveric experiments, Biomechanical simulation, patient-specificmodeling, Osteosynthesis

## Abstract

Word count: 257

The strategy for plate fixation of fractured bones in humans changed from absolute stability through relative stability to a new concept of a predefined range of elastic movement with mechanical amplitude limitation (“Biphasic Plate”,41medical, Bettlach, Schweiz).
This study aims to evaluate the stress distribution of the biphasic plate design under realistic boundary conditions, utilizing a comprehensive and integrated approach of in vivo, in vitro, and in silico analyses. The hypothesis is that the biphasic plate will exhibit a distinct stress distribution profile under real-world mechanical loads compared to conventional plate designs. To test this, an implantable vivo strain measurement system (“Fracture Monitor”, AO-Foundation, Davos Switzerland) and a camera system are employed for experimental data acquisition, while patient monitoring captures actual boundary conditions during daily activities.
Finite element simulations are performed on patient-specific 3D models generated from computed tomography imaging, allowing for detailed stress analysis. These simulations are validated through experiments on human cadaveric specimens in a custom-designed test rig by investigating the specific behavior of the biphasic plate with its two different modes (rigid and flex). These modes offer both the strength of the treatment and the flexibility within the fracture gap.
The key research question explores the behavior of the biphasic plate under true physiological conditions, particularly in the context of complex, multi-directional forces experienced during human movement.
By the chosen biomechanical testing setup, the in silico simulations could be validated, demonstrating the ability to accurately replicate the postulated motion sequence of the biphasic plate. This iteration emphasizes both validation and reproducibility as the key outcomes.

## Funding information

The study was partially funded by the Werner Siemens Foundation (WSS, Zug, Switzerland) as part of Project Smart Implants 2.0. In addition, institutional funding from Saarland University and University Hospital Tuebingen was used to cover personal costs and infrastructure.

## Funding statement

The author(s) declare that financial support was received for the research and/or publication of this article.

## Ethics statements

### Studies involving animal subjects

Generated Statement: No animal studies are presented in this manuscript.

### Studies involving human subjects

Generated Statement: The studies involving humans were approved by The ethics committee of Saarland Medical Board has approved the present study using human cadaveric specimens (Aerztekammer des Saarlandes, Germany, application number 195/24). The studies were conducted in accordance with the local legislation and institutional requirements. The human samples used in this study were acquired from Samples obtained from body donations at Saarland University. Written informed consent for participation was not required from the participants or the participants´ legal guardians/next of kin in accordance with the national legislation and institutional requirements. The patients/participants provided their written informed consent to participate in this study. Written informed consent was obtained from the individual(s) for the publication of any potentially identifiable images or data included in this article. The study was conducted under the Declaration of Helsinki and approved by the Ethics Committees of the University of Tuebingen (Protocol codes 317/2022BO2). Informed consent was obtained from all subjects involved in the study. . The studies were conducted in accordance with the local legislation and institutional requirements. The participants provided their written informed consent to participate in this study.

### Inclusion of identifiable human data

Generated Statement: Written informed consent was obtained from the individual(s) for the publication of any potentially identifiable images or data included in this article.

## Data availability statement

Generated Statement: The original contributions presented in the study are included in the article/supplementary material, further inquiries can be directed to the corresponding author/s.

## Generative AI disclosure

No Generative AI was used in the preparation of this manuscript.

# Integrated Study of the Distal Femur Biphasic Plate: Exploring In Vivo, In Vitro, and In Silico Methodologies

Annchristin Andres[1*], Kerstin Wickert[1*], Michael Roland[1], Marcel Orth[2], Benedikt Braun[3], Tina Histing[3], Stefan Diebels[1], Tim Pohlemann[2]

[1]Applied Mechanics, Saarland University, Saarbrücken, Germany
[2]Department of Trauma, Hand and Reconstruction Surgery, Saarland University Hospital, Homburg, Germany
[3]University Hospital Tuebingen on Behalf of the Eberhard-Karls-University Tuebingen, Faculty of Medicine, BG Hospital Tuebingen, Germany

*** Correspondence:**
Annchristin Andres, Kerstin Wickert
Applied Mechanics
Saarland University
Campus A4 2, 1. OG
D-66123 Saarbrücken
Germany
Phone: +49 681 302 2168
Fax: +49 681 302 3992
email: annchristin.andres@uni-saarland.de

**Key Words:**

biphasic plate, human cadaveric experiments, biomechanical simulation, patient-specific modeling, osteosynthesis

**Abstract**

The strategy for plate fixation of fractured bones in humans changed from absolute stability through relative stability to a new concept of a predefined range of elastic movement with mechanical amplitude limitation ("Biphasic Plate",41medical, Bettlach, Schweiz).

This study aims to evaluate the stress distribution of the biphasic plate design under realistic boundary conditions, utilizing a comprehensive and integrated approach of in vivo, in vitro, and in silico analyses. The hypothesis is that the biphasic plate will exhibit a distinct stress distribution profile under real-world mechanical loads compared to conventional plate designs. To test this, an implantable vivo strain measurement system ("Fracture Monitor", AO-Foundation, Davos Switzerland) and a camera system are employed for experimental data acquisition, while patient monitoring captures actual boundary conditions during daily activities.

Finite element simulations are performed on patient-specific 3D models generated from computed tomography imaging, allowing for detailed stress analysis. These simulations are validated through experiments on human cadaveric specimens in a custom-designed test rig by investigating the specific behavior of the biphasic plate with its two different modes (rigid and flex). These modes offer both the strength of the treatment and the flexibility within the fracture gap.

The key research question explores the behavior of the biphasic plate under true physiological conditions, particularly in the context of complex, multi-directional forces experienced during human movement.

By the chosen biomechanical testing setup, the in silico simulations could be validated, demonstrating the ability to accurately replicate the postulated motion sequence of the biphasic plate. This iteration emphasizes both validation and reproducibility as the key outcomes.

## 1. Introduction

The evolution of modern surgical fracture stabilization by plates started with introducing the principle of absolute stability after complete anatomic reduction to take advantage of the regular bone metabolism for direct bone healing [1]. The need for additional care of the soft tissue coverage and biology after high-energy trauma led to efforts to minimize the implant footprint and iatrogenic soft tissue impairment. The Limited Contact Dynamic Compression Plate (LCDCP), introduced by Gautier and Perren [2], is one prominent example. In addition, the indirect bridging of the fracture zone by a plate allowed the progression of the mainly undisturbed biological healing process of secondary bone healing by callus formation and natural callus maturation [3]. Taking into account the limited ability to create a controlled environment for the microbiomechanical conditions within the fracture gaps using the presently available bridging implants and increased knowledge about the required mechanical in vivo boundary conditions led to developments for allowing controlled micro movements within the plate-bone construct [4,5]. As a secondary effect, better long-term stability, especially in osteoporotic bone, could be detected by taking advantage of a damping effect [6]. Technical problems with the screws as dynamic elements in the plate-screw-bone construct led to the evolution of the semi-elastic concept towards implementing the dynamic component into the plate body as a "biphasic plate" [7]. This study also demonstrated the induction of significant enhancement of the mechanobiological aspects of fracture healing, leading to rapid and robust

callus formation while improving the strength and stiffness of the overall construct compared to conventional locking plates, especially in higher weight-bearing ranges [7]. Similarly, Epari and colleagues [8] found that biphasic plating exhibited a bi-linear stiffness response, providing more consistent interfragmentary movement and greater implant strength, which is particularly advantageous for complex fractures like those of the distal femur.

Alternative developments can be summarized in controlling the microbiological environment by combining constructs of various intra- and extramedullary implants and additional strategies to limit invasivity and iatrogenic soft tissue damage. Examples are the Less Invasive Stabilization System (LISS-DF) and retrograde nailing, which demonstrated good healing rates and fewer complications like infection and nonunion [9,10]. Dual plating techniques, which use both lateral and medial locking plates, have shown promise in treating complex distal femur fractures, with studies [11] reporting higher union rates and potentially lower revision rates than single lateral plating. However, when applied with proper fixation principles, single-locked plates can also achieve successful outcomes in various distal femur fractures [12]. A systematic review and meta-analysis conducted by Tripathy and colleagues [13] although dual plating resulted in faster fracture healing, there were no significant differences in functional outcomes or complications compared to single plating. However, dual plating was associated with longer procedure times, raising concern about its clinical need. These findings suggest that single and dual plating can be effective, with the decision often depending on the fracture's complexity and the surgeon's preference. Double constructs, frequently applied in geriatric fracture situations with low bone quality, i.e., double plate or nail/plate combinations, are considered to be fully loadable, but high stiffness and stress shielding might delay fracture healing time [14,15]. In addition, in vivo sensing systems are under development for generating continuous strain data from the plate as a surrogate indicator for the progressing callus formation and hardening, as an important proof of concept and possibly a future way to individualize aftercare and rehabilitation by case-specific loading and activity recommendations [16–18]. The concept of a biphasic plate combining very high peak and fatigue stability with adequate micromovement conditions for callus formation enhancement might be the necessary step forward to provide controlled movement, limited soft tissue impairment, and superior early and long-term stability even in prolonged healing situations [19]. This study aims to add mechanical data on the plate behavior in realistic in vitro loading conditions and combine the findings with an established in silico simulation model already successfully applied to clinical healing predictions [20]. Further research and clinical studies are needed to fully explore the potential of biphasic plates in improving patient outcomes and advancing fracture treatment.

## 2. Methods

### 2.1 Experimental Setup

The local ethical committee approved the biomechanical experiment (Aerztekammer des Saarlandes, Germany, application number 195/24). The cadaveric femur came from body donation from the Institute of Anatomy and Cell Biology from Saarland University. They using the preservation methods according to Weigner, described in literature for veterinary uses [21]. The demographic data of the donor stated a 75-year-old female individual, 46 kg of weight, who passed away for reasons independent of bone conditions. The fracture was simulated by an osteotomy (Colibri II, DePuy Synthes, Norderstedt, Germany, oscillating blade, 0,8mm) with a 30° angle to the shaft axis comparable to an OTA/AO classification fracture type 33A2 (see Figure 1C) [22]. The biphasic plate was fixed with a total of 9 head-locking screws, six screws in the distal plate head, and three proximal cortical. The AO Fracture Monitor (see Figure 1B (4)) was mounted on the biphasic plate using two screws, each tightened with a torque of 1.5 Nm. This biofeedback sensor system monitors the progression of bone healing at a frequency of 10 Hz via a strain gauge. Data is transmitted wirelessly via Bluetooth to a cloud for further

evaluation through an app on a smartphone [17]. The experiment was executed on a custom-designed testing device (see Figure 1A), validated in a previous work from our team [18].The specimen was clamped into a particular mold clamping (Figure 1A (3)) system to best accommodate the bone's complex shape. A motor (Figure 1A (1)) is positioned on the proximal side, driving a spindle to apply a force to the bone. The motor rotated at 0.25 mm/s with each step, compressing the femur by 0.25 mm.

## 2.2 In Silico Setup

The cadaveric specimen was scanned together with a six-rod calibration phantom (QRM-BDC/6, QRM GmbH Moehrendorf, Germany) with a Somatom Definition AS64 CT scanner (Siemens Healthineers, Erlangen, Germany). The following settings were applied: tube voltage: 120 kVp, tube current: 96 mA, and 0.6 mm slice thickness. The generated DICOM data set was used to create the computational model for the biomechanical finite element simulation. The biphasic plate computer-aided design (CAD) model, provided by AO Foundation, was added and aligned appropriately after segmenting the cadaveric bone model in Simpleware ScanIP™ (Synopsys, Mountain View, CA, United States). Bolts were generated in ScanIP™ and positioned at the existing screw locations. The plate has Young's modulus of 200 GPa and a Poisson's ratio of 0.3 [8], while the bone's material properties are defined based on the CT data and the calibration phantom described in Wickert et al.[18]. The properties of the fracture gap, carefully selected from relevant literature [23], ensure the model's validity. All elements used in the finite element FE model were C3D10 (ten-node tetrahedral elements with four integration points). The plate and pin form a firm connection in the model. The input file loads into Abaqus™ (Dassault Systems, Velizy-Villacoublay. France) for analysis, where the model undergoes a series of six simulation steps, each applying a concentrated force based on the experimental load, normalized and distributed across the nodes at the proximal end of the femur (force values shown in Figure 2A). The model defines a surface-to-surface contact for the meandering gap of the biphasic plate, with tangential behavior set as frictionless and usual as hard contact, ensuring a thorough and complete analysis.

## 2.3 Patient-specific Biomechanical Models

The simulation of the patients follows the same approach as the in silico simulation of the cadaveric specimen. Therefore, 3D models are generated for each patient (see Table 1) based on their clinical imaging data and their clinical specifications, which include the anthropometric properties of the bone, the fracture situation, the location and positioning of the biphasic plate, the number, length, angle, and positioning of the screws, and patient-specific material properties derived from the analysis of the gray values.

High-resolution adaptive FE meshes are then generated using ScanIP™, also with quadratic elements of C3D10-type. In the meshes, node sets at the distal and proximal ends of the bones are defined to apply boundary conditions. Here, the hip force is the load derived from the measured patient data (see supplementary material Figure 7) or the Orthoload™ database [24]. The data sets are scaled by the corresponding patient´s weight and distributed on the marked nodes. The distal node set defines the distal epiphysis and the proximal epiphysis. All force components, i.e., medial/lateral as $F_x$, proximal/distal as $F_z$, and anterior/posterior as $F_y$, are always applied to the proximal node set as a concentrated force. Translation in all three spatial directions is blocked at the distal epiphysis. Homogeneous material properties are assigned within ScanIP™, with values for the implant, interfragmentary nail, and fracture gap as described above [8,23,25]. To determine the relationship between elasticity and bone density, the grayscale values from the CT data are mapped to the Hounsfield scale and corresponding

local mechanical properties of the bone [26–29]. The simulation workflow can also be found in various papers from our interdisciplinary team [30–35].

## 3. Results

### 3.1 In Vitro

The motor rotated the spindle at a speed of 0.25 mm/s, advancing by 0.25 mm with each step. Figure 2A shows the measured force values after each step and the clamped, treated specimen (Figure 2B). The in vitro behavior of the biphasic plate is also illustrated, including its two modes: opened (Figure 2C) and closed (Figure 2D) meander patterns.

### 3.2 In Silico

Figure 3 compares experimental and simulation data for relative change in length across six steps. The x-axis represents the different steps of the process (Step 1 to Step 6), as shown in the values of Figure 2A, while the y-axis shows the relative change in length. The raw experimental data is depicted as light blue, with significant scatter, while the smoothed experimental data is shown as a solid blue line, providing a more apparent trend. Red crosses mark the data points from the simulation, highlighting how the simulation results align with the experimental outcomes at each step. Overall, the smoothed experimental data closely follows the trend of the simulation, indicating a strong agreement between the two. However, some deviations are visible at specific steps, where the simulation data either slightly over- or underestimates the relative change in length.



In addition to the correlation between in vitro experiments and simulation, the correct simulation of the primary mechanism of the biphasic plate is also important. The image, Figure 4, consists of three parts: two graphs labeled A and B and a stress distribution image labeled C. Figure 4A shows the relationship between load in Newton [N] and interfragmentary motion (IFM) in millimeters [mm] for the near cortex of a bone, with a steady increase in load as IFM rises, followed by a sharper increase beyond 0.2 mm. Figure 4B depicts a similar relationship for the far cortex, where the IFM range extends to 2 mm, showing a non-linear rise in load, mainly after 1 mm. The third part, Figure 4C, is a color-coded contour map illustrating a biphasic plate's von Mises stress distribution, with stress values ranging from 0 to 850 N/mm², i.e., MPa. The highest stress concentrations are visible in specific plate regions, indicating potential areas of failure. Together, these elements represent a biomechanical analysis of fracture fixation, focusing on load distribution and IFM in a biphasic plate under stress. The results are comparable with the studies by Epari and colleagues [8]. The aim was to validate the simulation setup from two sides to obtain valid, reproducible in vivo simulation results. On the one hand, the in vitro experiments carry out the validation through alignment of the recorded measurements data from the fracture monitor and the simulation results (see Figure 3), as already shown in preliminary work by Wickert et al. [18], secondly in Figure 4, by comparing the simulation setup with the results from the previous study on the biphasic plate [8].

### 3.3 In Vivo

The following section presents the results of patient-based in vivo studies. By analyzing data from real clinical scenarios, we aim to understand better how the biphasic plate behaves in patients with accurate gait data. The results in Figure 5 show that the maximum load on the

biphasic plate is observed at the edge and not centrally in the middle of the plate in all patients. The medial-lateral and posterior-anterior force components, therefore, influence the stress distribution. In addition, the main point of force at the femoral head creates a lever arm that further influences the stress distribution. In particular, the primary application of force at the femoral head in the femur leads to a superposition of axial compressive and bending stresses, consistent with Pauwels' findings [36] on the biomechanical forces in the hip joint. The supplementary material contains a more detailed analysis of screw positioning for each patient.

## 4. Discussion

The biphasic nature of the plate we studied, which balances stiffness and flexibility, is a crucial area of investigation. Limited micromotion, combined with high overall stiffness and fatigue strength, is presently considered to be the best compromise for adapting to the variant biomechanical conditions needed throughout the timeline of fracture healing [7,37]. For the first time, the present study compared controlled biomechanical data transferred into an innovative in silico simulation model to a patient-based simulation of a real-life situation. A deeper understanding of real-life micromechanics within a fracture area might be possible using experimental and computational methods.

*In vitro* Epari and colleagues [8] investigated the behavior of the biphasic plate using a bone substitute material with the following material properties: Young's modulus of 7 GPa and a Poisson's ratio of 0.3. The focus of this work included the experimental investigation of the biphasic plate in a setting using human cadaveric bones. A simple fracture type according to AO classification was chosen based on patient cases and combined to correlate the results [8]. The behavior of the biphasic plate was successfully tested on the human cadaveric bone under axial loading conditions. The experiment demonstrated the plate's two distinct phases (rigid and flex) and provided valuable data for validating the biomechanical FE analysis.

*In silico,* this integrated study focuses on correlating experimental findings with simulation outcomes to create more robust predictive models. Epari and colleagues [38] serve as a foundation where computational models were reconstructed to simulate the behavior of the biphasic plate. In this step, the reproduction of the properties of the biphasic plate and, thus, the verification of the simulation we created were decisive. The results show that the mechanism could be reproduced correctly in the fracture gap movement and the stress distribution. However, our simulation also considered the material properties of the cortical and cancellous bone and selected a fracture gap that closely aligns with the patient cases examined later in vivo. The difference lies primarily in a reduction in the fracture width of 20 mm, as selected by Epari and colleagues [8].

*In vivo* The simulation of the in vivo cases provides decisive insights into the actual patient's behavior. Above all, it is possible to simulate the stress distribution on the plate during a step forward. It is particularly noticeable here that the medial/lateral and posterior/anterior portions of the force cause the stress distribution to deviate significantly from that of the in silico studies, which is not surprising, however, as a purely axial load was applied in silico both in the previous paper [8] and in our replicated simulation. This was also set relatively low at 1000 N, as studies on hip forces such as those carried out by Bergmann and colleagues [39,40] show that proximal/distal forces of around 2500 N are regular. Likewise, the lever arm through the femoral head leads to further changes in the stress distribution, which Pauwels [36] described previously. This work does not focus on the screw positions, but it emphasizes that the plate uses a fixed working length and screw configuration. Previous work [41,42] has already described the importance of screw positions and the effects of plate screw density. In the present patient simulations, only patient 2 corresponds; see supplementary material Figure 6B, which meets

these requirements. Accordingly, the different screw positionings naturally also influence the stress distributions.

A significant limitation of the current study is that biological factors like genetic factors, physical health, and medical conditions cannot be considered in the simulation. Of course, this also applies to our in vitro experiments, as they use human preparations but cannot fully reproduce complex biological systems. Since no healing simulation was performed, making precise statements about the bone healing process or the long-term results is impossible. In addition, the 3D models and segmentation were created in close consultation with the treating physicians to ensure anatomical accuracy. Despite these efforts, minor errors in the segmentation are still possible. These differences can lead to minor deviations from the actual anatomy of the bone.

## 5. Conclusion

This study addresses the limitations of each individual approach by integrating in vivo, in vitro, and in silico methodologies. While in vivo studies provide real-world insights, they are enhanced by the precision and control of in vitro and silico methods. Combining these approaches leads to a more comprehensive understanding of the biphasic plate's performance, helping to improve its design and clinical application. The ultimate goal is to ensure patients receive implants that stabilize fractures and support optimal healing and long-term outcomes as minimally invasive as possible. The results from the simulation closely matched the experimental data, confirming the accuracy of the FE analysis workflow. Under axial loading, the maximum stress was concentrated at the center of the plate, above the meander pattern. However, when patient-specific models were analyzed under in vivo conditions, with force components in all three planes (sagittal, frontal, and transverse), a trend emerged, showing that the maximum stresses are distributed along the lateral sides of the biphasic plates.

## 6. Ethics Statement

The ethics committee of Saarland Medical Board has approved the present study using human cadaveric specimens (Aerztekammer des Saarlandes, Germany, application number 195/24). The studies were conducted in accordance with the local legislation and institutional requirements. The human samples used in this study were acquired from Samples obtained from body donations at Saarland University. Written informed consent for participation was not required from the participants or the participants´ legal guardians/next of kin in accordance with the national legislation and institutional requirements. The patients/participants provided their written informed consent to participate in this study. Written informed consent was obtained from the individual(s) for the publication of any potentially identifiable images or data included in this article. The study was conducted under the Declaration of Helsinki and approved by the Ethics Committees of the University of Tuebingen (Protocol codes 317/2022BO2). Informed consent was obtained from all subjects involved in the study.

## 7. Data Availability statement

The original contributions presented in the study are included in the article/supplementary material; further inquiries can be directed to the corresponding author. Researchers who wish to request access to data should send an email clearly indicating the research purpose. Every request must be reviewed by the responsible institutional review boards, considering the risk of patient reidentification and compliance with the applicable data protection rules.

## 8. Conflict of Interest

TP is president and board member of the AO Foundation, Switzerland, and extended board member of the German Society of Orthopaedic Trauma Surgery (DGU), the German Society of Orthopaedic Surgery and Traumatology (DGOU), and the German Society of Surgery (DGCH). TP is also the spokesman of the medical advisory board of the German Ministry of Defence. TP and Saarland University hold parts of the Biphasic Plate Patent (EP3331462B1).

The remaining authors declare that the research was conducted without commercial or financial relationships that could be constructed as a potential conflict of interest.

## 9. Funding

The study was partially funded by the Werner Siemens Foundation (WSS, Zug, Switzerland) as part of Project Smart Implants 2.0. In addition, institutional funding from Saarland University and University Hospital Tuebingen was used to cover personal costs and infrastructure.

## 10. Acknowledgments

The authors thank Katja Schäfer, Irina Scheck, and Prof. Thomas Tschernig from the Institute of Anatomy and Cell Biology, Saarland University, for their help during the specimen preparation. The authors would also like to thank the people who decided during their lifetime to donate themselves to science and teaching after their decease.

The authors also thank Dr. Dorothea Kerner and Dr. Felix Frenzel from the Clinic of Diagnostic and Interventional Radiology, Saarland University, for performing the CT scan of the human cadaveric specimen.

## 11. Figure Legends

*Figure 1: A Self-designed and built testing device consists of the following components: (1) stepper motor (2) measuring sensors (3) clamping system B clamped femur with distal fracture (C), treated with Biphasic Plate and equipped with (4) AO Fracture Monitor.*

*Figure 2: A Results from the experiment: Normal force of the Biphasic Plate during axial loading B clamped human cadaveric fractured specimen treated with Biphasic Plate and AO Fracture Monitor C rigid phase, the slot is "open" D flex phase, the slot is "closed".*

*Figure 3: Relative change in length over the applied load steps from Figure 2A (step 1 – step 6) compared between the in-vitro results (blue line) and the in silico results (red cross).*

*Figure 4: Load in Newton over IFM in millimeters for A near cortex, B far cortex, and C, the corresponding stress results described as von Mises stress in megapascal of the in silico experiment of the biphasic plate.*

*Figure 5: Von Mises stress results in MPa for the in vivo investigations for A Patient 1, B Patient 2, C Patient 3, and D Patient 4.*

## 12. Tables

| **Patient ID** | Bodyweight [kg] | Gender | Age | Side | Fracture (AO Classification) | Number of Screws | Revision Surgery/ Pseudarthrosis | Additional Information |
|---|---|---|---|---|---|---|---|---|
| Patient 1 | 70 | Male | 1945 | Left | 33A3 | 10 | No | Additional distal femur fracture on the contralateral side |
| Patient 2 | 105 | Male | 1961 | Right | 33A2 | 11 | Yes | Previous distal femur fracture many years earlier |
| Patient 3 | 90 | Male | | Right | 33A3 | 8 | | |
| Patient 4 | 63 | Male | | Left | 33A2 | 7 | Yes | Knee Implant, Intramedullary Nail, Locking Attachment plate |

*Table 1: Patient Information*

## 13. Literature


1. Perren, S. M., Russenberger, M., Steinemann, S., Müller, M. E. & Allgöwer, M. A dynamic compression plate. *Acta Orthop Scand Suppl* **125**, 31–41 (1969).
2. Gautier E., P. S. M. Limited Contact Dynamic Compression Plate (LC-DCP) - biomechanical research as basis to new plate design. *Orthopade* **21**, 11–23 (1992).
3. Gerber, C., Mast, J. W. & Ganz, R. Biological internal fixation of fractures. *Arch Orthop Trauma Surg* **109**, 295–303 (1990).
4. Richter, H. *et al.* Dynamization at the near cortex in locking plate osteosynthesis by means of dynamic locking screws: An experimental study of transverse tibial osteotomies in sheep. *Journal of Bone and Joint Surgery - American Volume* **97**, 208–215 (2015).
5. Bottlang, M. & Feist, F. Biomechanics of far cortical locking. *J Orthop Trauma* **25 Suppl 1**, S21-8 (2011).
6. Pohlemann, T. *et al.* Dynamic locking screw improves fixation strength in osteoporotic bone: an in vitro study on an artificial bone model. *Int Orthop* **39**, 761–768 (2015).
7. Hofmann-Fliri, L., Epari, D. R., Schwyn, R., Zeiter, S. & Windolf, M. Biphasic Plating – In vivo study of a novel fixation concept to enhance mechanobiological fracture healing. *Injury* **51**, 1751–1758 (2020).
8. Epari, D. R. *et al.* Biphasic plating improves the mechanical performance of locked plating for distal femur fractures. *J Biomech* **115**, 110192 (2021).
9. Schütz, M., Schäfer, M., Bail, H., Wenda, K. & Haas, N. Neue osteosyntheseverfahren bei distalen femurfrakturen. *Zentralbl Chir* **130**, 307–313 (2005).
10. Rosenkranz, J. et al. New minimally invasive methods of stbilizing distal femoral fractures. *Revue Therapeutique* **60**, 757–761 (2003).
11. Bologna, M. G. *et al.* Dual plate fixation results in improved union rates in comminuted distal femur fractures compared to single plate fixation. *J Orthop* **18**, 76–79 (2020).
12. Virk, J. S. *et al.* Distal femur locking plate: The answer to all distal femoral fractures. *Journal of Clinical and Diagnostic Research* **10**, RC01–RC05 (2016).
13. Tripathy, S. K. *et al.* Dual-Plating in Distal Femur Fracture: A Systematic Review and Limited Meta-analysis. *Indian J Orthop* **56**, 183–207 (2022).
14. DeKeyser, G. J. *et al.* Biomechanical and anatomical considerations for dual plating of distal femur fractures: a systematic literature review. *Arch Orthop Trauma Surg* **142**, 2597–2609 (2022).
15. Wähnert, D. *et al.* Double plating in Vancouver type B1 periprosthetic proximal femur fractures: A biomechanical study. *Journal of Orthopaedic Research* **35**, 234–239 (2017).
16. Ernst, M., Richards, R. G. & Windolf, M. Smart implants in fracture care – only buzzword or real opportunity? *Injury* **52**, S101–S105 (2021).
17. Windolf, M. *et al.* Continuous Implant Load Monitoring to Assess Bone Healing Status—Evidence from Animal Testing. *Medicina (Lithuania)* **58**, (2022).

18. Wickert, K. *et al.* Experimental and virtual testing of bone-implant systems equipped with the AO Fracture Monitor with regard to interfragmentary movement. *Front Bioeng Biotechnol* **12**, (2024).

19. Agarwal, N. Plate Osteosynthesis : Newer Tools and Recent Updates. 8–14 (2023) doi:10.4103/juoa.juoa.

20. Braun, B. J. *et al.* Individualized Determination of the Mechanical Fracture Environment After Tibial Exchange Nailing—A Simulation-Based Feasibility Study. *Front Surg* **8**, 1–9 (2021).

21. Janczyk, P., Weigner, J., Luebke-Becker, A., Kaessmeyer, S. & Plendl, J. Nitrite pickling salt as an alternative to formaldehyde for embalming in veterinary anatomy-A study based on histo- and microbiological analyses. *Annals of Anatomy* **193**, 71–75 (2011).

22. Müller, M.E., Koch, P., Nazarian, S., Schatzker, J. Tibia/Fibula = 4. In: The Comprehensive Classification of Fractures of Long Bones. *Springer, Berlin, Heidelberg* https://doi.org/https://doi.org/10.1007/978-3-642-61261-9_7 (1990) doi:https://doi.org/10.1007/978-3-642-61261-9_7.

23. Claes, L. E. & Heigele, C. A. Magnitudes of local stress and strain along bony surfaces predict the course and type of fracture healing. *J Biomech* **32**, 255–266 (1999).

24. Orthoload - Loading of Orthopaedic Implants. https://orthoload.com/ (2024).

25. Imam, MA. & Fraker, AC. Titanium alloys as implant materials. *In: Brown S, Lemons J, editors. Medical Applications of Titanium and Its Alloys: The Material and Biological Issues. West Conshohicken, PA: ASTM International* 3–16 (1996).

26. Hvid, I., Bentzen, S. M., Linde, F., Mosekilde, L. & Pongsoipetch, B. X-ray quantitative computed tomography: The relations to physical properties of proximal tibial trabecular bone specimens. *J Biomech* **22**, 837–844 (1989).

27. Rho, J. Y., Hobatho, M. C. & Ashman, R. B. Relations of mechanical properties to density and CT numbers in human bone. *Med Eng Phys* **17**, 347–355 (1995).

28. Zannoni, C., Mantovani, R. & Viceconti, M. Material properties assignment to finite element models of bone structures: A new method. *Med Eng Phys* **20**, 735–740 (1999).

29. Cattaneo, P. M., Dalstra, M. & Frich, L. H. A three-dimensional finite element model from computed tomography data: A semi-automated method. *Proc Inst Mech Eng H* **215**, 203–213 (2001).

30. Roland, M., Diebels, S., Wickert, K., Pohlemann, T. & Ganse, B. Finite element simulations of smart fracture plates capable of cyclic shortening and lengthening: which stroke for which fracture? *Front Bioeng Biotechnol* **12**, 1–14 (2024).

31. Orth, M. *et al.* Simulation-based prediction of bone healing and treatment recommendations for lower leg fractures: Effects of motion, weight-bearing and fibular mechanics. *Front Bioeng Biotechnol* **11**, 1–13 (2023).

32. Braun, B. J. *et al.* Individualized Determination of the Mechanical Fracture Environment After Tibial Exchange Nailing—A Simulation-Based Feasibility Study. *Front Surg* **8**, 1–9 (2021).

33. Braun, B. J. *et al.* Bewegungsanalyse und muskuloskeletale Simulation in der Pseudarthrosentherapie – Erfahrungen und erste klinische Ergebnisse. *Die Unfallchirurgie* **125**, 619–627 (2022).

34. Roland, M. *et al.* An algorithmic strategy for the simulation of bone healing directly on computed tomography data. *Pamm* **15**, 105–106 (2015).

35. Roland, M. *et al.* Reappraisal of clinical trauma trials: the critical impact of anthropometric parameters on fracture gap micro-mechanics—observations from a simulation-based study. *Sci Rep* **13**, 1–14 (2023).

36. Pauwels, F. *Gesammelte Abhandlungen Zur Funktionellen Anatomie Des Bewegungsapparates*. (Springer Berlin Heidelberg, 1965).

37. Tufekci, P. *et al.* Early mechanical stimulation only permits timely bone healing in sheep. *Journal of Orthopaedic Research* **36**, 1790–1796 (2018).

38. Epari, D. R., Kassi, J. P., Schell, H. & Duda, G. N. Timely fracture-healing requires optimization of axial fixation stability. *Journal of Bone and Joint Surgery* **89**, 1575–1585 (2007).

39. Bergmann, G. *et al.* Hip forces and gait patterns from rountine activities. *J Biomech* **34**, 859–871 (2001).

40. Bergmann, G. *et al.* Realistic loads for testing hip implants. *Biomed Mater Eng* **20**, 65–75 (2010).

41. Windolf, M. & Perren, S. Basic mechanobiology of bone healing. in *Minimally Invasive Plate Osteosynthesis (MIPO). Stuttgart, New York: AO Foundation/Georg Thieme* 13–30 (2012). doi:10.1055/b-0034-87595.

42. Wagner, M. & Leung, F. K. Implants. in *Minimally Invasive Plate Osteosynthesis - Secon Edition. Stuttgart, New York: AO Foundation/Georg Thieme* 65–72 (2012).

Figure 1.TIF

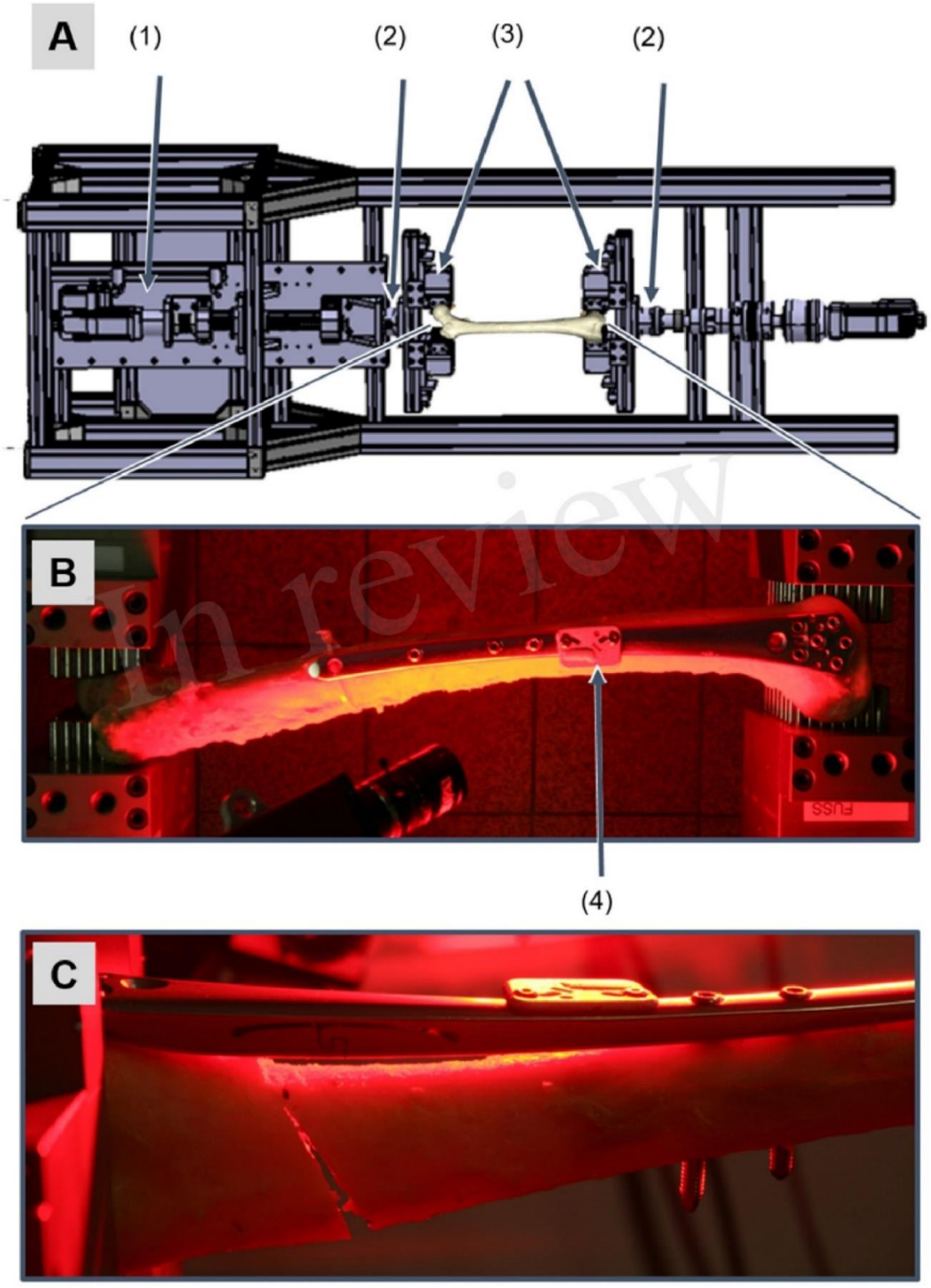

Figure 2.TIF

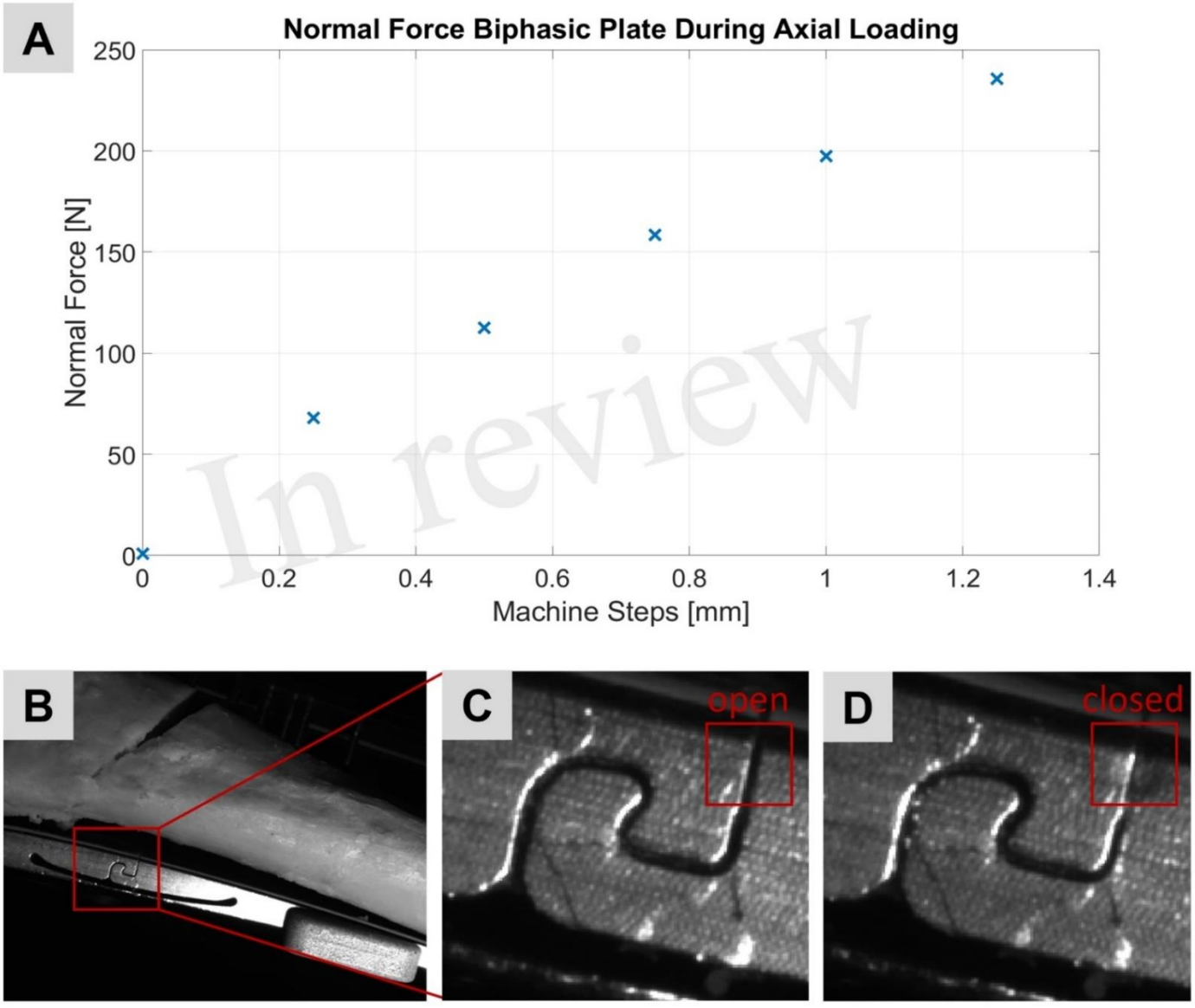
A
Normal Force Biphasic Plate During Axial Loading
Normal Force [N]
250
200
150
100
50
0
0
0.2
0.4
0.6
0.8
1
1.2
1.4
Machine Steps [mm]
In review
B
C
open
D
closed

Figure 3.TIF



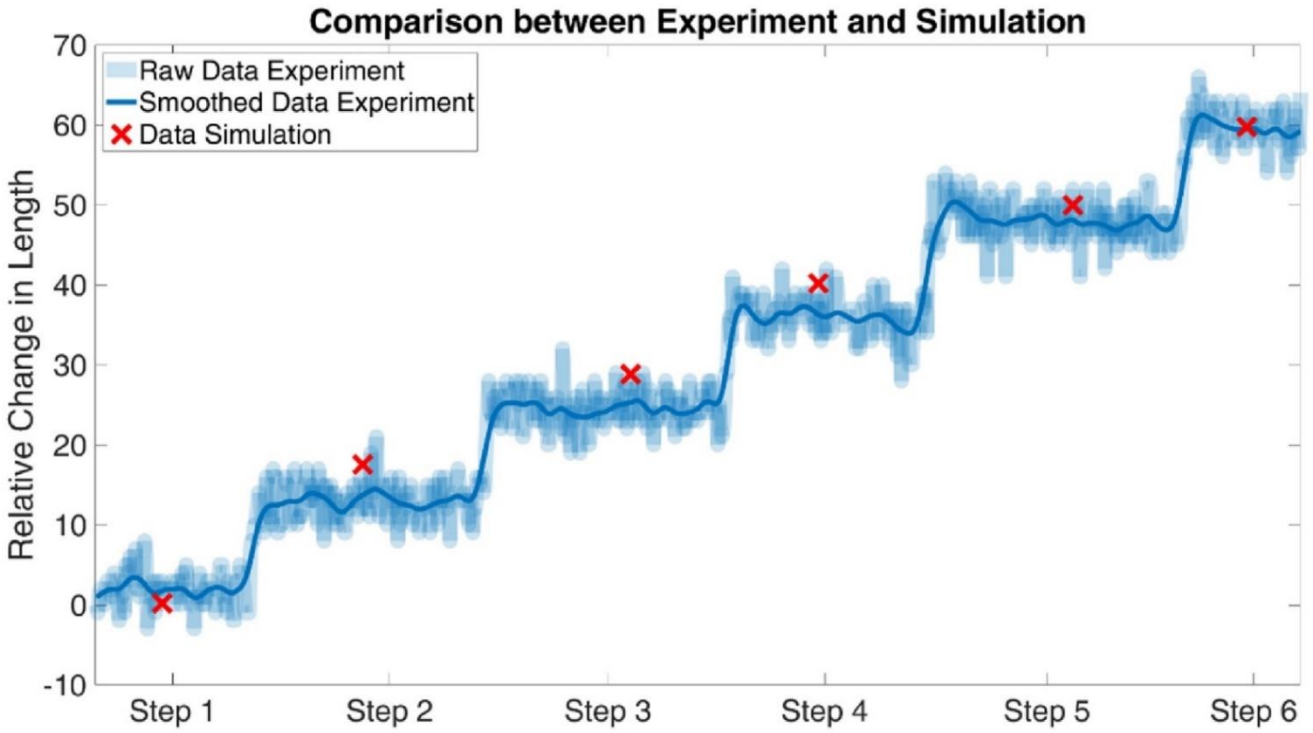

Figure 4.TIF

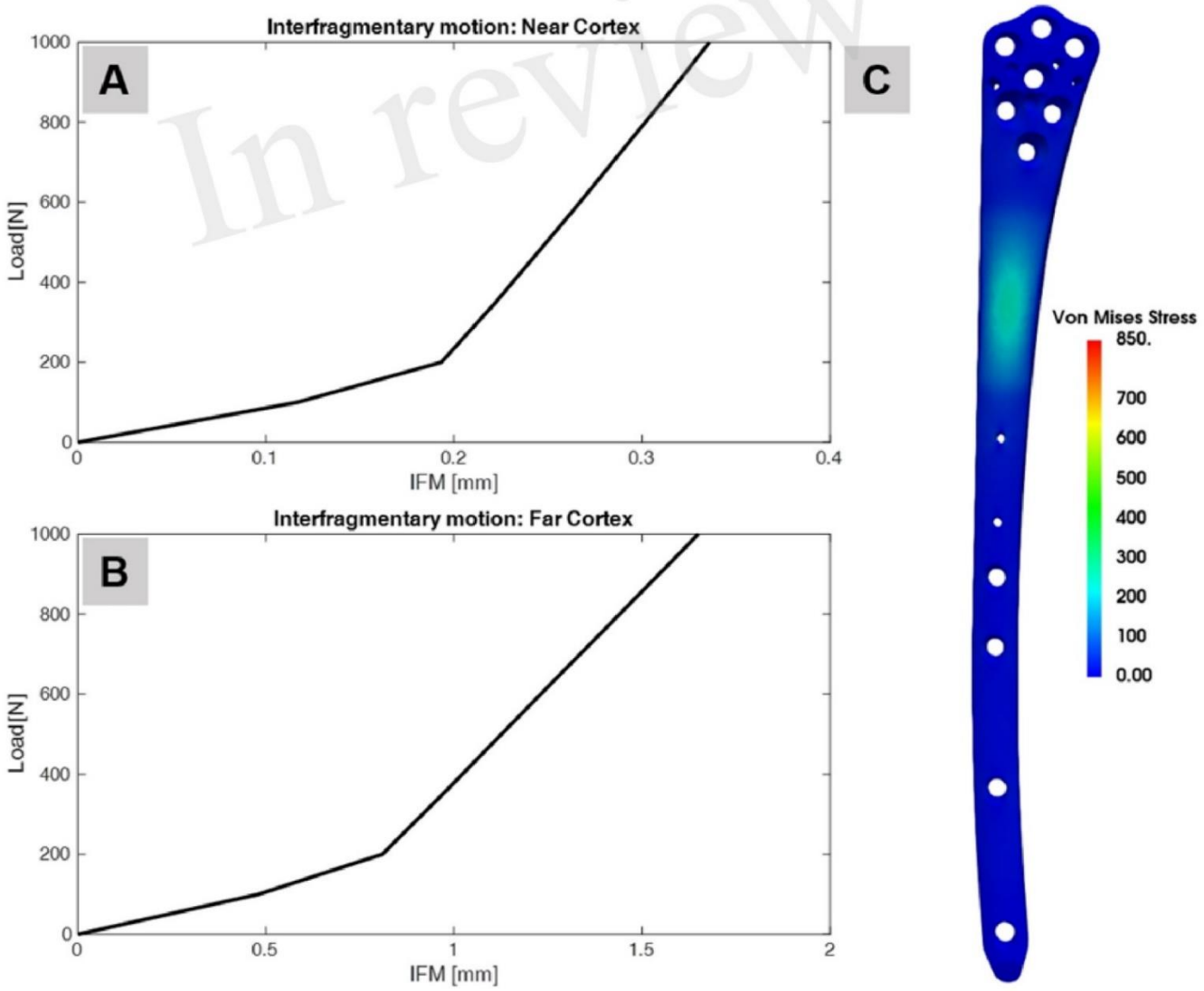


A
B
C
D
Von Mises Stress
0.0 100 200 300 400 500 600 700 800 900 1000.0

## 1. Supplementary material


Figure 6: Screw positions for A Patient 1, B Patient 2, C Patient 3 and D Patient 4.

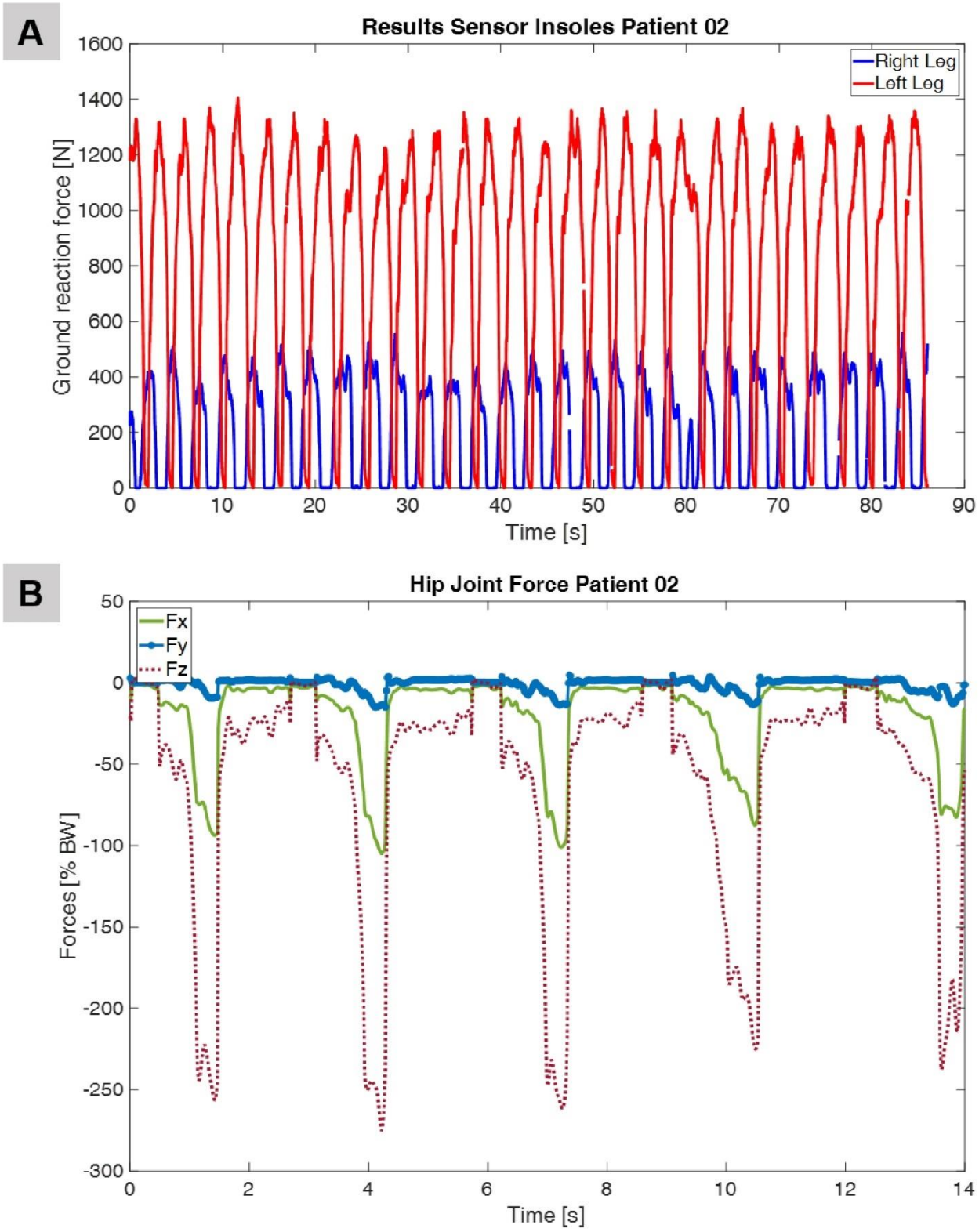


Figure 7: A Ground reaction force over time, recorded two days postoperatively under the recommended weight-bearing conditions, B Hip joint force over time, derived from the musculoskeletal modeling system AnyBody, using input data from the motion capture system during the same two-day postoperative measurement session.

### 9.1.4 CT-, 3D-Scan and Manufacturer-Based Implant Models: A Comparative Finite Element Study on Implant Geometry and Interfragmentary Movement in Distal Radius Fracture Fixation (Paper 4)

Authors:

**K. Wickert,** A. Andres, M. Roland, D. Crepulja, B. Braun, T. Histing, R. Leibinger, F. Reinauer and S. Diebels

Publication status:

In progress

# CT-, 3D-Scan and Manufacturer-Based Implant Models: A Comparative Finite Element Study on Implant Geometry and Interfragmentary Movement in Distal Radius Fracture Fixation

Kerstin Wickert[1*], Annchristin Andres[1], Michael Roland[1], Danijel Crepulja[1], Benedikt Braun[2], Tina Histing[2], Ralf Leibinger[3], Frank Reinauer[3], Stefan Diebels[1]

1. Applied Mechanics, Saarland University, Saarbrücken, Germany
2. Department of Trauma and Reconstructive Surgery at the Eberhard Karls University Tübingen, BG Klinik Tübingen, Germany
3. KLS Martin SE & Co. KG, 78532 Tuttlingen, Germany

* Correspondence:
Kerstin Wickert
Applied Mechanics
Saarland University
Campus A4 2, 1.OG
D-66123 Saarbrücken
Germany
phone: +49 681 302 2168
email: kerstin.wickert@uni-saarland.de

## Abstract

The accuracy of patient-specific finite element simulations in orthopedic biomechanics depend highly on the source and thus quality of the anatomical data and implant geometry. This study investigates the influence of three different implant geometry sources (computed-tomography-based, three-dimensional surface scan-based, and original manufacturer data) on biomechanical outcomes in a distal radius model under physiologically relevant loading conditions.

A distal radius fracture was created and stabilized using an additive manufactured locking plate. Each implant dataset was integrated into the same bone geometry, derived from imaging data. Musculoskeletal joint loads (extension-flexion) were applied at the distal radius, based on inverse dynamics simulations. The implant geometry sources differ in mesh density, surface quality, and positioning, resulting in varying levels of computational complexity. Interfragmentary movement and von Mises stress distributions were evaluated in the near and far cortex regions to assess sensitivity to implant representation.

Substantial differences in interfragmentary movement are observed in the near cortex, which are strongly linked to variations in implant positioning across datasets. In contrast, the far cortex showed relatively consistent results. The model based on manufacturer data exhibited the highest mesh density and longest computation times, while the computed tomography-based model offered the most efficient setup. Notably, three-dimensional scan data required extensive preprocessing to ensure mesh quality.

Implant geometry and positioning significantly affect local mechanical behavior in finite element simulations of fracture fixation. The findings highlight the need for standardized geometry integration workflows and support the future use of statistical implant models in larger patient-specific studies where manufacturer data is unavailable.

**Keywords**: distal radius fracture, additive manufactured implant, subject-specific analysis, osteosyntheses, orthopedic trauma surgery, biomechanical simulation

## Introduction

With advancing age, the risk of fracture development increases significantly. Distal radius fractures are reported to occur most frequently between the ages of 50 and 80 years [1]. Among individuals over the age of 65, this fracture type represents one of the most common fractures of the upper extremity, second only to proximal femur fractures [2]. In industrialized countries, this trend is largely attributed to an aging population. The progressive loss of bone mass and structural integrity associated with aging further influences treatment and outcome [3].

Overall, approximately 5-10% of all fractures are associated with impaired healing, including cases in which bone union fails to occur completely and also implant failure [4].

The underlying causes are diverse, ranging from mechanical overloading to implant failure. Biomechanical simulations have become an important tool for addressing clinically relevant questions. Finite element (FE) analysis has long been established as a reliable method for the numerical simulation of physical problems. Early use in orthopedic biomechanics focused on analyzing bone loading patterns [5].

However, in medical research, numerous patient-specific and experimental factors influence the outcomes, making it challenging to establish a reproducible simulation workflow that consistently delivers valid results. It is already known that the segmentation of the data has an influence on the simulation results [6]. Among the key determinants of simulation accuracy are the generation of the geometric model, the definition of boundary conditions, and the assignment of material properties to the individual components.

This study specifically investigates the impact of implant dataset generation on the accuracy of simulation results. Augat et al. addressed various factors influencing biomechanical simulations and their effects on outcome quality, emphasizing that biomechanical models should be *appropriate, reliable, valid,* and *relevant* [7]. In line with this, the U.S. Food and Drug Administration has published a comprehensive guidance document outlining how reports on computational modeling studies - particularly those involving FE analyses - should be prepared when submitting medical devices for regulatory approval [8]. The modeling approach and simulation setup were guided by established practices for credibility assessment in computational modeling, as outlined in ASME V&V 40 (2018), particularly in the context of medical device evaluation [9].

Building on this foundation, the present study investigates the effect of implant geometry generation on the accuracy of FE simulation results. Using a distal radius fracture analysis as a representative example, the study examines how different approaches to generating implant geometries influence simulation outcomes. Three types of implant datasets were analyzed: (1) segmented implant geometries reconstructed from computed tomography (CT) scans, (2) geometries derived from 3D scanning, and (3) the original manufacturer-provided dataset, including screws. The objective is to assess whether the choice of dataset type introduces measurable differences in simulation accuracy and to provide insights into the impact of geometric data quality on FE-based biomechanical analyses.

# Methods

## Computational Model

A radius (see Figure 1 A) builds the basis to generate the computational model and is additionally used as the initial data set to generate the three computational models for the FE analysis.

A fracture, type (2R3A2) according to AO classification was created with Geomagic Freeform™ software (Geomagic Freefrom Plus/Touch X, 3D Systems, Inc.) [10]. The working principle is based on pottery work. The following steps are executed: (1) Import radius surface in stereolithography (STL) format, (2) Convert the surface to clay model, (3) Fracture generation using freeform scraper tool, freeform hot wax tool to smoothen fracture edges and Boolean operations (uniform, subtract). With this workflow three parts were generated (distal part, fracture and proximal part). (4) Export of the fractured radius for further data analysis in STL format. (5) Import of the fractured radius and subsequent generation of a fracture mask to work in the following with an volume mesh. This fractured radius (distal and proximal part) was printed with an 3D printer for demonstration purpose.

The Geomagic Freeform™ software was additionally used to plan with the surgeon the osteotomy line for the individual implant. With this basis the individual solution was manufactured by KLS Martin SE & Co. KG. Three computational models were generated, each based on implant data from a different source (manufacturer, CT scan, 3D scan), resulting in varying levels of geometric complexity.

*Manufacturer model:* The implant including screws were imported in STL format to the initial data set. There was no alignment needed, because this dataset was used for implant planning and positioning (see Figure 1 D).

*CT scan model:* For imaging, the 3D-printed fractured radius, including the individual implant, was acquired using computed tomography (SOMATOM Definition AS, SIEMENS, Erlangen, Germany) with a slice thickness of 0.6 mm. For image segmentation of the implant, a mask was created using threshold methods. Additional steps to fill holes in the mask and suppress noise were performed utilizing a morphological closing filter and a recursive Gaussian smoothing filter. A detailed segmentation workflow is published by the authors [11], [12], [13], [14],. Subsequently, the mask was imported to the initial data set for alignment (see Figure 1 B). Simpleware™ (Synopsys, Mountain View, CA, United States) was used for image segmentation.

*3D scan model:* The implant was scanned with a 3D scanner including a rotary table for image acquisition (GOM Scan 1, Carl Zeiss AG, Oberkochen, Germany). To capture every side of the implant, several scanning series were needed. During one round of rotation, the rotary table stopped eight times to take a shot. For the second scanning series the implant was placed on the other side. Overall sixteen shots were executed. The two scanning series were subsequently aligned and merged to generate a complete 3D reconstruction of the implant, resulting in a single STL file representing the entire geometry. In the following, the 3D scanned model was imported into the initial data set and aligned to the correct position (see Figure 1 C). To reduce mesh

complexity and element count, screws were modeled as cylindrical bolts with identical diameter.

All implant datasets were imported into the initial data set containing the freeform fracture. Since this dataset served as the basis for the manufacturer's surgical planning, the position of the manufacturer's implant model was used as a reference to align the other two models (derived from CT scan and 3D scan).

Fracture [15] and implant [16] are assigned as homogeneous material parameters according to literature. The material properties of the radius (cortical and cancellous bone) are also assigned from literature [17]. Additionally, node sets for force application and boundary conditions for the FE simulation are defined at the distal and proximal epiphysis. An adaptive meshing was created using quadratic elements with straight edges type C3D10. This work was also done using the Simpleware™ software. Material assignment and node sets were equal in all computational models.

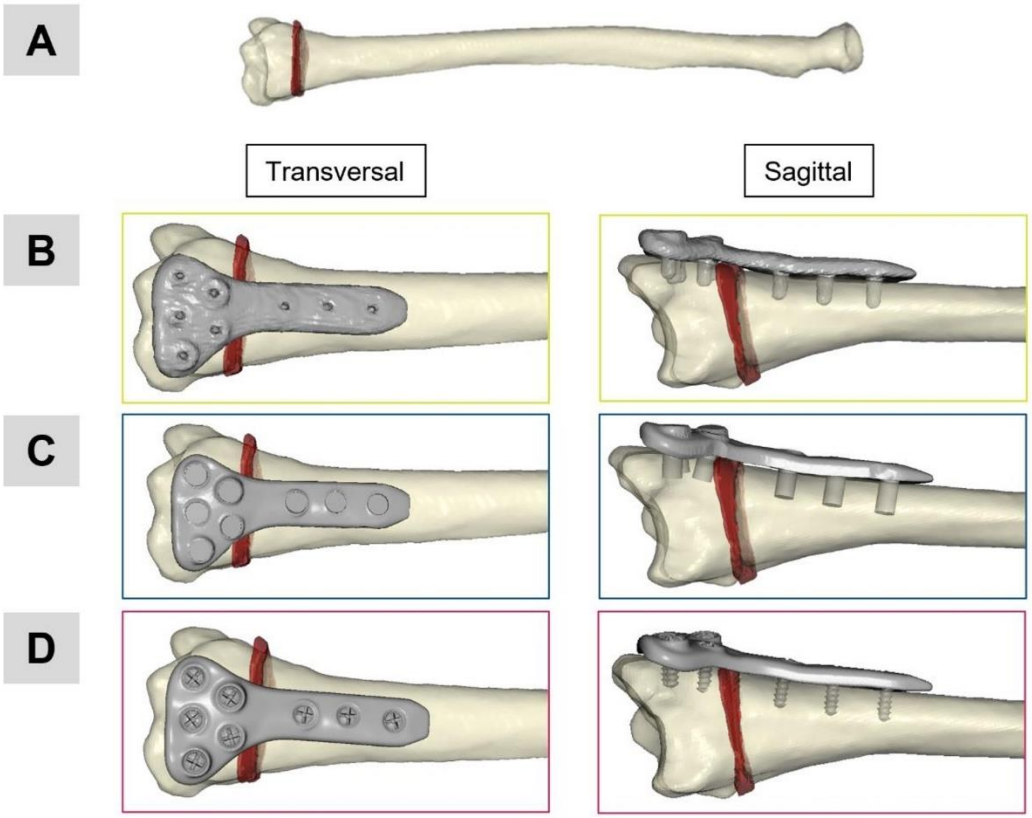


*Figure 1: A: CT Scan as the basis to create an artificial distal radius fracture (AO/OTA 2R3A2) (red=fracture gap). Also used for individual treatment planning, B: Computational model of the implant from CT scan, C: Computational model of the implant from 3D scan, D: Data set from manufacturer. All models are shown in transversal and sagittal direction.*

Table 1 summarizes the three different computational models (CT scan, 3D scan, and manufacturer dataset).

| Model | Element type | Number of elements | Size of input file |
|---|---|---|---|
| CT scan | Quadratic tetrahedra | 11,002 | 13,661 KB |
| 3D scan | Quadratic tetrahedra | 99,420 | 32,063 KB |
| Manufacturer | Quadratic tetrahedra | 1,093,061 | 239,464 KB |

*Table 1: Computational model (CT scan, 3D scan, manufacturer) information at a glance concerning element type, number of elements and size of input file.*

## Loading Scenario

Daily activities, used as loading scenarios, represent realistic conditions for testing bone-implant systems by evaluating implant stiffness or interfragmentary movement [18]. Flexion and extension as a daily activity were selected for this treatment approach. Monitoring is therefore a suitable method to assess physical activity during the healing period and to establish the basis for subject-specific loading conditions. To capture the movement, subjects were equipped with a motion measurement system (Xsens™ Technology B.V., Enschede, Netherlands) [19]. In this case the wrist joint angle (see Figure 2A) are captured during extension flexion (see Figure 2 B) as a part of daily activity. These data are used in musculoskeletal simulations to calculate subject-specific joint forces (see Figure 2 C), separated into their anatomical axes (see Figure 2 D). The computations were done using the AnyBody™ Software (AnyBody Technology A/S, Aalborg, Denmark).

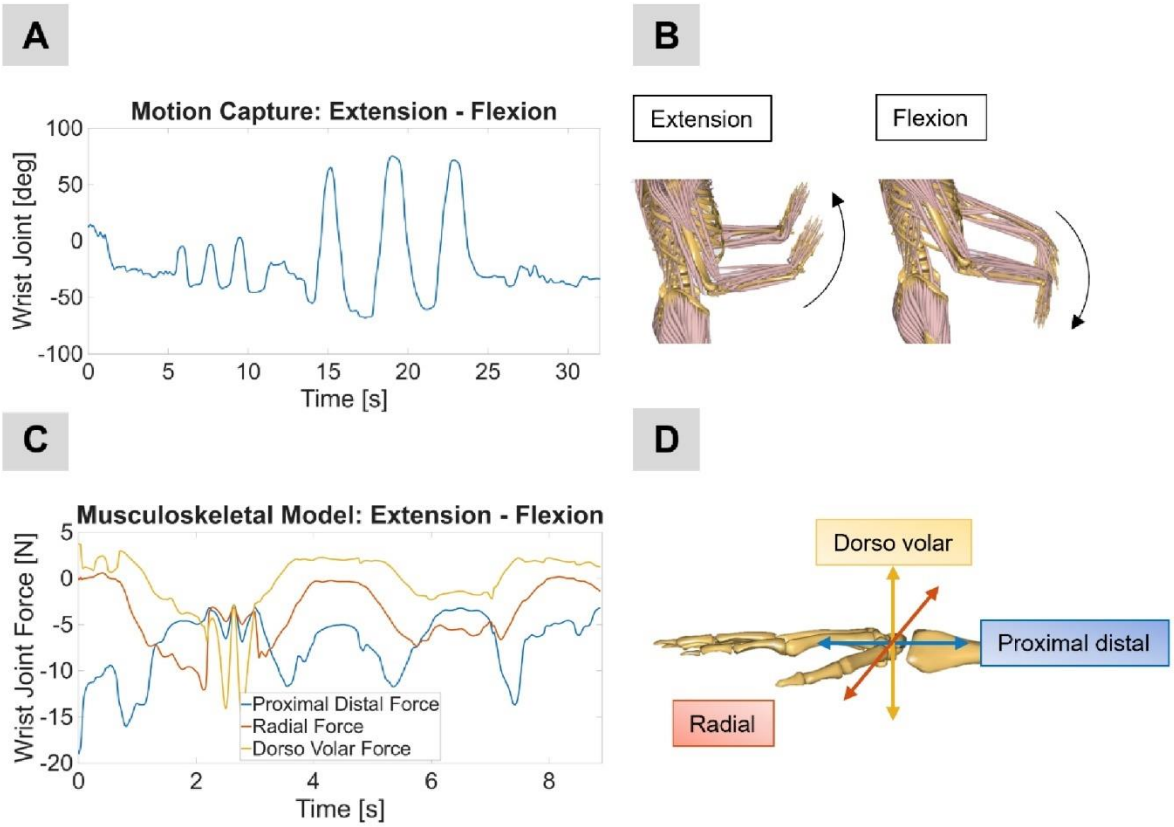


*Figure 2: A: Motion capture of extension and flexion, B: Movement of extension and flexion in a musculoskeletal model, C: Calculated wrist joint forces from musculoskeletal model. Used as loading scenario in simulation, D: Body directions using the example of the wrist.*

The estimated force values were then applied as loading scenarios in the simulation environment on the defined node sets. The established workflow of this procedure is already published by the authors [11].

### Finite Element Simulation

All three computational models were imported into Abaqus™ (Dassault Systemes, Vélizy-Villacoublay, France). At first, the bone-implant systems had to be aligned, that the acting wrist joint forces were applied accurate according to the body axes.

The wrist joint forces are applied as concentrated forces on the node set at the distal end segment of the radius. The force application of the wrist joint forces is applied iteratively, until the wrist joint force values of the musculoskeletal model have been processed. The proximal end segment is fixed. For evaluation purposes different areas of interest were observed. (1) Displacement of the implant surface above the fracture gap (2) interfragmentary movement near cortex (3) interfragmentary movement far cortex and (4) Maximum von Mises stress of the implant at the force extremum in dorso volar direction (-15 N) (see Figure 2 C). The displacements as well as the interfragmentary movement were determined by choosing two node on the surface calculating the displacement during each increment (see Figure 3 D).

## Results

Figure 3 representing for all three data sets the areas of interest, implant surface and interfragmentary movement near and far cortex, during the movement of extension and flexion. The displacement of the implant's surface and the interfragmentary movement near cortex are smaller in comparison to the interfragmentary movement far cortex.

The implant provides sufficient stability at the fracture site while allowing greater motion on the opposite side (far cortex). This leads to increased interfragmentary movement (see Figure 3 B) compared with the implant-adjacent (near cortex) side (see Figure 3 C) or the micromotions at the implant surface (see Figure 3 A). The individual computational models show only minor differences. While the implant displacements and the interfragmentary movement at the far cortex are very similar across all models, larger deviations can be observed in the interfragmentary movement at the near cortex. Differences in interfragmentary movement were primarily observed in the near cortex region across the three implant models (CT-based, 3D-scan-based, and manufacturer design). These deviations can be attributed to variations in implant positioning, which directly influence the local mechanical environment adjacent to the implant. In contrast, the far cortex region showed only minor differences in interfragmentary displacement between models. This can be explained by the more indirect load transfer in this area, which makes it less sensitive to small geometric or positional deviations of the implant. Overall, the results highlight the dominant role of implant positioning in determining local stability, particularly at the near cortex.

Clear differences can also be observed in both the number of elements and the size of the input file, which contains the complete model information, including bone, fracture, implant, and node sets (see Table 1). These differences are also critical for the computational performance of the simulations. While the CT-based model completed the simulation within a few minutes, the simulation time increased rapidly

with a higher element count, resulting in the manufacturer-provided model requiring several hours to simulate physiologically relevant loading scenarios.

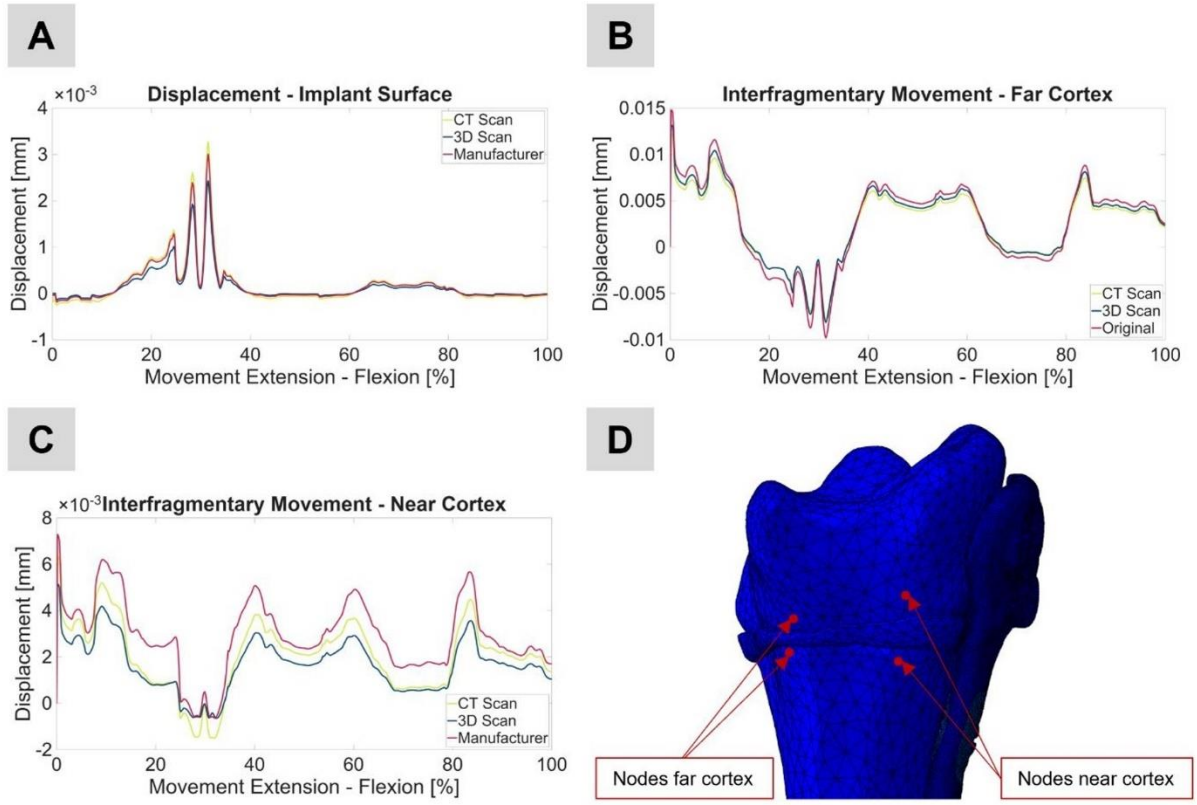


*Figure 3: Simulation results concerning the displacement during the movement of extension – flexion on A: the implant surface, B: the radius' surface far cortex, and C: the radius' surface near cortex, D: Nodes chosen for evaluation. Two nodes near cortex and two nodes far cortex for displacement evaluation.*

Figure 4 illustrates the von Mises stress distribution on the implant surface. While the overall stress patterns appear similar across all three models, the maximum stress values differ notably. The CT-based model exhibited a peak von Mises stress of 38 MPa (see Figure 4 A), compared to 63 MPa for the 3D scan-based model (see Figure 4 B) and 75 MPa for the manufacturer model (see Figure 4 C). These differences in peak stress can be attributed primarily to variations in mesh density. The higher-resolution meshes of the 3D and manufacturer models allow for a more accurate resolution of local stress concentrations, particularly around screw holes and geometrical transitions. Additionally, small deviations in implant positioning between models may lead to local changes in load transfer and bending moments, further contributing to variations in peak stress values. Despite these differences, the general stress distribution remains consistent, indicating that the global load response is preserved across geometry sources. Similar observations have been reported in the literature, where finer meshes were shown to capture more pronounced local stress peaks, especially in regions with geometric discontinuities or contact interfaces [20].

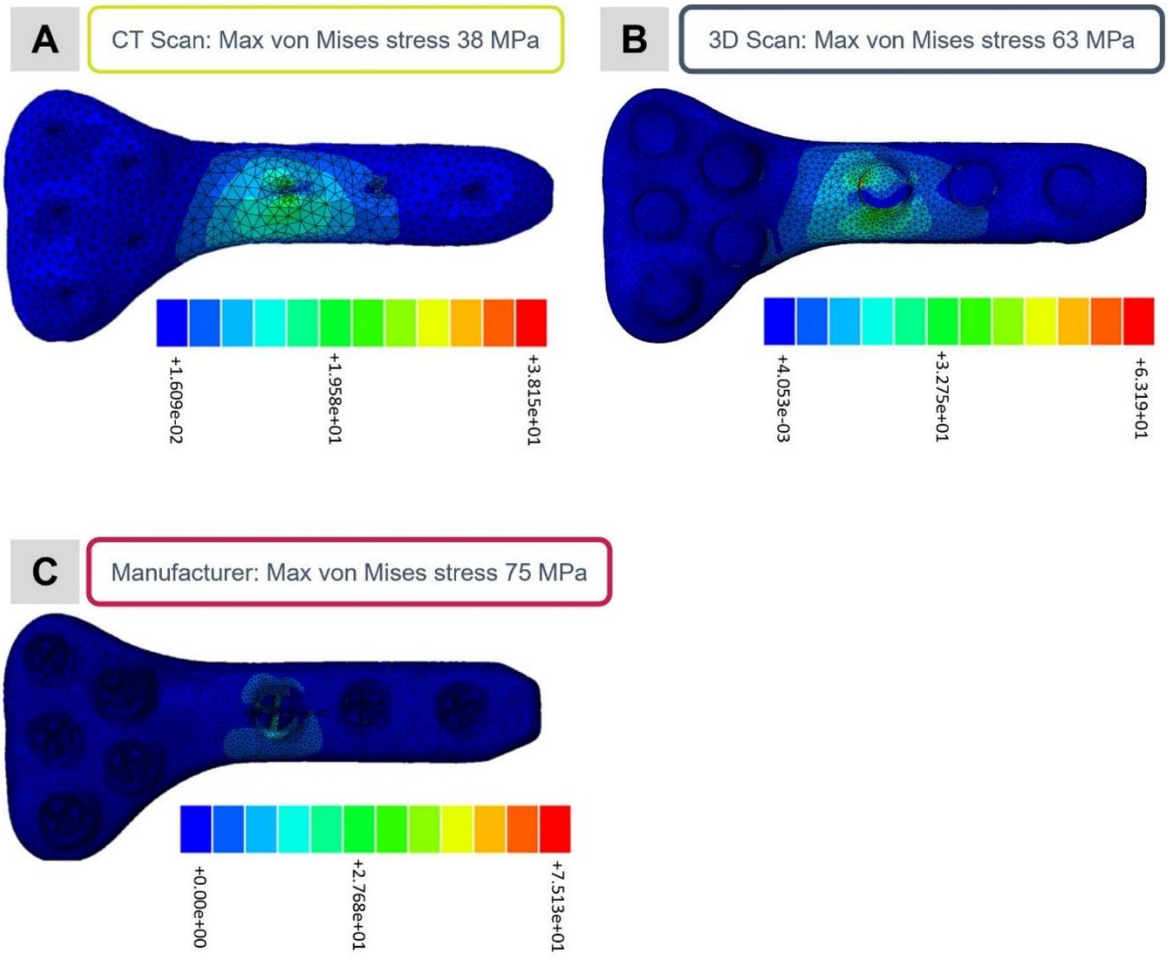


*Figure 4: Stress distribution of von Mises stress A: CT scan, B: 3D scan and C: Manufacturer model.*

The analysis of each region is strongly influenced by the selected nodes of the FE mesh. Minor discrepancies can also be attributed to slight variations in the alignment of the individual models. The manufacturer's planning model served as a reference for the alignment of the other two models (CT-based and 3D-scan-based), which were positioned manually. The Supplementary Material includes Figure 5, illustrating the deviations of the implant surfaces obtained from the 3D (see Figure 5 A) and CT scans (see Figure 5 B), as well as an additional figure demonstrating the quality of the 3D-scanned implant compared to the manufacturer's reference model (see Figure 5 C).

## Discussion

The presented workflow has been established for a single subject-specific model and provides a foundation for application in a larger cohort to confirm the reproducibility and validity of the results. Nevertheless, a challenge is the limited accessibility of manufacturers implant data, which are normally subjected to confidentiality agreements and intellectual property restrictions. In this case, statistical bone models [21] in combination with a generic or statistical implant could provide a solution to investigate for broader cohort studies while maintaining a standardized framework. This would enable systematic investigations into interindividual variability without relying on proprietary implant geometries.

The main differences, comparing the three models, were observed in the illustration of the screws and in the positioning of the implant. Particularly in the near cortex region, the influence of implant positioning became evident, as local interfragmentary movement varied depending on the spatial alignment of the fixation device. While the general geometry of the bone remained consistent across models, even small deviations in implant location led to measurable differences in mechanical response.

In addition to the biomechanical effects, practical aspects such as data preparation and computational cost played a significant role. The three models differed substantially in mesh density and input file size, ranging from 11,002 elements (13,661 KB) in the CT-based model to over one million elements (239,464 KB) in the manufacturer-specific model (see Table 1). Accordingly, simulation run times increased with model complexity [20]. Furthermore, extensive preprocessing was required, particularly for the 3D-scan and manufacturer models. The 3D implant surface, for instance, required cleaning, hole filling, and remeshing. Similarly, the manufacturer implant data had to be provided in a suitable format before mesh generation could take place. These aspects highlight the trade-off between anatomical or geometric fidelity and computational feasibility, which must be considered when scaling such simulations to larger cohorts. As highlighted by Murphy et al. [22], computational time remains a critical factor in patient-specific FE modeling, especially when high-resolution surface scans are used to generate detailed meshes for biomechanical analysis. The time window for patient-specific solutions is relatively narrow between imaging and treatment. As a result, computationally intensive simulations are more suitable for research purposes and are not yet feasible for routine clinical use. Instead, models that are sufficiently accurate for the specific question, yet simplified enough to allow for analysis and computation within a short timeframe, are more appropriate for clinical application.

In this study the focus is on comparing the influence of different implant datasets, rather than simulating the entire healing process, which partially justifies the linear assumption. Moreover, although the flexion-extension movement represents a clinically relevant loading scenario [23], the model does not include soft tissues or active muscle forces, which in vivo contribute significantly to joint mechanics, load sharing, and constraint. Patient-specific FE models are increasingly valued for their potential to link individual anatomy, geometry, and loading conditions to biomechanical metrics that may inform clinical decision-making (e.g. implant design, risk estimations, optimization). Imaging modalities such as CT allow for faithful reconstruction of bone geometry and, when segmented appropriately, also cortical and trabecular compartments [24]. By integrating patient-specific geometry with musculoskeletal load data, one can simulate individualized stresses, displacements, and interfragmentary movement - offering insight beyond generic or population-averaged models [13], [25].

A notable limitation of the present FE model is the assumption of linear elastic material behavior, which is justifiable only for relatively small deformations and strains. This simplification neglects non-linearities, plasticity, damage accumulation, or viscoelastic effects that may become relevant under higher loads. However, translation of these models into clinical practice remains limited. Challenges include the need for standardized workflows, validation against in vivo or experimental data, handling of proprietary implant geometries, and ensuring acceptable turnaround times for clinical

applicability. Nonetheless, if your modeling approach can robustly quantify the effect of geometry source on simulation outputs, it may guide surgeons, implant manufacturers, or researchers in understanding sensitivity limits of patient-specific simulations. Over time, with improvements in imaging, preprocessing automation, and computational resources, such models may support personalized surgical planning, implant selection, or risk stratification in fracture fixation and biomechanics.

## Conclusion

This study introduces an insight into influences on biomechanical simulations concerning implant data sources. However, these investigations only cover one factor that can influence the simulation results. Other factors, such as the influence of the selected test scenario, reproducibility, or other factors in the simulation area (e.g., meshing), still need to be investigated. Differences in the simulation results can be attributed primarily to the implant position near the cortex.

## Data availability statement

The original contributions presented in the study are included in the article/ supplementary material, further inquiries can be directed to the corresponding author.

## Author contributions

KW: Methodology, Formal Analysis, Investigation, Visualization, Writing – Original Draft, Writing – Review and Editing

AA: Resources, Visualization, Writing – Review and Editing

MR: Supervision, Writing – Review and Editing

DC: Resources, Investigation, Writing – Review and Editing

BB: Investigation, Data Curation, Supervision, Writing – Review and Editing

TH: Supervision, Funding acquisition, Writing – Review and Editing

RL: Data Curation, Resources, Writing – Review and Editing

FR: Resources, Supervision, Funding acquisition, Writing – Review and Editing

SD: Supervision, Funding acquisition, Writing – Review and Editing

## Funding

This work was funded by the German Federal Ministry of Research, Technology and Space (BMFTR), previously German Federal Ministry Education and Research (BMBF) under the grant “FKZ: 13GW0572”.

## Conflict of interest

The authors RL and FR are employees of KLS Martin SE & Co. KG, and therefore, they have received/will receive benefits for personal or professional use from KLS Martin SE & Co. KG related directly or indirectly to the subject of this manuscript.

## References


[1] A. M. Koski, A. Patala, E. Patala, and R. Sund, ‘Incidence of osteoporotic fractures in elderly women and men in Finland during 2005–2006: A population-based study’, Scand J Surg, vol. 103, no. 3, pp. 215–221, 2014, doi: 10.1177/1457496914525554.

[2] K. Reiland, B. Haastert, W. Arend, B. Klüppelholz, J. Windolf, A. Icks, S. Thelen, and S. Andrich, ‘Epidemiology of distal radius fractures in Germany: Incidence rates and trends based on inpatient and outpatient data’, *Osteoporos Int*, vol. 35, pp. 317–326, 2024, doi: 10.1007/s00198-023-06904-6.

[3] C. K. Ugwoke, D. Albano, N. Umek, I. Dumić-Čule, and Ž. Snoj, ‘Application of virtual reality systems in bone trauma procedures’, *Medicina (Kaunas)*, vol. 59, no. 3, p. 562, 2023, doi: 10.3390/medicina59030562.

[4] T. A. Einhorn and L. C. Gerstenfeld, ‘Fracture healing: Mechanisms and interventions’, *Nat Rev Rheumatol*, vol. 11, no. 1, pp. 45–54, 2015, doi: 10.1038/nrrheum.2014.164.

[5] R. Huiskes and E. Y. Chao, ‘A survey of finite element analysis in orthopedic biomechanics: The first decade’, *J Biomech*, vol. 16, no. 6, pp. 385–409, 1983, doi: 10.1016/0021-9290(83)90072-6.

[6] E. Saillard, M. Gardegaront, A. Levillain, F. Bermond, D. Mitton, J.-B. Pialat, C. Confavreux, T. Grenier, and H. Follet, ‘Finite element models with automatic computed tomography bone segmentation for failure load computation’, *Sci Rep*, vol. 14, p. 16576, 2024, doi: 10.1038/s41598-024-66934-w.

[7] P. Augat, M. W. Hast, G. Schemitsch, M. Heyland, A. Trepczynski, E. Borgiani, G. Russow, S. Märdian, G. N. Duda, M. Hollensteiner, M. Bottlang, and E. H. Schemitsch, ‘Biomechanical models: Key considerations in study design’, *OTA Int*, vol. 4, no. 2 (suppl.), pp. e099(1–6), 2021, doi: 10.1097/OI9.0000000000000099.

[8] U.S. Food and Drug Administration (FDA), *Reporting of Computational Modeling Studies in Medical Device Submissions*, Center for Devices and Radiological Health, Rockville, MD, Rep. FDA-2013-D-1530, Sept. 2016.

[9] The American Society of Mechanical Engineers (ASME), *V&V 40 – Assessing credibility of computational modeling through verification and validation: Application to medical devices*, ASME, New York, NY, 2018, ISBN 978-0-7918-7204-8.

[10] M. E. Müller, P. Koch, S. Nazarian, and J. Schatzker, ‘Tibia/Fibula = 4’, in *The Comprehensive Classification of Fractures of Long Bones*, Springer, Berlin, Heidelberg, 1990, doi: 10.1007/978-3-642-61261-9_7.

[11] A. Andres, M. Roland, K. Wickert, B. Ganse, T. Pohlemann, M. Orth, and S. Diebels, ‘Individual postoperative and preoperative workflow for patients with fractures of the lower extremities’, *Clin Biomech (Bristol)*, p. 106503, Mar. 22, 2025, doi: 10.1016/j.clinbiomech.2025.106503.

[12] M. Roland, S. Diebels, M. Orth, T. Pohlemann, B. Bouillon, and T. Tjardes, ‘Reappraisal of clinical trauma trials: The critical impact of anthropometric parameters on fracture gap micro-mechanics—observations from a simulation-based study’, *Sci Rep*, vol. 13, p. 20450, 2023, doi: 10.1038/s41598-023-47910-2.

[13] B. J. Braun, M. Orth, S. Diebels, K. Wickert, A. Andres, J. Gawlitza, A. Bücker, T. Pohlemann, and M. Roland, ‘Individualized determination of the mechanical fracture environment after tibial exchange nailing: A simulation-based feasibility study’, *Front Surg*, vol. 8, p. 749209, 2021, doi: 10.3389/fsurg.2021.749209.

[14] K. Wickert, M. Roland, A. Andres, S. Diebels, B. Ganse, D. Kerner, F. Frenzel, T. Tschernig, M. Ernst, M. Windolf, M. Müller, T. Pohlemann, and M. Orth, ‘Experimental and virtual testing of bone-implant systems equipped with the AO Fracture Monitor with regard to interfragmentary movement’, *Front Bioeng Biotechnol*, vol. 12, p. 1370837, 2024, doi: 10.3389/fbioe.2024.1370837.

[15] L. E. Claes and C. A. Heigele, ‘Magnitudes of local stress and strain along bony surfaces predict the course and type of fracture healing’, *J Biomech*, vol. 32, no. 3, pp. 255–266, 1999, doi: 10.1016/S0021-9290(98)00153-5.

[16] M. A. Imam and A. C. Fraker, ‘Titanium alloys as implant materials’, in *Medical Applications of Titanium and Its Alloys: The Material and Biological Issues*, S. A. Brown and J. E. Lemons, Eds., ASTM International, 1996, pp. 3–16.

[17] A. Synek, Y. Chevalier, S. F. Baumbach, and D. H. Pahr, ‘The influence of bone density and anisotropy in finite element models of distal radius fracture osteosynthesis: Evaluations and comparison to experiments’, *J Biomech*, vol. 48, no. 15, pp. 4116–4123, 2015, doi: 10.1016/j.jbiomech.2015.10.012.

[18] Y. A. Behnam, A. Anantha Krishnan, R. List, and C. W. Clary, ‘In vitro verification of simulated daily activities using implant-specific kinematics from in vivo measurements’, *Bioengineering*, vol. 11, p. 1108, 2024, doi: 10.3390/bioengineering11111108.

[19] A. Andres, M. Roland, K. Wickert, S. Diebels, J. Stöckl, S. Herrmann, F. Reinauer, R. Leibinger, A. Pavlov, L. Schuppener, D. Schäfer, T. Histing, and B. J. Braun, ‘Advantages of digital twin technology in orthopedic trauma surgery: Exploring different clinical use cases’, *Sci Rep*, vol. 15, p. 19987, 2025, doi: 10.1038/s41598-025-04792-w.

[20] C. Falcinelli, F. Valente, M. Vasta, and T. Traini, ‘Finite element analysis in implant dentistry: State of the art and future directions’, *Dent Mater*, vol. 39, no. 6, pp. 539–556, 2023, doi: 10.1016/j.dental.2023.04.002.

[21] X. Cai, Y. Wu, J. Huang, L. Wang, Y. Xu, and S. Lu, ‘Application of statistical shape models in orthopedics: A narrative review’, *Innov Med*, Nov. 1, 2024, Chinese Medical Association, doi: 10.1016/j.imed.2024.05.001.

[22] E. K. Murphy, J. Smith, M. A. Kokko, S. B. Rutkove, and R. J. Halter, ‘Rapid patient-specific FEM meshes from 3D smartphone-based scans’, *Physiol Meas*, vol. 45, no. 2, p. 025008, 2024, doi: 10.1088/1361-6579/ad26d2.

[23] J. Y. Ryu, W. P. Cooney III, L. J. Askew, A. N. An, and E. Y. Chao, ‘Functional ranges of motion of the wrist joint’, *J Hand Surg Am*, vol. 16, no. 3, pp. 409–419, 1991, doi: 10.1016/0363-5023(91)90006-W.

[24] P. Pankaj, ‘Patient-specific modelling of bone and bone-implant systems: The challenges’, *Int J Numer Method Biomed Eng*, vol. 29, no. 2, pp. 233–249, 2013, doi: 10.1002/cnm.2536.

[25] A. Andres, M. Roland, K. Wickert, S. Diebels, D. Truhn, T. Histing, and B. Braun, ‘Predicting the effect of individual weight-bearing on tibial load and fracture healing after tibial plateau fractures – introduction of a biomechanical simulation model’, *Front Bioeng Biotechnol*, vol. 13, 2025, doi: 10.3389/fbioe.2025.1659029.

## Supplementary Material

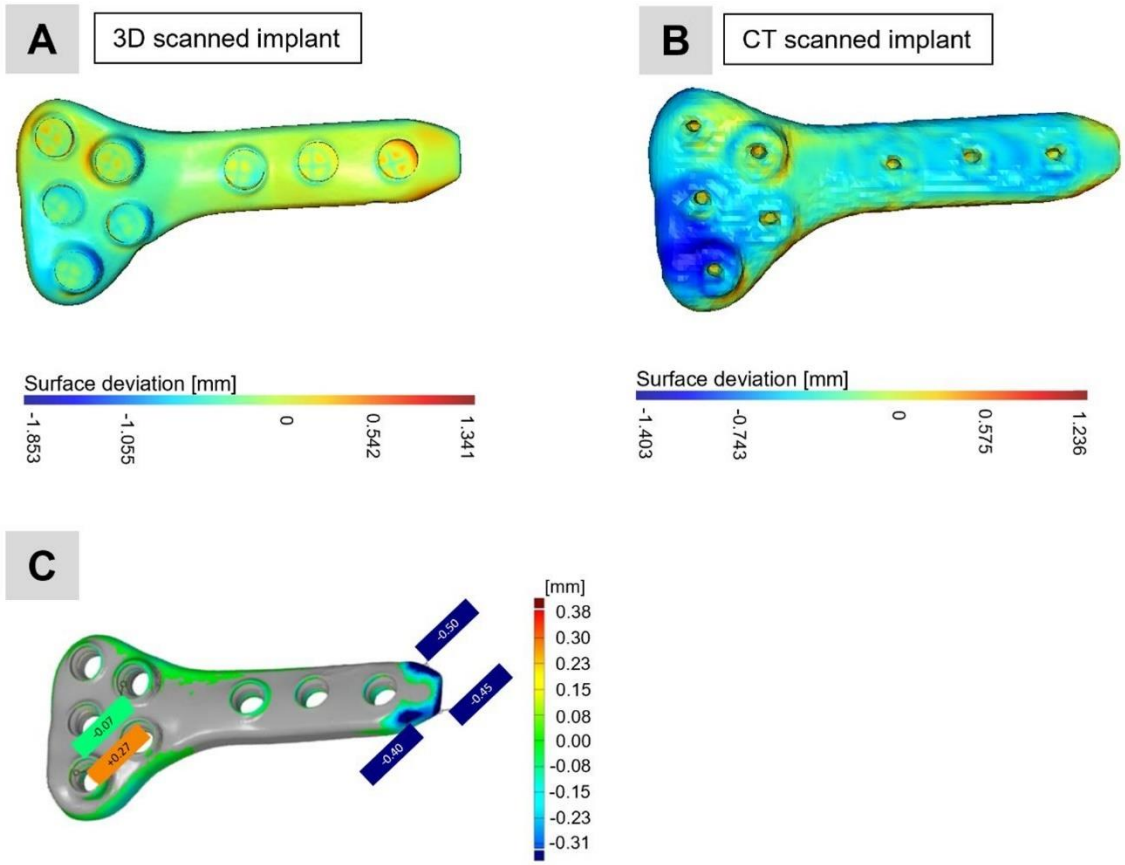


*Figure 5: Surface deviation of the A: 3D scanned implant position and B: Surface deviation of the CT scanned implant position compared to the manufactured implant (reference), C: Surface deviation of the 3D scanned implant in comparison to the manufacturer data set.*

## 9.2 Further Publications of the author

B. J. Braun, M. Orth, S. Diebels, **K. Wickert**, A. Andres, J. Gawlitza, A. Bücker, T. Pohlemann, and M. Roland, 'Individualized determination of the mechanical fracture environment after tibial exchange nailing—A simulation-based feasibility study', *Front Surg*, vol. 8, p. 749209, 2021, doi: 10.3389/fsurg.2021.749209.

B. Ganse, M. Orth, M. Roland, S. Diebels, P. Motzki, S. Seelecke, S. Kirsch, F. Welsch, A. Andres, **K. Wickert**, B. J. Braun, and T. Pohlemann, 'Concepts and clinical aspects of active implants for the treatment of bone fractures', *Acta Biomater*, vol. 146, pp. 1–9, 2022, doi:10.1016/j.actbio.2022.05.001.

M. Orth, B. Ganse, A. Andres, **K. Wickert**, E. Warmerdam, M. Müller, S. Diebels, M. Roland, and T. Pohlemann, 'Simulation-based prediction of bone healing and treatment recommendations for lower leg fractures: Effects of motion, weight-bearing and fibular mechanics', *Front Bioeng Biotechnol, vol. 11, 2023, doi: 10.3389/fbioe.2023.1067845.*

M. Roland, S. Diebels, **K. Wickert**, T. Pohlemann, and B. Ganse, 'Finite element simulations of smart fracture plates capable of cyclic shortening and lengthening: which stroke for which fracture?', *Front Bioeng Biotechnol*, vol. 12, 2024, doi: 10.3389/fbioe.2024.1420047.

A. Andres, M. Roland, **K. Wickert**, S. Diebels, J. Stöckl, S. Herrmann, F. Reinauer, R. Leibinger, A. Pavlov, L. Schuppener, D. Schäfer, T. Histing and B.J. Braun , 'Advantages of digital twin technology in orthopedic trauma surgery – Exploring different clinical use cases', *Sci Rep*, vol. 15, p. 19987, 2025, doi: 10.1038/s41598-025-04792-w.

A. Andres, **K. Wickert**, E. Gneiting, F. Binmoeller, S. Diebels, and M. Roland, 'Simulation of a custom-made temporomandibular joint—An academic view on an industrial workflow', *Bioengineering*, vol. 12, p. 545, 2025, doi: 10.3390/bioengineering12050545.

A. Andres, M. Roland, **K. Wickert**, B. Ganse, T. Pohlemann, M. Orth, and S. Diebels, 'Individual postoperative and preoperative workflow for patients with fractures of the lower extremities', *Clin Biomech (Bristol)*, p. 106503, 2025, doi: 10.1016/j.clinbiomech.2025.106503.

A. Andres, M. Roland, **K. Wickert**, S. Diebels, D. Truhn, T. Histing and B. Braun ,'Predicting the effect of individual weight-bearing on tibial load and fracture healing after tibial plateau fractures – introduction of a biomechanical simulation model', *Front Bioeng Biotechnol, vol. 13, 2025, doi: 10.3389/fbioe.2025.1659029.*

# Eidesstattliche Versicherung

Hiermit versichere ich an Eides statt, dass ich die vorliegende Arbeit selbstständig und ohne Benutzung anderer als der angegebenen Hilfsmittel angefertigt habe. Die aus anderen Quellen oder indirekt übernommenen Daten und Konzepte sind unter Angabe der Quelle gekennzeichnet.

Die Arbeit wurde bisher weder im In- noch im Ausland in gleicher oder ähnlicher Form in einem Verfahren zur Erlangung eines akademischen Grades vorgelegt.

Ich erkläre darüber hinaus mit meiner Unterschrift, dass ich

- keine im Merkblatt „Hinweise zur Vermeidung von Plagiaten“ der Naturwissenschaftlich-Technischen Fakultät beschriebene Form des Plagiats begangen habe.
- Alle Methoden, Daten und Arbeitsabläufe wahrheitsgetreu dokumentiert habe und
- keine Daten manipuliert habe.

| | |
|---|---|
| Ort, Datum | Unterschrift |